An integral model for continuous HF releases

Ott, Søren

Publication date:
2001

Document Version
Publisher's PDF, also known as Version of record

Risø–R–1293(EN)

An integral model for continuous HF releases

Søren Ott

Risø National Laboratory, Roskilde, Denmark
October 2001

Abstract This report describes the development of an integral model for the dispersion of HF clouds, which is part of the work done by Risø in the URAHFREP project. URAHFREP, *Understanding dispersion of industrial Releases of Anhydrous Hydrogen Fluoride and the associated Risk to the Environment and People*, is a project sponsored by the European Commission under contract ENV4-CT97-0630.

The main objective has been to model the possible influence of HF thermodynamics on the dispersion of atmospheric HF clouds. Both negative buoyancy (heavy gas) effects and positive buoyancy effects are possible depending on concentration, humidity and other factors. A main question is under which conditions these effects are strong enough to dominate naturally occurring fluctuations and produce plume lift-off. The URAHFREP field trials showed only weak signs of positive buoyancy in plumes produced for 0.1 kg/s liquid spray releases.

HF can form polymers in the gas phase and it forms highly non-ideal liquid mixtures with water. It is demonstrated that the HF thermodynamics needed for the dispersion model can be described by exact thermodynamical relations. The treatment is based on the fugacity concept, which is explained in some detail emphasizing the link to measurements. Existing experimental data are scarce and of varying quality. The best data have been selected and analysed in order to obtain properties on the saturation curve. A relatively simple rings–and–chains model for the self-association in the gas phase is proposed, and it is demonstrated that the model is capable of reproducing independent measurements (not used to tune the model), in particular it predicts the enthalpy and the anomalous specific heat of HF very satisfactorily. Exact relations describing phase equilibria for the water-HF system are set up, and the role of the mixing enthalpy is demonstrated. This is used to derive a simple four parameter model for the mixture. Finally the model is successfully tested against fog chamber experiments.

The dispersion model is a more-or-less standard integral model with some additional features. The ideas and assumptions of integral models is explained and the various scaling regimes for cloud growth are discussed. Re-analyzing the Prairie Grass data set it is found that boundary layer scaling is superior to mixed layer scaling, and hence the height of the boundary layer has no direct impact on the dispersion in the lower part of the boundary layer (including lift-off due to natural convection). The model is tested against data from the URAHFREP field trials. Reasonable agreement is found. In most cases (all except one) the experiments showed no signs of buoyancy effects which is in agreement with model predictions. In Trial 12 reduced ground level concentrations were observed as well as an elevation of the cloud centroid. This behaviour is captured by the model. A case study is made in order to determine the conditions necessary for HF induced buoyancy to have an effects on ground level concentrations. The possibility of including added mass is discussed and dynamic equations compatible with the level of complexity of an integral model are derived in the appendix.

ISBN

87–550–2942–6; 87–550–2943–4(Internet)

Print: Pitney Bowes Management Services Denmark A/S · 2001

Contents

1 Introduction

This report presents a simple model for atmospheric dispersion of Hydrogen Fluorid (HF) clouds. The motivation is to understand what influence the peculiar thermodynamics of mixtures of HF with moist air can have on dispersing HF clouds. The influence is mediated by density changes which may cause an HF cloud to become both positively and negatively buoyant. The crucial point in terms of risk assessment applications is whether large HF plumes can lift-off the ground. If so this could be regarded as an inherent safety factor of the substance that could reduce safety distances.

Modelling the density is therefore a primary aim to which the first half of this report is devoted. In order to obtain the density a complete mass and enthalpy balance must be set up which takes possible condensation of hydrofluoric acid (liquid HF/water mixtures) into account. Theory, experimental data and models are reviewed and discussed. A simple thermodynamic model is proposed and tested against experimental data.

The second half of the report is devoted to the development of a simple dispersion model capable of reproducing what we believe are the main features of HF dispersion. Surface layer scaling is the basis for our understanding of dispersion in general is used in the interpretation of experimental data and will be explaines in some detail. The importance of a clear distinction between relative and absolute turbulent diffusion is also emphasized. The dispersion model is based on the relative diffusion (or two-particle) concept, and an effort is made to tune it to experimental relative diffusion data. Such data are as yet scarce, and the data resulting from the URAHFREP field trials (Ott and Jørgensen 2001) are in fact among the best available, therefore these are used frequently throughout the report.

The ideal model should combine simplicity with accuracy, and making such a model can be complicated. Simplicity is obtained by treating only selected aspects of reality whereas accuracy is obtained by selecting the right aspects and treat them in the right way. This requires a basic understanding of the phenomenology. Unfortunately, there is little empirical knowledge of HF clouds. We know that mixtures of HF and humid air get hot and become positively buoyant, but effects of this on the dispersion of HF plumes is uncertain. In the URAHFREP tests only faint indications of positive buoyancy effects were observed and in the Goldfish experiments only negative buoyancy was observed (Blewitt, Yohn, Koopman and Brown 1987). Consequently, lift-off of an HF cloud has never been observed during an experimental release. This only exclude the possibility of a lift-off in the conditions under which the experiments were made. In the Goldfish experiments the relative humidities seem to have bin too low and in the URAHFREP experiments the release rates may have been too low for lift-off to be detectable. This lack of experimental evidence of HF induced lift-off is an obvious difficulty for the modeller. Without simple visual observations the understanding of the phenomenology cannot be said to be complete. The purpose of the URAHFREP trials was to provide such understanding by collecting high quality data from HF dispersion experiments. The trials showed that buoyancy effects in HF clouds were small under the given conditions and no lift-off was seen. This in itself is a valuable result, but it is difficult to generalize to situations where a lift-off might occur. Hall and Walker (1997) has pointed out that the experiments can be conceived as down-scaled versions of larger releases. Scaling to larger release rates makes the results applicable to larger, and more hazardous releases. In the trials buoyancy effects were insignificant for 0.1 kg/s HF releases when the relative humidity was less than 90% or the windspeed was above 2 m/s. Using scaling we may infer from

this that 10 kg/s releases show insignificant buoyancy effects when the relative humidity is less than 90% or the windspeed is above 5 m/s. Conversely, the behaviour of a 10 kg/s release at lower windspeeds than 5 m/s is not covered by the experiments, and the results do not rule out the possibility of lift-off for such a release. Thus the experiments rule out the possibility of lift-off in many situations, and a model should reproduce this. It should be mentioned that the ten model calculations made by Chhibber and Kaiser (1996) for a 10 kg/s HF release under various meteorological conditions are in agreement with the experimental findings.

More emphasis has been put on modelling the behaviour up to the point where lift off may occur than on the lift-off itself. We know little about the behaviour of an HF plume after lift-off. It is a question whether the plume takes off as a well organized entity, the way an integral model treats it, or it becomes fluffy and disintegrates so that large fractions of it are left on the ground. There are numerous studies of buoyant releases from elevated sources (stacks), but we have no knowledge of field experiments with positively buoyant ground releases. HF plumes are unique because they are heavy near the source. Therefore elevated releases can be expected to fall to the ground and spread out before becoming positively buoyant and possibly begin to rise again. This was simulated in the wind tunnel study of Hall and Walker (2000) who studied plume rise from buoyant area sources. Here the lift-off of buoyant plumes tended to be disorganized. The concentrations on the ground are in some cases greatly reduced immediately downwind of the lift-off point, but seldom to zero. Smoke plumes from a fire do not always leave the ground, even if they are hotter than an HF can ever get. Therefore it is most likely that an HF plumes lifting off the ground do not simply rocked to the sky, even under conditions that favour plume rise the most.

Lift-off can be expected to be influenced by atmospheric stability. In stable conditions plume rise is limited by the density stratification which may prevent the plume from rising beyond a certain height. In convective conditions plume rise is a self-propelling process due to the unstable density profile. This means that even passive plumes exhibit plume rise, as was observed in the wind tunnel experiments of Willis and Deardorff (1976). We interpret reduced cross-plume integrated concentrations observed in dispersion experiments in the convective surface layer in the same way. Under these conditions plumes are very irregular and dominated by horizontal as well as vertical wind fluctuations and temperature differences. A passive plume on the ground may therefore become positively buoyant because of heating from the ground and form a rising thermal and this may resemble the change to slightly positive buoyancy in an HF cloud.

At large distances, where the plume has been well mixed with the boundary layer, buoyancy has no effect. Here the concentration can be estimated from the boundary layer height, a suitable plume width and the windspeed. HF can harm certain plants at low concentration levels so the final stage of the dispersion could be relevant for major spills. Closer to the source plume rise could have a mitigating effect in terms of reduced concentrations on the ground, and a main point is to determine more precisely which conditions are required. This calls for a model capable of defining the limiting case.

2 HF thermodynamics

2.1 Properties of HF

HF gas is one of the least ideal gases known. Saturated HF vapour is for example about four times denser than expected from the ideal gas law. The specific heat at constant pressure C_P varies dramatically with temperature with a maximum about 10K above the boiling point where values of C_P are some 30 times larger than the classical value $\frac{7}{2}R$ for a stiff diatomic molecule. The normal boiling point of HF, 292.69K, is also much higher than the boiling points of HCl and HBr. The explanation for this behaviour is the strong tendency for the HF molecules to form polymers (sometimes called 'oligomers' or just 'clusters'). The diatomic HF monomer is a very stable molecule, even at very high temperatures, that can be regarded as an invariant building block for the formation of the polymers. Crystaline HF consists of long zig-zag chains of HF molecules connected by hydrogen bonds (i.e. -HF-HF-HF-HF-). The zigs and zags occur at the F atoms so that the segment HF-H bends 120^o.1 while the segment F-HF is straight. There is less direct evidence for polymers in the liquid phase and in the gas phase. Only the dimer $(HF)_2$, the tetramer $(HF)_4$ and the hexamer $(HF)_6$ have been positively identified in the gas phase.

The polymerization has two important effects. Firstly, it increases the density. Saturated HF vapour is much denser than air even if the formula weight of HF is only 20 g/mol compared to 29 g/mol for air. Secondly, polymerization influences the enthalpy. It requires an enthalpy of about 25kJ/mol to break a hydrogen bond in a polymer. When the gas is expanded (or mixed with dry air or N_2) the polymers break up and the gas cools substantially. When for example 1 mole of HF is mixed with 10 moles of dry air (both originally at 1 bar and room temperature) the temperature drops about 30K. The effect is somewhat akin to the dilution and subsequent evaporation of an aerosol spray. Here the heat of vaporisation of the liquid aerosols gives a negative contribution to the enthalpy budget. The heat of polymerization (the excess enthapy in proper terms) of HF gas acts in a similar way. In fact the excess enthalpy of saturated HF vapour is almost as large as the heat of vaporization. So in a way the gas can be regarded as only halfway evaporated.

Things are more complicated when water is present. Liquid HF is highly hygroscopic and HF is soluble in water in any proportion. Liquid mixtures of HF and water is called hydrofluoric acid. In terms of pH it is not a very strong acid, but it is still very aggressive chemical that attacks almost anything (including glass). The heat of mixing is very large, so that the partial enthaltpies of HF and water in hydrofloric acid is much lower than for the pure liquids. At the same time the vapour pressure is very low and the boiling point of 50% hydrofluoric acid is higher than that of water. Therefore mixtures of HF gas and humid air produce a fog of hydrofluoric acid droplets which is remarkably stable. A reaction can also take place in the gas phase resulting in the formation of a $HF \cdot H_2O$ complex, which has been observed spectroscopically. However, the gaseous reaction is relatively unimportant because of the small value of the reaction constant. Because of the low enthalpy of hydrofluoric acid the fog formation tends to raise the temperature of the mixture. Fog formation therefore has the direct opposite effect of de-polymerization. There is no rule telling which of these effects is the strongest. Depending on concentration and humidity the temperature may rise or it may drop.

An atmospheric release of HF goes through a rather complicated sequence. Near the release point the HF concentration is high with possible HF aerosol (in case of

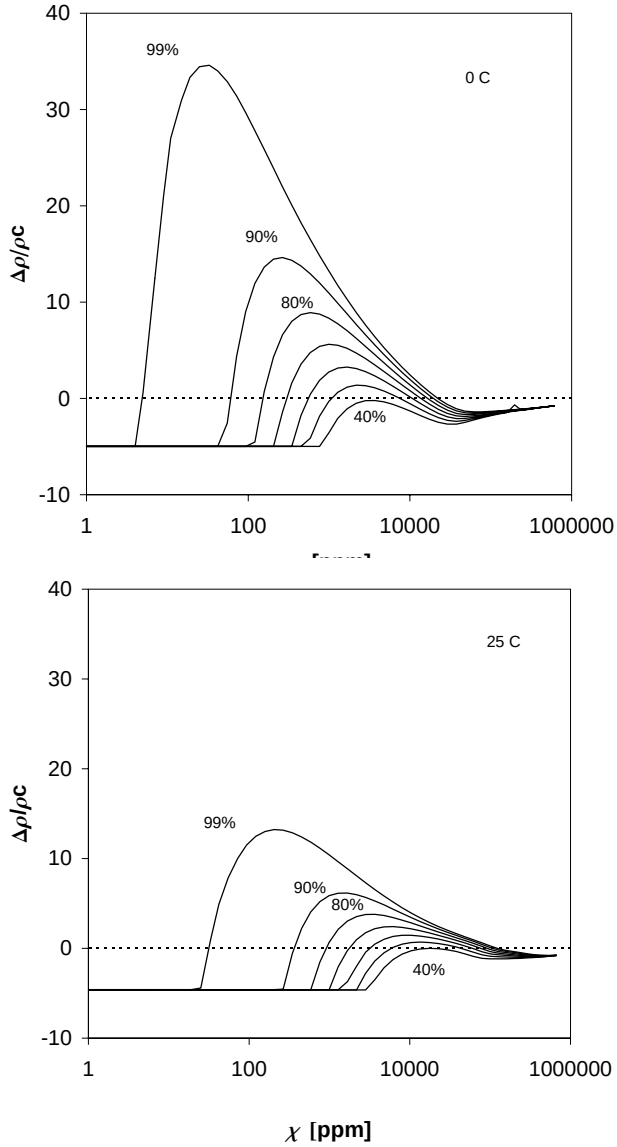

Figure 1. Buoyancy factors for adiabatic mixtures of HF and humid air. Ambient temperatures 0°C *(upper) and* 25°C *(lower). In all cases the HF initially liquid and* 15°C

a spray release). As air is entrained de-polymerization and evaporation of droplets cools the cloud so that it becomes denser than air and falls to the ground. As more humid air is mixed into the cloud the water vapour will join HF vapour to form hydrofluoric acid fog and HF droplets will absorb moisture. As a result the boiling point of the droplets is raised to about 110°C and the water vapour pressure becomes extremely low. Therefore there is very little water vapour present in the cloud at this point, the cloud is hot and lighter than air. The condensation of water ceases at some point and the concentration of water vapour in the gas phase starts to increase. Along with this the concentration of HF in the droplets starts to decrease and the droplets gradually evaporate. The evaporation of the aerosol lowers the temperature of the cloud so that it becomes slightly denser than air just before the aerosol disappears.

The non-constant buoyancy of mixtures of HF with humid air is illustrated in figure 1, which is based on the model developed below. The ordinate is the

'buoyancy factor' $(\rho_a - \rho)/(\rho c)$, where ρ_a is the density of the air, ρ is the density of the mixture and c is the HF concentration (mass by mass), i.e. the ratio between (buoyancy force) and (HF mass times g). The buoyancy factor is constant for buoyancy conserving substances, and for example equal to $(M_a - M)/M$ for an ideal gas (Ms are molecular weights).

2.2 Theory

In this section we briefly review some basic thermodynamic relations for non-ideal mixtures. Most of what follows can be found in textbooks (Guggenheim 1957, Moore 1972). The main point is to distinguish fundamental thermodynamics relations from empirical relations and to make clear which measurements are required to characterize the thermodynamics of HF and HF mixtures.

The starting point is the well-known fundamental differentials:

$$\mathrm{d}\,H(P,T,\mathbf{n}) = T\,\mathrm{d}S(P,T,\mathbf{n}) + V(P,T,\mathbf{n})\,\mathrm{d}P + \sum_j G_j(P,T,\mathbf{n})\mathrm{d}n_j \quad (1)$$

$$\mathrm{d}\,G(P,T,\mathbf{n}) = -S(P,T,\mathbf{n})\,\mathrm{d}T + V(P,T,\mathbf{n})\,\mathrm{d}P + \sum_j G_j(P,T,\mathbf{n})\,\mathrm{d}n_j \quad (2)$$

In the following we will often use the following relation to instead of (2)

$$\mathrm{d}\,\frac{G(P,T,\mathbf{n})}{T} = -\frac{H(P,T,\mathbf{n})}{T^2}\,\mathrm{d}T + \frac{V(P,T,\mathbf{n})}{T}\,\mathrm{d}P + \sum_j \frac{G_j(P,T,\mathbf{n})}{T}\,\mathrm{d}n_j \quad (3)$$

$\mathbf{n} = (n_1, n_2, \ldots, n_N)$ defines the molar composition in terms of 'basic components'. These are the molecules that survive in the gas phase as $P \to 0$. For the HF-water-air system the basic components are: HF monomers, H_2O and dry air (which we will regard as an inert gas). For HF-air-water gas the basic molecules are themselves stable, even if at higher pressures complexes such as HF polymers $(HF)_q$, the complex $HF \cdot H_2O$ and possibly others are formed. It is convenient not to treat complexes (including polymers) as distinct species, but to let $\mathbf{n}$ count the basic components before the formation of complexes. In this way $\mathbf{n}$ is independent of pressure and temperature. We also define the molar fractions

$$x_j = \frac{n_j}{n_1 + n_2 + \cdots + n_N} \quad (4)$$

Again x_j counts the relative amount of species j including molecules bound in complexes.

G_j is the chemical potential for species j, which is equal to the partial free energy, viz.

$$G_j(P,T,\mathbf{n}) = \frac{\partial G(P,T,\mathbf{n})}{\partial n_j} \quad (5)$$

Other partial quantities are defined in a similar way, e.g. partial volume $V_j = \frac{\partial V}{\partial n_j}$, partial enthalpy etc. We recall that generally $X = \sum n_j X_j$, in particular we have the Gibbs-Duhem relation

$$G = \sum n_j G_j \quad (6)$$

In equilibrium the requirement is that G_j has the same value for all phases.

An ideal gas obeys the ideal gas law (shown here for n moles of the gas)

$$V^I(P,T) = \frac{nRT}{P} \quad (7)$$

A non-ideal gas can be represented by the similar equation

$$Z(P,T,\mathbf{n})V(P,T,\mathbf{n}) = \frac{RT}{P}\sum_j n_j \quad (8)$$

where Z is the *association factor*, which is also sometimes called the 'compressibility factor'). From (7) and (2) it follows that

$$G^I(P,T) - G^I(P',T) = \int_{P'}^{P} \frac{\partial G^I}{\partial P}\,\mathrm{d}P = \int_{P'}^{P} V^I\,\mathrm{d}P = nRT\,\log\frac{P}{P'} \tag{9}$$

We recall that the enthalpy of an ideal gas is independent of pressure because

$$\frac{\partial H^I}{\partial P} = -T^2\,\frac{\partial^2 G^I/T}{\partial P \partial T} = -T^2 \frac{\partial R/P}{\partial T} = 0 \tag{10}$$

H^I does not incorporate contributions from inter-molecular interactions, they are absent in ideal gases, but it does incorporate contributions from translation, rotation and vibrations of individual molecules. These can be measured by spectroscopy.

The free energy of a mixture of gases is not simply additive since an extra term, due to mixing entropy, must be added. Thus for an ideal mixture of ideal gases we have

$$G(P,T,\mathbf{n}) = \sum_j n_j G_j^I(P,T,\mathbf{n}) + RT\sum_j n_j \log x_j = \sum_j n_j G_j^I(x_j P,T) \tag{11}$$

In other words, the partial free energy is equal to the free energies of the component evaluated at the *partial pressure* $x_j P$ as if the other components were missing. For non-ideal gases containing complexes made up of several different component, it is not clear how a 'partial pressure' of a component should be defined. However, at low pressure the gas will approach an ideal mixture of the basic components. It is therefore possible to measure the ideal free energy $G_j^I(P,T)$ at low pressures and extrapolate to finite pressures by means of (9). Ideal gas properties can be determined directly from measurements of P, V and T or it can be calculated using statistical mechanics and spectroscopic data. For fixed T, $G_j^I(P,T)$ varies as the logarithm of P so there must be a 'pressure' f_j for which

$$G_j(P,T,\mathbf{n}) = G_j^I(f_j(P,T,\mathbf{n}),T) \tag{12}$$

f_j is called the *fugacity* of species j. At low pressure the fugacity equals the partial pressure, i.e. $\frac{f_j}{x_j P} \to 1$ for $P \to 0$.

It is instructive to define also the partial excess free energy. It is equal to the difference between the partial free energy of the real gas and the free energy of the corresponding ideal gas evaluated at the 'ideal' partial pressure $x_j P$, viz.

$$\begin{aligned} G_j^E(P,T,\mathbf{n}) &\equiv G_j(P,T,\mathbf{n}) - G_j^I(x_j P,T) \\ &= G_j^I(f_j,T) - G_j^I(x_j P,T) = RT\log\frac{f_j}{x_j P} \end{aligned} \tag{13}$$

Since $G_j^E \to 0$ for $P \to 0$ we have

$$\begin{aligned} RT\log\frac{f_j}{x_j P} &= G_j^E(P,T,\mathbf{n}) = \int_0^P \frac{\partial G_j^E}{\partial P}\,\mathrm{d}P = \int_0^P \left(V_j(P,T,\mathbf{n}) - \frac{RT}{P}\right)\,\mathrm{d}P \\ &= \frac{\partial}{\partial n_j}\int_0^P \left(V(P,T,\mathbf{n}) - \frac{RT}{P}\sum_j n_j\right)\,\mathrm{d}P \end{aligned} \tag{14}$$

This expresses the fugacity in terms of the *excess volume* $V(P,T,\mathbf{n}) - \frac{nRT}{P}$, a quantity that can be measured directly. We can also define the partial excess enthalpy

$$H_j^E(P,T,\mathbf{n}) \equiv H_j(P,T,\mathbf{n}) - H_j^I(T) = -T^2 \frac{\partial G_j^E(P,T,\mathbf{n})/T}{\partial T} \tag{15}$$

where $H_j^I(T) = \lim_{P\to 0} H_j(P,T,\mathbf{n})$ is the partial enthalpy of the corresponding ideal gas.

Using fugacities we may now write (3) as

$$\begin{aligned}
\mathrm{d}\,\frac{G(P,T,\mathbf{n})}{T} &= \mathrm{d}\sum_j n_j \frac{G_j^I(f_j,T)}{T} \\
&= \sum_j n_j \left(\frac{R}{f_j}\frac{\partial f_j(P,T,\mathbf{n})}{\partial T} - \frac{H_j^I(T)}{T^2} \right) \mathrm{d}T \\
&+ \sum_j n_j \frac{R}{f_j}\frac{\partial f_j(P,T,\mathbf{n})}{\partial P}\,\mathrm{d}P \\
&+ \sum_j \left(\frac{G_j}{T} + \sum_i n_i \frac{R}{f_i}\frac{\partial f_i(T,P,\mathbf{n}))}{\partial n_j} \right) \mathrm{d}n_j
\end{aligned} \tag{16}$$

Comparing the terms involving $\mathrm{d}n_j$ in (3) and (16) we find that

$$\sum_i n_i \frac{1}{f_i}\frac{\partial f_i}{\partial n_j} = 0 \tag{17}$$

Equation (17) leads to an exact form of the Duhem-Margules rule.

Until this point we have used P, T and $\mathbf{n}$ as independent variables. It is natural to try T and the fugacities $\mathbf{f} = (f_1,\ldots,f_N)$. With these variables the pressure differential is

$$\mathrm{d}P = -\frac{H^E}{VT}\,\mathrm{d}T + \sum_j n_j \frac{RT}{f_j V}\,\mathrm{d}f_j \tag{18}$$

so that

$$\sum_j f_j \frac{\partial P(T,\mathbf{f})}{\partial f_j} = \frac{RT}{V}\sum_j n_j = Z(T,\mathbf{f})P \tag{19}$$

This is the equation of state for the gas from which all other thermodynamic quantities can be derived. The key point is therefore to determine the function $P(T,\mathbf{f})$.

The following discussion is limited to the case $N = 2$. This is done in order not to overcrowd equations with subscripts, but the generalization to arbitrary N is straight forward. We can always write $P(T,f_1,f_2)$ as a Taylor series with T-dependent coefficients

$$P(T,f_1,f_2) = \sum_{q=0}^{\infty}\sum_{r=0}^{\infty} \tilde{K}_{q,r}(T)\, f_1^q\, f_2^r \tag{20}$$

For small pressures we have $P = f_1 + f_2$, hence $\tilde{K}_{0,0} = 0$, and $\tilde{K}_{1,0} = \tilde{K}_{0,1} = 1$, otherwise there are no restrictions. The coefficients $\tilde{K}_{qr}$ can be interpreted in terms of a simple model gas. The model gas is an ideal mixture of complexes, where each complex is an ideal gas. The partial pressure P_{qr} of the $(q:r)$ complex (consisting of q molecules of species 1 and r molecules of species 2) is given by

$$P_{qr} = \tilde{K}_{qr}(T)\, p_1^q\, p_2^r \tag{21}$$

where $p_1 = P_{1,0}$ and $p_2 = P_{0,1}$ are the partial pressures of the monomers. In the model the coefficient $\tilde{K}_{q,r}(T)$ on the right hand side of (20) therefore acts as an equilibrium constant for the formation of the $(q:r)$ complex. In order to complete the picture it should be verified that p_1 and p_2 are in fact the fugacities of the two species. From the ideal gas law it follows that

$$RTn_1 = V\sum_{q\,r} qP_{qr} = Vp_1\frac{\partial P(T,p_1,p_2)}{\partial p_1} \tag{22}$$

and

$$RTn_2 = V\sum_{q\,r} rP_{qr} = Vp_2\frac{\partial P(T,p_1,p_2)}{\partial f_2} \tag{23}$$

Hence for fixed T

$$\mathrm{d}P = \frac{n_1RT}{Vp_1}\,\mathrm{d}p_1 + \frac{n_2RT}{Vp_2}\,\mathrm{d}p_2 \tag{24}$$

so that the excess free energy of the model is equal to

$$\int_0^P \left(V - (n_1+n_2)\frac{RT}{P}\right)\,\mathrm{d}P = n_1RT\log\frac{p_1}{x_1P} + n_2RT\log\frac{p_2}{x_2P} \tag{25}$$

It finally follows from (14) that $p_1 = f_1$ and $p_2 = f_2$. This mean that the model can actually reproduce the thermodynamics of the real gas. It is, however, still a model because the interactions are regarded as purely 'chemical' in the sense that molecules are either free or locked into complexes. In real gases molecules can attract or repel each other without forming complexes, and such interactions are not part of the model. The model may therefore be right for the wrong reasons. It would obviously be embarrassing if any of the coefficients were negative, and this can happen. At low pressure the molar excess volume approaches the constant value $V^{E0} = -RT(\tilde{K}_{2,0}x_1^2 + \tilde{K}_{1,1}x_1x_2 + \tilde{K}_{0,2}x_2^2)$. For a pure substance ($x_1 = 1$ and $x_2 = 0$) this reduces to $V^{E0} = -RT\tilde{K}_{2,0}$. The excess volume is therefore negative at low pressure if $\tilde{K}_{2,0}$ is positive. V^{E0} can be estimated from van der Waal constants, e.g. Weast (1986), and for most gases it is indeed negative, He and H_2 are among the few exceptions. There is of course no such thing as a Helium polymer and the weak non-ideality of He must be explained in other ways. Conversely, if the coefficients are all positive it is not possible to falsify the simple model by measuring macroscopic thermodynamic properties of the gas. For HF there is evidence only for a few polymer species so that, according to the simple model, $P(f)$ is a simple polynomial. However, even if only a few polymers are present, $P(f)$ could be a more complicated function because of non-ideal behaviour.

If we want to improve the simple chemical model we must work in a more general setting where the chemical composition is specified in terms of the actual molecules present. In other words, each $(q:r)$ complex is treated as a component with a corresponding mole number ν_{qr}, where of course

$$n_1 = \sum_{qr} q\,\nu_{qr} \qquad \text{and} \qquad n_2 = \sum_{qr} r\,\nu_{qr} \tag{26}$$

In this setting we imagine that ν_{qr} can be controlled independently together with P and T. This may not actually be technically possible because it will bring the gas out of equilibrium, but the free energy and other thermodynamic functions can still be defined theoretically. Thus we may form a partial free energy G_{qr} for each complex and a fugacity f_{qr} so that

$$G_{qr}(P,T,\nu) = \frac{\partial G}{\partial \nu_{qr}} = G^I_{qr}(f_{qr},T) \tag{27}$$

The equilibrium condition is that

$$G^I_{qr}(f_{qr},T) = qG^I_1(f_{1,0},T) + rG^I_2(f_{0,1},T) \tag{28}$$

In equilibrium we therefore have

$$\begin{aligned} G^E(P,T,n_1,n_2) &= \sum_{qr} \nu_{qr}\, G_{qr}(P,T,\nu) - n_1 G_1^I(x_1 P,T) - n_2 G_2^I(x_2 P,T) \\ &= n_1 RT \log \frac{f_{1,0}}{x_1 P} + n_2 RT \log \frac{f_{0,1}}{x_2 P} \end{aligned} \tag{29}$$

Using (13) it follows that in equilibrium $f_{1,0} = f_1$ and $f_{0,1} = f_2$. In other words, the fugacities of the momomers are the same whether or not we count polymers as separate species.
From (9) and (28) we get

$$f_{pq} = K_{qr}(T)\, f_1^q\, f_2^r \tag{30}$$

where

$$K_{qr}(T) = \exp\left(\frac{qG_1^I(P',T) + rG_2^I(P',T) - G_{qr}^I(P',T)}{RT} \right) P'^{1-q-r} \tag{31}$$

K_{qr} is the equilibrium constant for the formation of the $(q : r)$ complex used normally by chemists and it is of course always positive and will in general differ from $\tilde{K}_{qr}$. In order to relate the equilibrium constants K_{qr} to the coefficients $\tilde{K}_{qr}$ we must use a theory of some kind to express P as a function of the fugacities f_{qr}. In equilibrium we then use (30) to find $P(T, f_1, f_2)$ and finally make a Taylor expansion to determine $\tilde{K}_{qr}$. This we may of course lead to negative $\tilde{K}_{qr}$. The simplest possible way to link P to the fugacities is to assume that the complexes are ideal gases, but that is merely a re-statement of the simple chemical model. In order to make improvements it is therefore necessary to take the non-ideal behaviour of the complexes into account. This requires a microscopic description of the interactions between complexes.

We now turn to the gas-liquid equilibrium. In order to distinguish properties of the two phases we use superscript ^{l} for liquid and ^{g} for gas. When there is only one component in the system, say HF, the condition for equilibrium is that (the superscript ^{o} indicates a pure substance)

$$G^{lo}(P_s^o(T),T) = G^{go}(P_s^o(T),T) \tag{32}$$

where both Gs are molar free energies (chemical potentials) and $P_s^o(T)$ is the saturation pressure. We can also use the saturation fugacity $f_s^o(T)$, i.e.

$$G^{lo}(P_s^o(T),T) = G^{Igo}(f_s^o(T),T) \tag{33}$$

Evaluating $\frac{\mathrm{d}G/T}{\mathrm{d}T}$ for both sides of (32) it follows that

$$-\frac{H^{lo}}{T^2} + \frac{V^{lo}}{T}\frac{\mathrm{d}P_s^o}{\mathrm{d}T} = -\frac{H^{go}}{T^2} + \frac{V^{go}}{T}\frac{\mathrm{d}P_s^o}{\mathrm{d}T} \tag{34}$$

which is of course just the usual Clausius-Clapeyron equation. From (33) it follows in the same way that

$$-\frac{H^{lo}}{T^2} + \frac{V^{lo}}{T}\frac{\mathrm{d}P_s^o}{\mathrm{d}T} = -\frac{H^{Igo}}{T^2} + \frac{R}{f_s^o}\frac{\mathrm{d}f_s^o}{\mathrm{d}T} \tag{35}$$

Combining (33) and (35) we get

$$\log \frac{f_s^o(T)}{f_s^o(T')} = \int_{T'}^{T} \left(\frac{H^{Igo} - H^{lo}}{RT^2} + V^l \frac{\mathrm{d}P_s^o}{\mathrm{d}T} \right) \mathrm{d}T \tag{36}$$

This relation can be used to determine the saturation fugacity $f_s^o(T)$ from experimental data. The quantities on the right hand side are all directly measurable (and it is generally safe to ignore $V^{lo}\mathrm{d}P_s^o/\mathrm{d}T$), so only a single value $f_s^o(T')$ needs to be known.

For two-phase mixtures we reserve $\mathbf{n} = (n_1, \ldots, n_N)$ and $\mathbf{x} = (x_1, \ldots, x_N)$ to specify the molar composition in the liquid phase and use $\mathbf{m} = (m_1, \ldots, m_N)$ and $\mathbf{y} = (y_1, \ldots, y_N)$ to denote the molar composition and molar fractions in the gas phase. For constant P and T, $\mathbf{y}$ is a complicated function of $\mathbf{x}$.

The equilibrium condition is that

$$G_j^l(P_s, T, \mathbf{n}) = G_j^g(P_s, T, \mathbf{m}) = G_j^{Ig}(f_j, T) \tag{37}$$

For an ideal liquid mixture the free energy is defined as

$$G^{Il}(P_s, T, \mathbf{n}) = \sum_j n_j \left(G_j^{\mathrm{o}}(P_{sj}^{\mathrm{o}}(T), T) + RT \log x_j \right) \tag{38}$$

where G_j^{o} is the (real) free energy of the mixture and P_{sj}^{o} is the vapour pressure of the pure jth component. The last term in (38) accounts for the mixing entropy. We define the free energy of mixing as the difference between the real and the ideal free energy, viz.

$$G_{\mathrm{mix}} = G^l - G^{Il} \tag{39}$$

This is a useful quantity. From (9), (37) and (38) it follows that

$$\begin{aligned} G_{\mathrm{mix}}(P_s, T, \mathbf{n}) &= \sum_j n_j (G_j^{Ig}(f_{sj}) - G_j^{Ig}(f_{sj}^{\mathrm{o}}) - RT \log x_j) \\ &= RT \sum_i n_i \log \frac{f_{si}}{x_i f_{si}^{\mathrm{o}}} \end{aligned} \tag{40}$$

For an ideal mixture, where the left hand side vanishes, we obtain $f_{sj} = x_j f_{sj}^{\mathrm{o}}$, which is recognized as Raoult's law if fugacities are replaced by the corresponding partial pressures. Note that due to (17) we have

$$\log \frac{f_{sj}}{x_j f_{sj}^{\mathrm{o}}} = \frac{\partial}{\partial n_j} \sum_i n_i \log \frac{f_{si}}{x_i f_{si}^{\mathrm{o}}} = \frac{\partial G_{\mathrm{mix}}(P_s, T, \mathbf{n})}{RT \partial n_j} \tag{41}$$

Now we can use (3) to get

$$\frac{\mathrm{d}G_{\mathrm{mix}}(P_s(T), T, \mathbf{x})/T}{\mathrm{d}T} = -\frac{H^l - H^{lo}}{T^2} + \frac{V^l - V^{lo}}{T^2} \frac{\mathrm{d}P_s}{\mathrm{d}T} \tag{42}$$

The last term is negligibly small because the liquid volume is small. The leading term involves the mixing enthalpy $H_{\mathrm{mix}} \equiv H^l - H^{lo}$. This quantity is directly measurable, since -H_{mix} is the amount of heat generated by mixing the liquid from pure liquid components at constant temperature. This can be done with good accuracy using bomb calorimetry.

In this section we have derived useful relations from fundamental thermodynamics. No additional assumptions have been made, hence the relations need no further validation. The investigation shows that a gas consisting of a mixture of interacting components is characterized by the function $P(T, \mathbf{k})$ and that liquid-gas equilibrium is governed by an exact form of Duhem-Margules rule involving fugacities.

2.3 Data sources

The amount of experimental thermodynamic data for HF is not impressive and most sources are rather old.

Association factors (densities) have been measured by Thorpe and Hambly (1889), Simons and Hildebrand (1924), Fredenhagen and Wellmann (1932) Fredenhagen (1933), Fredenhagen (1934), Long, Hildebrand and Morell (1943) and

Strohmeier and Briegleb (1953). Strohmeier and Briegleb (1953) measured the association constant for constant T down to small pressures. A static method was used: the gas was trapped in a container end weighed. This data set is of particularly high quality although the pressure range leaves a gap up to the saturation pressure.

Franck and Meyer (1959) used a dynamic method to measure $C_P(T)$at constant P. The results show an interesting large peak of $C_P(T)$ occurring about 10 K above the boiling point.

Satutated vapour pressure measurements are available from Gore (1869) (the data are reproduced in *Gmelins Handbuch der anorganischen Chemie* (1959)), Simons and Hildebrand (1924), Fredenhagen (1933), Franck and Spalthoff (1957) and Jarry and Davies (1953).

Hu, White and Johnston (1953) measured C_p along the saturation curve from 14.8K up to the normal boiling point. The heat of fusion and the heat of vaporisation at the normal boiling point were also determined.

Smith (1958), using spectroscopy, found stong evidence for the presence of the tetramer and the hexamer in IR gas absorption spectra. No other polymers could be identified outside the region of monomer absorption, but weak dimer peaks were identified in the monomer absorption band. The amount of dimer was judged to be rather low and varying weakly with temperature.

Potter (1957) reported enthalpies and C_P for HF in the ideal gas state. The calculations were based on spectroscopic measurements. Fredenhagen (1934) measured the heat of vaporisation from the liquid to ideal gas state by boiling liquid HF in vacuum.

Vanderzee and Rodenburg (1970) reviewed data available up to 1969 and discussed problems connected with estimates of excess properties, in particular the excess enthalpy. It was found that differences between the measurements of Strohmeier and Briegleb (1953) and Franck and Meyer (1959) could be reconciled if careful smoothing of data was performed and if the temperature measurements of Franck and Meyer (1959) were adjusted upward by 0.5 to 2.0 K (the experimental error of T was reported to be ± 1 K). A set of analysed values of excess properties was then compiled based on the two datasets supplemented by the data of Hu et al. (1953) on the saturation curve and the data of Potter (1957) for the ideal gas. These analysed data have since been widely recognized as the best available source of information. They cover a relatively narrow range of temperatures and therefore we have recompiled the data in order to obtain a wider range of values along the saturation curve.

Since then it appears that there has been only two experimental investigation of pure HF. Schotte (1987) measured adiabatic temperature changes of HF gas mixed with dry air in a fog chamber. Since dry air can be regarded as an inert species the mixing corresponds to an adiabatic expansion which creates a large temperature drop due to de-polymerization. The results are difficult to relate directly to basic thermodynamical properties, but they can serve as model test cases. The fog chamber technique, like other dynamic techniques, is difficult because adiabatic conditions are difficult to control, and the accuracy of these experiments is unknown. Gall (author of the article in Kirk-Othmer 1980) point out that measurements by dynamic and static methods may give different results if there is a significant time constant associated with the mobile equilibrium between the hydrogen fluoride polymers. Lately the observations were confirmed in similar experiments performed by Kemp and Newland (2000). These experiments are part of the URAHFREP project.

The composition of the vapour phase over aqueous solutions of HF have been measured by e. g. Brosheer, Lenfesty and Elmore (1947), Munter, Aepli and Kossatz (1947) and Munter, Aepli and Kossatz (1949). From these and other datasets

Vieweg (1963) compiled a table of recommended 'partial pressures' of HF and H_2O as a function of the temperature and composition of the liquid. Direct measurements of partial pressures are not possible, whereas the total pressure and the chemical composition of the vapour can be obtained more easily. Some authors report the data as partial pressures meaning $y_{\rm HF}P$, where $y_{\rm HF}$ is the molar fraction of HF *monomer* and P is the total pressure. Vieweg (1963) calculate partial pressures on the basis of the (apparent) molar weight of HF, $ZM_{\rm HF}$, in order to include the effect of polymerisation. The values of Z used for this are not provided so it only possible to work back to the chemical composition when $Z \approx 1$, which is, however, a very good approximation except for the highest HF concentrations.

The only more resent work is that of Miki, Maeno and Maruhashi (1990) who measured vapour and liquid compositions at the normal boiling point. Mike *et al.* found deviations from Munter's H_2O vapour pressures for HF solution containing more than 50% HF (by weight). In this region the vapour consists of less than 10% H_2O, so the discrepancy might not be so important. Activity coefficients were also given (The activity coefficient of HF is $\gamma_{\rm HF} \equiv \frac{y_{\rm HF}P}{x_{\rm HF}p^o_{\rm HF}}$ where $x_{\rm HF}$ is the molar fraction of HF in the liquid and $p^o_{\rm HF}$ is the vapour pressure of pure HF liquid). The results for $\gamma_{\rm HF}$ were in agreement with previous work while discrepancies were found for $\gamma_{\rm H_2O}$ for HF concentrations (in the liquid phase) higher than 40%.

The enthalpy of hydrofluoric acid at 25° C was studied by Johnson, Smith and Hubbard (1973), who mixed liquid HF with water in a bomb calorimeter. The measurements cover HF concentrations up to 50% (mol/mol). Kirk-Othmer (1980) and *Gmelins Handbuch der anorganischen Chemie* (1959) cite results for higher concentrations.

Schotte (1987) also measured temperature changes of HF gas mixed with humid air. These experiments demonstrate the formation of hydrofluoric acid fog under adiabatic mixing. A temperature rise was observed when HF was mixed with humid air, whereas the temperature dropped when HF was mixed with dry air. This was confirmed in experiments by Kemp and Newland (2000). A detailed quantitative agreement was not found, which is most likely due to inherent experimental difficulties of the method. The investigations were extended to mixtures of HF gas, butane and dry/humid air and it was found that the liquid butane merely acts as an inert species.

2.4 Properties of pure HF

Below we list correlations for some thermodynamic quantities derived from these sources. Parts of the analysis is similar to the analysis of Vanderzee and Rodenburg (1970) who used graphical analysis on the same datasets.

In the temperature range of interest here the specific heat on the ideal state (Potter 1957) fits the correlation

$$C_p^I(T) = 29.144\,\mathrm{J/molK} + 1.2310^{-}4(T - 298.16\mathrm{K})\mathrm{J/molK}^2 \qquad (43)$$

This is only a small correction to the classical value $C_p^I = \frac{7}{2}R$. The table only contains data for $T > 298.16$ K, but it is probably safe to extrapolate down to 200 K.

Both the excess enthalpy $H^{Es}(T)$ and the excess free energy $G^{Es}(T)$ of saturated HF vapour can be obtained by combining data from different experiments. In order to do this we choose a data point at the relatively high temperature $T_1 = 317.15$K and the relatively low pressure $P_1 = 15465$ Pa (116 Torr), where the gas is close to the ideal state. The chosen point is an intersection between Strohmeier and Briegleb's (1953) constant T and Franck and Meyer's (1959) constant P measurements. We adopt the values $G^E(T_1, P1) = -25$ J/mol and

$H^E(T_1, P1) = -293\,\mathrm{J/mol}$ from Vanderzee and Rodenburg (1970). Both values are small so we could have chosen to estimate them from a model. Franck and Meyer's (1959) C_p data together with (43) yields the excess specific heat yield $C_p^E \equiv C_p - C_p^I$, and numerical integration can be used to obtain

$$\begin{aligned} H^E(T_2, P1) &= H^E(T_1, P_1) + \int_{T_1}^{T_2} C_p^E(t, P_1)\,\mathrm{d}T \\ \frac{G^E(T_2, P1)}{T_2} &= \frac{G^E(T_1, P1)}{T_1} + \frac{H^E(T_2, P1)}{T_2} \\ &- \frac{H^E(T_1, P1)}{T_1} \int_{T_1}^{T_2} \frac{C_p^E(t, P_1)}{T}\,\mathrm{d}T \end{aligned} \tag{44}$$

Taking $T_2 = 247\,\mathrm{K}$, the boiling point at P_1, we end up with two data points on the saturation curve: $G^{Es}(T_2) = G^E(T_2, P1) = -499.9\,\mathrm{J/mol}$ and $H^{Esg}(T_2) = H^E(T_2, P1) = -6011\,\mathrm{J/mol}$.

Various measurements of saturation pressure are available (Gore 1869, Simons 1924, Jarry and Davies 1953). The data are well represented by the following correlation (Clough, Grist and Wheatley 1987a)

$$P_s(T) = P_b\, \exp\left[A\left(1/T - 1/T_b\right) + C\log T/T_b + D(T - T_b) + E(T^2 - T_b^2)\right] \tag{45}$$

where $P_b = 1\,\mathrm{Bar}$, $T_b = 292.69\mathrm{K}$ is the normal boiling point and

$$\begin{aligned} A &= 5959.1\,\mathrm{K} \\ C &= -24.14 \\ D &= 6.560710^{-2}\,\mathrm{K}^{-1} \\ E &= -2.293410^{-5}\,\mathrm{K}^{-2} \end{aligned} \tag{46}$$

The heat of vaporization $-\Delta H_s = H_{sg} - H_{sl}$ is related to the saturated vapour pressure via

$$\Delta H_s = (V_{gs} - V_{ls})\,T\,\frac{\mathrm{d}P_s}{\mathrm{d}T} \tag{47}$$

The specific volume of the vapour, V_{gs}, can be inferred from the association factor Z_s. Based on the experimental data of Fredenhagen (1933) and Franck and Spalthoff (1957), Jarry and Davies (1953) and the analysed data of Vanderzee and Rodenburg (1970) we propose the following correlation for Z_s, which extends the temperature range of the correlation given by Vanderzee and Rodenburg.

$$Z_s(T) = 1 + \frac{A}{\left[\left(\frac{T}{T_m}\right)^2 + B\right]^{\frac{1}{3}}} \tag{48}$$

where

$$\begin{aligned} A &= 1.1309 \\ B &= 0.0469 \end{aligned}$$

$$T_m = 234.94\,\mathrm{K} \tag{49}$$

The specific volumes of the liquid, V_{ls}, is given by (Simons and Bouknight 1932, Vanderzee and Rodenburg 1970)

$$\rho_{ls} = 1002.0\,\mathrm{kg/m^3} - 2.2625\,\mathrm{kg/m^3K}\,(T - 273.15\,\mathrm{K}) + 3.15\,10^{-3}\,\mathrm{kg/m^3K^2}(T - 273.15\,\mathrm{K}) \tag{50}$$

The specific heat of the liquid measured by Hu et al. (1953) can be correlated very closely by

$$\begin{aligned} C_{psl} = \quad & 51.935\,\mathrm{J/molK} + 14.795\,10^{-2}\,\mathrm{J/molK^2}\,(T - 298.15\,\mathrm{K}) \\ + \quad & 5.8898\,10^{-4}\,\mathrm{J/molK^3}\,(T - 298.15\,\mathrm{K})^2 \end{aligned} \tag{51}$$

It seems that the measurements were not C_p, but $\frac{\mathrm{d}H_{sl}}{\mathrm{d}T} = C_{pl} + \frac{\partial H_l(T,P_s(T)}{\partial P}\frac{\mathrm{d}P_S}{\mathrm{d}T}$. However, the difference is negligible because H_l is nearly independent of pressure.

From (51) and (43) we may form the liquid excess specific heat $C^E_{psl} = C_{psl} - C^I_p$ and get the liquid excess enthalpy

$$H^E_{sl}(T) = H^E_{sl}(T_2) + \int_{T_2}^{T} + C^E_{psl}\,\mathrm{d}T \tag{52}$$

where the term $\frac{\partial H_l(T,P_s}{\partial P}\frac{\mathrm{d}P_S}{\mathrm{d}T}$ has been neglected because it is (probably) already contained in the measured values. The results are shown as the thin line in figure 7, which also shows the analysed experimental values of Vanderzee and Rodenburg (1970).

For the excess free energy we have

$$\frac{\mathrm{d}G^E s/T}{\mathrm{d}T} = -\frac{H^E_{ls}(T)}{+}\frac{V^E_{sl}}{T}\frac{\mathrm{d}P_s(T)}{\mathrm{d}T} \tag{53}$$

where $V^E_{sl}(T) = V_{sl}(T) - V^I(T)$. Equation (53) can be integrated numerically. The results are in good agreement with the analysed values of Vanderzee and Rodenburg (1970) as can be seen in figure 4 (actually the fugacity $f_s = P_s \exp(G^E s/RT)$ is shown, not $G^E s$).

2.5 HF Models

Various authors have analysed HF vapour data in terms the simple polymer model described above. With only one 'basic component', the HF monomer, we have

$$P = f_1 + \tilde{K}_2(T) f_1^2 + \tilde{K}_3(T) f_1^3 + \ldots \tag{54}$$

where fugacity f_1 is determined from the excess volume

$$RT \log \frac{f_1}{P} = \int_0^P \left(V(P,T,\mathbf{n}) - \frac{RT}{P} \right) \mathrm{d}P \tag{55}$$

Based on the density measurements of Thorpe and Hambly (1889) and their own measurements Simons and Hildebrand (1924) proposed to model gaseous HF as consisting of monomers and hexamers $(HF)_6$.

Fredenhagen and Wellmann (1932) argued for the existence of even larger polymers at high pressure and smaller polymers (dimers) at low pressures. Briegleb (1941) proposed a model consisting a polymer chains of any length and made rough estimates of $\tilde{K}_n$ up to $n = 11$ using Fredenhagen's (1933) data. Hu et al. (1953), using Long et al.'s (1943) data, found $\tilde{K}_{n+1}/\tilde{K}_n$ to be approximately independent of n for $n > 2$ so that

$$P = f_1 + \frac{\tilde{K}_2 f_1^2}{1 - \tilde{K}_3/\tilde{K}_2 f_1} \tag{56}$$

Franck and Meyer (1959) tested three models against their C_P data. The models were: a simplified version of (56)

$$P = \frac{f_1}{1 - \tilde{K}_2 f_1} \tag{57}$$

An analogy to Simons and Hildebrand's (1924) 1-6 model

$$P = f_1 + \tilde{K}_n f_1^n \tag{58}$$

and a combination of the two

$$P = \frac{f_1}{1 - \tilde{K}_2^c f_1} + \tilde{K}_n^r f_1^n \tag{59}$$

Here the n-mer comes in two version: a chain corresponding to the term $\tilde{K}_n^c f_1^n$ and a ring corresponding to $\tilde{K}_n^r f_1$. The best fit was obtained for third model with $n = 6$, which was slightly better than the second model (also with $n = 6$), and distinctively better than the first model. In the third model the main contribution comes from monomers, dimers and hexamers. This model is very similar to the so-called 1-2-6 model used by Clough, Grist and Wheatley (1987b) in the DRIFT code (see also Webber, Jones, Tickle and Wren 1992, Clough et al. 1987a). In this model

$$P = f_1 + \tilde{K}_2 f_1^2 + \tilde{K}_6 f_1^6 \tag{60}$$

Maclean, Rosetti and Rosetti (1962) evaluated this and similar models against the data of Strohmeier and Briegleb (1953). They found that the 1-2-6 model was better than a 1-2-q-6 model for q=3,4 or 5. They also tested models with few parameters and polymers of all sizes, i.e. similar to those tested by Franck and Meyer (1959). These performed slightly better.

$P(f_1, T)$ can be obtained from density data by numerical integration of (55). This should in principle determine the coefficients $\tilde{K}_n(T)$ in (54). Briegleb and Strohmeier (1953) analysed their data in terms of a model with polymers up to $(HF)_9$. According to these calculations the dimer dominates at low pressures (together with the monomer) while $(HF)_6$, $(HF)_7$ and $(HF)_8$ dominate near saturation. It should be realized, however, that an unequivocal determination of the nine parameters $\tilde{K}_n(T)$ requires that the experimental curve $P(f_1, T)$ is extremely accurate. Polynomials of high order are deceptive in the sense that two very different sets of coefficients may produce almost identical functional values on a limited interval. Therefore slightly different methods for obtaining the polynomial that makes the 'best' fit to the data may produce very different coefficients. An attempt to repeat Briegleb and Strohmeier's (1953) results gave a range of results depending on the fitting strategy. All fits were good, but none of them reproduced Breigleb and Strohmeier's results in detail. Although there is some uncertainty in the determination of $\tilde{K}_n(T)$, the overall trend is that $\tilde{K}_n(T)$ grows approximately exponentially with n as in Franck and Meyer's (1959) chain model.

Smith (1958) made spectroscopic measurements and found no evidence for other polymers than the dimer, the tetramer and the hexamer and of these he judged the dimer to be relatively unimportant. It was concluded that $\tilde{K}_2$ is most likely not an equilibrium constant, but must be explained as an effect of non-ideality of the monomer gas. Smith show that a 1-4-6 model with non-ideal behaviour is able to reproduce Strohmeier and Briegleb's (1953) association factor data.

Schotte (1980) rejected all previous models and proposed a modified 1-2-6-8 model where

$$P = \frac{f_1 + K_2 f_1^2 + K_6 f_1^6 + K_8 f_1^8}{\phi(f_1, T)} \tag{61}$$

Here $K_q f_1^q$ is assumed to be the fugacity of $(HF)_q$. The function ϕ is a fugacity coefficient so that $K_q f_1^q/\phi = P y_q$, where y_q is the molar fraction of $(HF)_q$ (the same ϕ is assumed to work for all q). In this model the polymers are therefore treated both as chemically reacting and as non-ideal gases in themselves. In order to determine ϕ Schotte assumes that the monomers obey the Peng-Robinson equation of state (Peng and Robinson 1976).

A number of other models treat the polymers as non-ideal gases, e.g. Redington (1982) and Galindo, Whitehead, Jackson and Burgess (1997), where a review of recent developments can be found. Common to these models is that they reproduce data well, although at the expense of a vast number of adjustable parameters.

We may conclude that a large number of models is available, and there is little data to back them up. It is difficult to say which one is best suited for a dispersion model, because, excepts for the oldest ones, they all rely on the analysed dataset of Vanderzee and Rodenburg (1970), which in turn is based mainly on the P–V–T measurements of Strohmeier and Briegleb (1953), with the C_p data of Franck and Meyer (1959) used for consistency a check (there were inconsistencies) and the calorimetric data of Hu et al. (1953) for the saturation curve. Although these data are undoubtedly the best available, they cover a limited range of pressures and temperatures. The core of the data consists of $Z(P,T)$ vs. P curves for just a handful of temperatures, and there are gaps in measurements near saturation. It is therefore clear that more high quality P–V–T data would improve the situation. Some of the models spend hundreds of adjustable constants to reproduce these curves. This may seem a bit of an overkill, but it is actually difficult to reproduce the behaviour close to saturation with a small number of adjustable parameters. There are fewer problems away from the saturation curve, and here the simpler models give good results.

The question is whether it is important to have great accuracy near saturation in dispersion calculation. For a spray release, which we may take as a standard example, high concentrations are found in the jet near the source, where the dynamics is dominated by the momentum induced at the source. It therefore does not matter much if the density is miscalculated for high concentrations (above 10%, say). It is far more important to reproduce enthalpies and phase equilibria at lower concentrations, where buoyancy forces have time to act. In this regime formation of hydrofluoric acid droplets with low vapour pressure which tends to decrease HF concentrations in the gas phase and enhance de-polymerization. Therefore the HF polymers play an indirect role. They are mostly not there, but they leave the enthalpy of de-polymerization behind them as a contribution to the enthalpy budget. With pure liquid HF in the initial phase it is eventually the excess enthalpy that enters the enthalpy budget, and therefore it is important that this quantity is accurately reproduced. Equally important is of course the contribution from the mixing enthalpy in the liquid phase, which determines the stability of the hydrofluoric acid fog.

2.6 Rings and chains

We propose to use a simple model similar to Franck and Meyer's (1959) model with chains and a 6-ring. The polymers in the model are either chains or closed rings with more than six HF molecules, and the hydrogen bonds are assumed equivalent so that (the subscript $_1$ on f is dropped henceforth)

$$P = \frac{f + K_6 f^6}{1 - K_2 f} \tag{62}$$

This model is not very different from the 1-2-6 model, but it gives somewhat better results near the saturation pressure. We will refer to this model as the

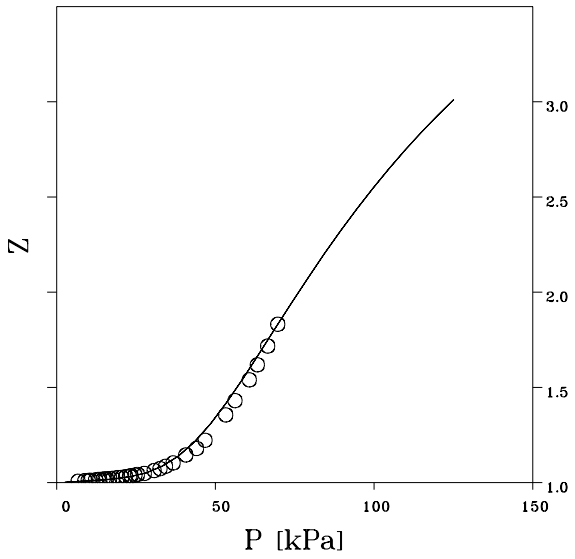

Figure 2. Comparison of Z predicted by the rings-and-chains model (line) with the experimental data of Strohmeier and Breigleb (circles) for 26°C.

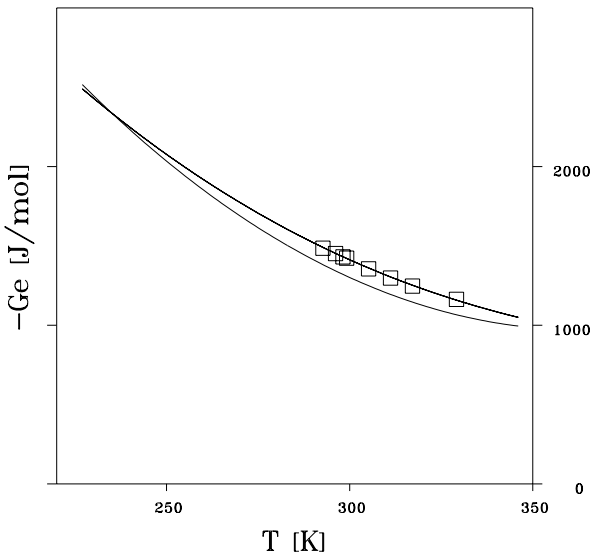

Figure 3. Excess free energy of saturated HF vapour. Thin line: derived from experimental data of Franck and Meyer and Hu, White and Johnston. Squares: analysed data of Vanderzee and Rodenburg. Thick line: rings-and-chains model predictions.

rings-and-chains model. The coefficients are modeled as

$$K_2(T) \quad = \quad \exp\left(\frac{A_2}{RT} + B_2\right) \text{ Pa}^{-1}$$

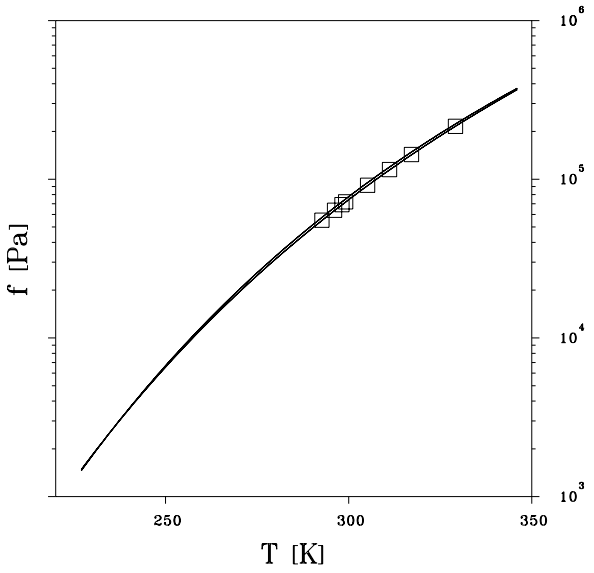

Figure 4. Fugacity saturated HF vapour. Thin line: derived from experimental data of Franck and Meyer and Hu, White and Johnston. Squares: analysed data of Vanderzee and Rodenburg. Thick line: rings-and-chains model prediction.

$$K_6(T) \quad = \quad \exp\left(\frac{A_6}{RT} + B_6\right) \text{ Pa}^{-5} \tag{63}$$

The four parameters A_2, B_2, A_6 and B_6 were estimated from the association factor data of Strohmeier and Briegleb (1953). The following procedure was followed. First, the HF fugacity was found by means of (14), which for a pure substance can be written as

$$\log \frac{f}{P} = \int_0^P \frac{1-Z}{ZP}\,\mathrm{d}P \tag{64}$$

The right hand side was evaluated by numerical integration of the association factor data. This was done by first fitting a polynomial of sufficiently high degree and then perform the integration analytically. The data points are so closely spaced that this effectively smoothes out the small experimental errors. The result is a table of values of corresponding values of Z and f for each of the six different temperatures where measurements were taken.

From (19), (62) and (63) it follows that

$$Z(f,T)P(f,T) = f\frac{\partial}{\partial f}P(f,T) = \frac{f + 6K_6f^6 - 5K_2K_6f^7}{(1-K_2f)^2} \tag{65}$$

Using this expression $K_2(T)$ and $K_6(T)$ were obtained for each of the six temperatures by fitting to the observed association factors. Finally the constants A_2, B_2, A_6 and B_6 were fitted to $K_2(T)$ and $K_6(T)$. This procedure yielded the following values

$$\begin{aligned} A_2 \quad &= 26585 \qquad \text{J/mol} \\ B_2 \quad &= -24.576 \end{aligned}$$

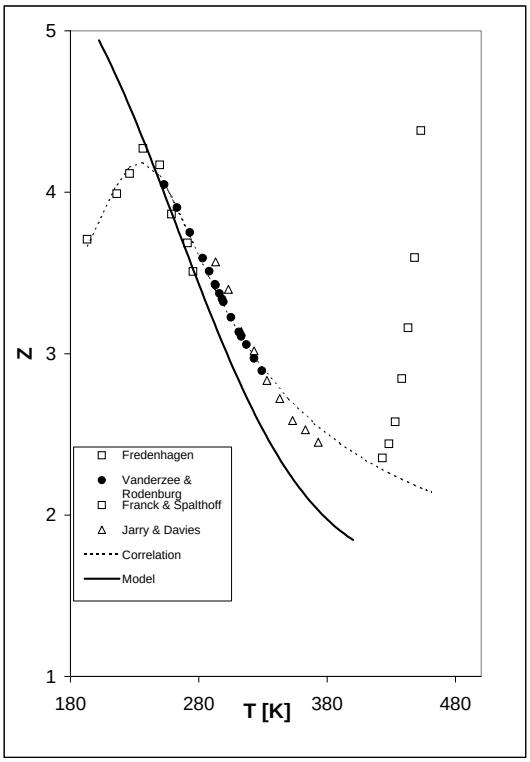

Figure 5. Comparison of Z for saturated vapour predicted by the rings-and-chains model (line) with experimental data.

$$\begin{aligned} A_6 &= 162649 \quad \text{J/mol} \\ B_6 &= -121.73 \end{aligned} \tag{66}$$

Figure 2 shows an example of the fit to the data. The line (model predictions) ends at the saturation pressure and it is obvious that more data for higher pressures would be very useful. Where data is available the fit is good, but not perfect. It is possible that the assumed temperature dependence (linearty with $1/T$) can be improved, but the narrow range of temperatures in the experiments makes this difficult.

In figure 3 we show the predicted excess free energy. The predictions are in almost exact agreement with the analysed data of Vanderzee and Rodenburg and deviating somewhat from the results from our data analysis (thin line).

Figure 4 shows results for the saturated vapour fugacity. Because of the wide range of values the model predictions and data are close, but actually there are differences of a few percent. The discrepancies are more evident from figure 5 where predicted values of Z along the saturation curve are shown together with experimental data from Fredenhagen (1933), Franck and Spalthoff (1957), Jarry and Davies (1953) and Vanderzee and Rodenburg (1970). The results are satisfactory in the temperature range of interest. The model does not reproduce the maximum at very low temperatures and it does not diverge at the critical temperature (461 K), but it performs rather well in between.

As a further check of the model, it was compared to the C_p data of Franck and Meyer (1959). For C_p the model predicts

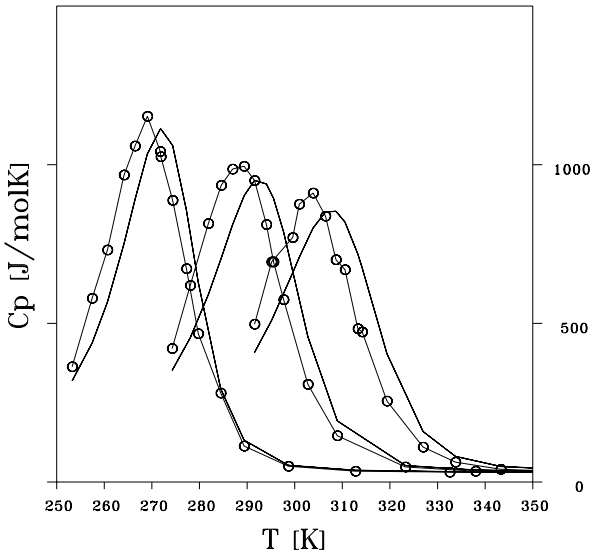

Figure 6. Comparison of C_p predicted by the rings-and-chains model (lines) with the data of Franck and Meyer (thin lines with circles). The three curves are for P= 83060, 42530 and 15465 Pa (the left peak).

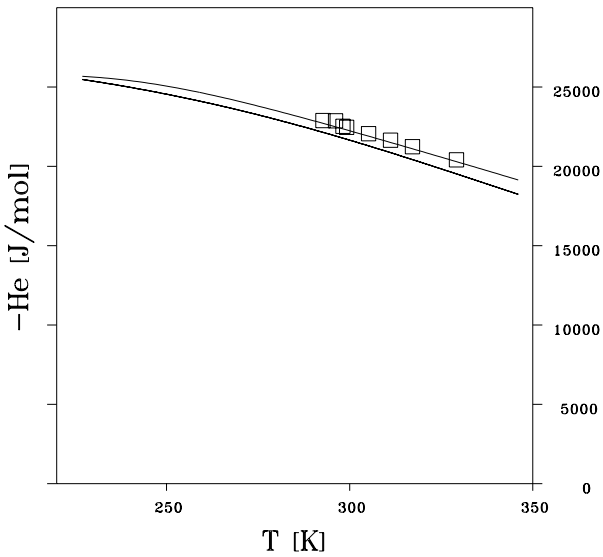

Figure 7. Excess enthalpy of saturated HF vapour. Thin line: derived from experimental data of Franck and Meyer and Hu, White and Johnston. Squares: analysed data of Vanderzee and Rodenburg. Thick line: rings-and-chains model predictions.

$$C_p - C_p^I = \frac{\partial H_E(T,P)}{\partial T} = \frac{\partial H_E(T,f)}{\partial T} + \frac{\partial H_E(T,f)}{\partial f}\frac{\partial f(T,P)}{\partial T}$$
$$= \frac{\partial H_E(T,f)}{\partial T} - \frac{\partial H_E(T,f)}{\partial f}\frac{fH_E}{RT^2} \quad (67)$$

which leads to a voluminous expression. It is noted that C_p is the heat capacity of a mass corresponding to one mol of HF monomers. Figure 6 shows the result of the comparison. The model reproduces nicely the large peaks of C_p. The maximum values are very well reproduced, but the peaks are at slightly higher temperatures than for the measurements. Vanderzee and Rodenburg (1970) noted the same tendency when comparing the datasets of Strohmeier and Briegleb (1953) and Franck and Meyer (1959) and attributed it to errors in the temperature measurements and suggested to shift the temperatures of Franck and Meyer one or two degrees up. Taking this into account the agreement is excellent. At the maxima C_p is about 50 times larger than C_p^I.

The model prediction of the excess enthalpy is given by

$$H_E(T,f) = -T^2\frac{\partial G_E(T,P)/T}{\partial T} = -RT^2\frac{\partial f(T,P)}{f\partial T} = \frac{RT^2}{ZP}\frac{\partial P(T,f)}{\partial T}$$
$$= -\frac{A_2K_2K_6 + A_2K_2f + A_6K_6f^5 - A_6K_2K_6f^6}{1 + 6K_6f^5 - 5K_2K_6f^6} \quad (68)$$

Figure 7 shows predicted excess enthalpies for saturated HF vapour (thick line) together with experimental data derived experiments (thin line). The experimental curve was made by numerical integration of the C_P data of Franck and Meyer (1959) along the 116 Torr isobar up to the saturation line and then follow the saturation line using the data of Hu et al. (1953). This data analysis agrees nicely with that of Vanderzee and Rodenburg (1970) (squares). The model consistently underpredicts $-H^{Eso}$, but the deviations are less than 3%. The Strohmeier and Breiglieb's dataset does not cover temperatures below 298.69K. Therefore the good agreement with data at much lower temperatures must be regarded as a lucky coincidence.

2.7 Phase equilibria

In the presence of water vapour the pressure is modeled as

$$P(f_1,f_2,T) = f_1 + \frac{f_2 + K_6(T)f_2^6}{1 - K_2(T)f_2}K_{12}(T)f_1f_2 \quad (69)$$

where we have chosen water as the first component and HF as the second component. Thus f_1 is the fugacity of water vapour and f_2 is the fugacity of HF vapour. The third term represents the partial pressure of the H_2O : HF complex. If we are in air we should add the partial pressure of dry air, which can be treated as an inert component.

The reaction of HF with water in the liquid phase is an exothermic process with important implications for HF dispersion. The main effect is to make droplets consisting of mixtures of HF and water much less volatile than droplets formed by any of the two substances in pure form. The effect of condensation is to raise the temperature of the cloud thereby decreasing the density. Depending on ambient temperature and humidity HF-water fog can typically persist down to HF concentrations of a fraction of a percent. When the fog evaporates the heat of condensation is supplied by the cloud, and the density may increase. Whether this

leads to a return of the cloud density to negative buoyancy depends on the reactions in the gas phase. If a substantial fraction of the HF ends up in the monomer state, the final density of the cloud is determined by the initial enthalpy in the storage tank, and be calculated without taking the intermediate reactions with water into account. Alternatively, if the association of HF with water persists in the gas phase this may bind enough enthalpy to affect the final buoyancy. The oligomerization has a similar effect, but only at high HF concentrations.

Thomas (1975) made spectroscopic measurements on HF-water vapour and found evidence for the HF : H_2O complex in the gas phase. Thomas found

$$K_{12}(315\text{K}) = 2.4\,10^{-6}\text{Pa}^{-1} \tag{70}$$

with an error bound of a factor of 2. The reaction constant is proportional to $e^{-\Delta H/RT}$ assuming that the entropy of association is independent of temperature. The enthalpy of association was determined as $\Delta H = -26\text{kJ/mol}\pm 5\text{kJ/mol}$. This leads to the relation

$$\frac{P_c}{f_2} = f_1\, K_{12}(315\text{K})\, \exp\left(-\frac{\Delta H}{R}\left(\frac{1}{T} - \frac{1}{315\text{K}}\right)\right) \tag{71}$$

where P_c is the partial pressure of the complex.

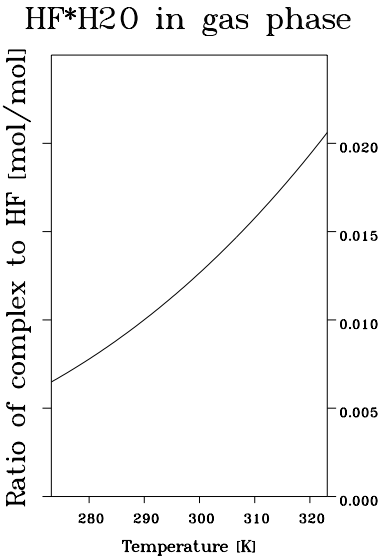

Figure 8. The ratio of partial pressures of HF-water complex and HF monomer in saturated water vapour as a function of temperature.

Figure 8 shows a plot of the ratio P_c/f_2 versus temperature assuming f_2 is equal to the saturated water vapour pressure. For relative humidities below 100% the ratio is correspondingly lower. The calculations show that about 99% of the HF ends up as free monomers in the final stage of the dispersion. The heat of vaporization of HF (to monomers) is about 31kJ/mol, which is comparable to the heat of dissociation. The effect on the enthalpy budget of the irreversible association of HF with H_2O in the gas phase is therefore comparable to the effect of a slight change of the heat of vaporization. Given the uncertainty of this number (certainly larger than 1%) it is justifiable to regard the HF-water reactions as reversible. It should therefore be safe to neglect the association of HF and water in the gas phase because the contribution to the enthalpy budget is insignificant.

Once we decide to ignore the water-HF association and other associations between chemical species in the gas phase we may write the pressure

$$P(f_1, f_2, T) = P_1(f_1, T) + P_2(f_2, T) + \ldots = f_1 + \frac{f_2 + K_6(T) f_2^6}{1 - K_2(T) f_2} + \ldots \qquad (72)$$

where partial pressures of other inert substances (e.g. dry air or butane) may be added. For the gas phase composition Dalton's law is replaced by

$$y_i = \frac{Z_i P_i}{\sum_j Z_j P j} \qquad (73)$$

where $Z_i P_i = f_i \partial P_i(T, f_i)/\partial f_i$, and only Z_2 is different from 1.

The situation is completely different for HF and water in the liquid phase. Here the interaction is very important and must not be ignored. Pouring liquid HF and water together leads to a violent reaction because of the extremely large mixing enthalpy of the two substances. Since the released heat is so large, it is effectively independent of T, because terms like $C_p \Delta T$ are only minor corrections. If we regard H_{mix} as independent of temperature and drop the last, small term in (42), we may integrate to obtain

$$G_{\mathrm{mix}}(P_s, T, x_2) \approx H_{\mathrm{mix}}(x_2) - T S_{\mathrm{mix}}(x_2) \qquad (74)$$

where S_{mix}, the mixing entropy, becomes independent of T because it is merely an integration constant. The composition is given by the molar fraction of one of the substances, and we choose to work with the HF fraction x_2. Both $H_{\mathrm{mix}}(x_2)$ and $S_{\mathrm{mix}}(x_2)$ vanish for $x_2 = 0$ and $x_2 = 1$ so we may write them as

$$\begin{aligned} H_{\mathrm{mix}}(x_2) &= (n_1 + n_2) x_2 (1 - x_2) M(x_2) \\ S_{\mathrm{mix}}(x_2) &= (n_1 + n_2) x_2 (1 - x_2) N(x_2) \end{aligned} \qquad (75)$$

M can be found from the mixing enthalpy measurements of Johnson et al. (1973), which seems to be the best and most recent source. The data cover HF concentrations up to 50%. It turns out that M is very close to linear in this range. A least square fit yields

$$M(x_2) = M_1 + M_2 x_2 \qquad (76)$$

where

$$M_1 = -18460\,\mathrm{J/mol} \qquad \text{and} \qquad M_2 = -19764\,\mathrm{J/mol} \qquad (77)$$

The correlation is accurate for concentrations in the range 1-50%, and still fairly good for larger concentrations, see figure 9. At very low HF concentrations there are peculiar large deviations, but they play no role since they are cancelled by the factor $x_2(1 - x_2)$. At larger HF concentrations the data are more scattered and the linear approximation probably not as accurate as below 50%. High concentration may not be so important for atmospheric releases because pure liquid HF is so hygroscopic that it effectively absorbs all available moisture in the air, even at noon in the Sahara desert. At very high liquid HF concentrations the enthalpy budget is therefore accurately determined by the simple assumption that all the water is in the liquid phase, and the equilibrium model is sufficiently accurate as long as it reproduces this behaviour. As more water gets into the droplets they get less hygroscopic and there will be an appreciable amount of water vapour present. In this range of concentrations model performance is more critical. Based on the measurements and model predictions of Schotte (1987) important liquid phase concentrations are roughly in the range $x_2 \sim 0.3 - 0.6$ (the fog disappears quickly

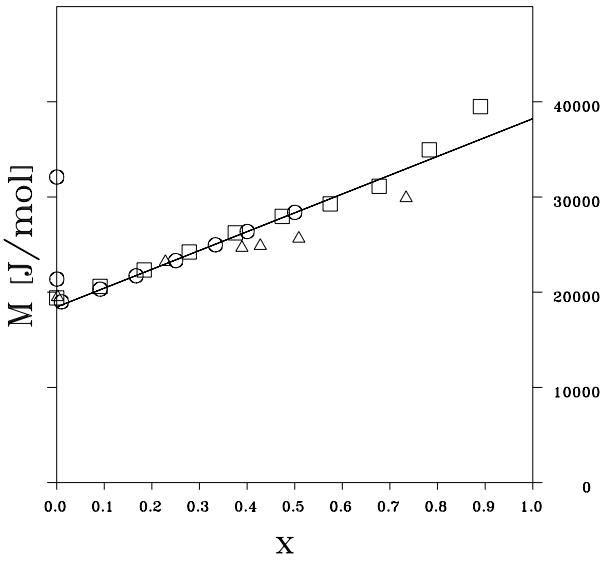

Figure 9. The function $M(x)$. Line: correlation (76). Circles: measurements of Johnson, Smith and Hubbard. Squares: data from Kirk-Othmer. Triangles: data from Gmelin.

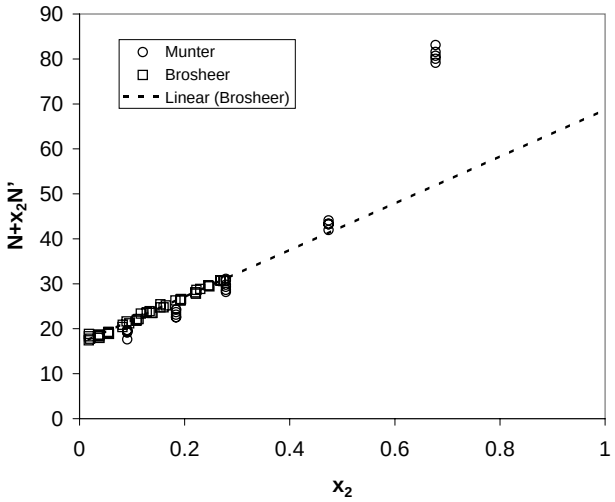

Figure 10. The function $N(x_2) + x_2 \mathrm{d}N(x_2)/\mathrm{d}x_2$

at lower concentrations), which is well covered by experimental data as far as M is concerned.
N can be found from vapour pressure and composition data. We may either use the relation

$$G_{\mathrm{mix}}(P_s, T, \mathbf{n}) = RT \sum_i n_i \log \frac{f_{si}}{x_i f_{si}^{\mathrm{o}}} \tag{78}$$

or we may use (41) to get expressions for each of the two species, i.e.

$$RT \log \frac{f_{s1}}{x_1 f_{s1}^o} = x_2^2 \left[(M - TN) - (1 - x_2) \frac{\mathrm{d}(M - TN)}{\mathrm{d}x_2} \right]$$
$$= x_2^2 \left[[M_1 - TN_1 + (2x_2 - 1)(M_2 - TN_2)] \right] \quad (79)$$

for water vapour and

$$RT \log \frac{f_{s2}}{x_1 f_{s2}^o} = (1 - x_2)^2 \left[[(M - TN) + x_2) \frac{\mathrm{d}(M - TN)}{\mathrm{d}x_2} \right]$$
$$= (1 - x_2)^2 \left[[M_1 - TN_1 + 2x_2(M_2 - TN_2)] \right] \quad (80)$$

for HF vapour. Pressure and composition data can be found in Brosheer et al. (1947) and Munter et al. (1949). Very similar methods were used for these two datasets. The measurements basically consist in chemical analysis of the vapours of hydrofluoric acid for a range of temperatures and liquid phase compositions. The results are reported as 'the partial pressures' of HF and water. We have assumed that the conversion from the measured composition was based on the ideal gas law. We prefer to use (80) because the HF data appear to be better than the water vapour data. The rings–and–chains model was used to convert measured molar fractions in the gas phase into fugacities. The vapour pressures over HF-water mixtures is relatively low except for HF concentrations very close to 100% and $f_{si} \approx y_i P$ is in fact adequate in most cases (a 7% correction is needed in one instance). The pure HF vapour fugacity f_{si}^{o} is also needed, and this quantity is substantially different from the vapour pressure, which other models use here. Both are strongly increasing functions of temperature, but the ratio between the two varies much less. It could be argued that it is be best to use fugacity values derived from measurements, but we use the model to determine f_{si}^{o} because the correlation we are aiming at is meant to be used in conjunction with the model and the model performs well with respect to reproducing this quantity (accurate to within a few percent). Since M has already been determined we can isolate $N + x_2 N'$ in (80). Figure 10 shows $N + x_2 N'$ determined in this way. The data covers temperatures between 298 K and 358 K. The data of Brosheer et al. (1947) show the least scatter, and they produce a nice straight line in the limited range of x_2 values (all less than 0.3). The values of $N - x_2 N'$ obtained from Munter et al. (1949) are in good agreement those obtained from Brosheer et al. (1947), although they appear to be slightly lower. Unfortunately, there are few data in the range $x_2 \sim 0.3 - 0.6$, and the temperatures are also higher than what can be expected in a cloud. However, measurements for the same x_2 and different T show little scatter indicating that N is indeed independent of T. More data for lower temperatures and $x_2 \sim 0.5$ would be helpful. Data is available from measurements of liquid and gas phase compositions at the normal boiling point. Some of these data are in the range $x_2 \sim 0.3 - 0.6$, but the temperatures are even higher (above 100°C in most cases) and the effect of polymerization is large, so these have not been used to determine N.

Based on the Brosheer et al. (1947) data we find

$$N(x_2) = N_1 + N_2 x_2 \quad (81)$$

where

$$N_1 = -16.598\,\mathrm{J/molK} \qquad \text{and} \qquad N_2 = -26.059\,\mathrm{J/molK} \quad (82)$$

This correlation is accurate for $x_2 < 0.5$, and from figure 10 it appears that the linear fit to $N(xz_2)$ is probably insufficient at higher concentrations. However, due to lack of data we will have to be content with the linear fit. In extreme cases this may lead to a 20% underestimate of the partial pressure of HF, which may

after all not be so bad. The tuning of the parameters with data for low x_2 values should ensure good performance at low HF concentration. Thus the model should be able to make accurate predictions of the concentration where the HF-water fog disappears.

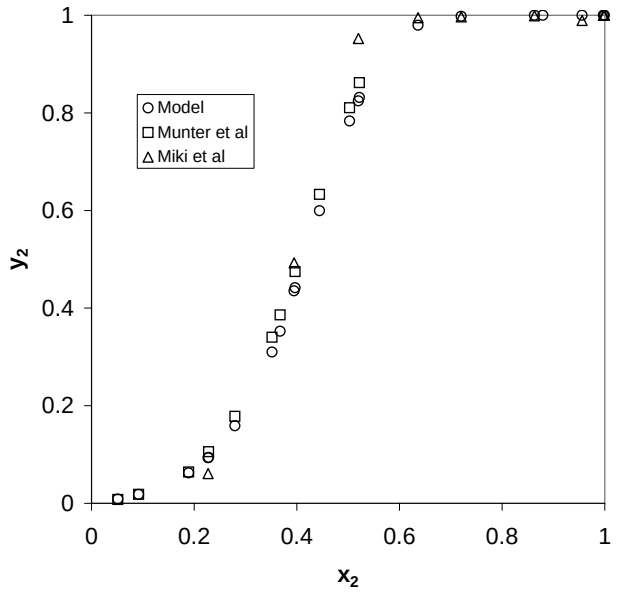

Figure 11. Predicted and measured values of the HF molar fraction in Hydrofluoric Acid vapour at the normal boiling point as a function of the HF molar fraction in the liquid phase.

In order to check the equilibrium model against independent data, we have calculated vapour phase composition (y_2) at the normal boiling point as a function of x_2. The results are shown in figure 11 together with measurements by Munter et al. (1947) and Miki et al. (1990). For these data polymerization has a large impact, but the model performs well. It should be noted that the normal boiling point is above 100°C for $x_2 < 0.5$. At these large temperatures and partial pressures, the influence of HF-water associations in the gas could be important.

The model has also been compared to the adiabatic mixing data of Schotte (1987) and Kemp and Newland (2000). The results are shown in figure 12 and figure 13. The model generally performs best at low concentrations where it reproduces Schotte data almost exactly. At high concentrations (above 10%, say) the temperatures predicted by the model are larger than those observed by Schotte, while they are smaller than those observed by Kemp and Newland.

Several methods to determine the phase equilibrium has been tried. The equations can be tricky to solve because of the drastic variation of the vapour pressures with T and x_2. The following procedure is robust and converges reasonably fast. In a dispersion calculation the composition of the mixture (HF, dry air and water) is given as well as the total enthalpy and the total (atmospheric) pressure. The first step is to determine the dew point and calculate the enthalpy at the dew point. Condensation uccurs if the total enthalpy H_{tot} is less than the dew point enthalpy. If there is no condensation the temperature is determined so as to yield the right enthalpy. Otherwise, the state is specified once we know the temperature and the fugacities. Starting with P and first guesses of T, f_1 and f_2 we may calculate y_2, x_2 and the amount of condensate and from these compute a new value H'_{tot} of the total enthalpy. We also use x_2, T and the equilibrium equations to determine new fugacities f'_1 and f'_2. The solution is a fixed point which is found by minimizing

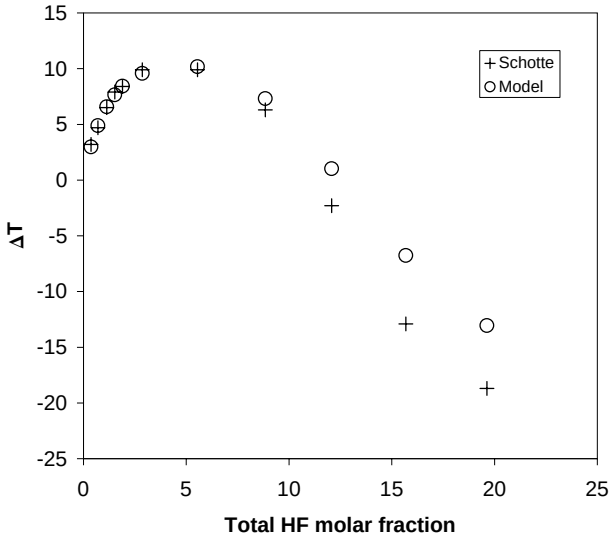

Figure 12. Predicted and measured values of the temperature change in mixtures of HF vapour and humid air vs. total HF molar fraction. Initial temperature $26°C$ *and 80% relative humidity.*

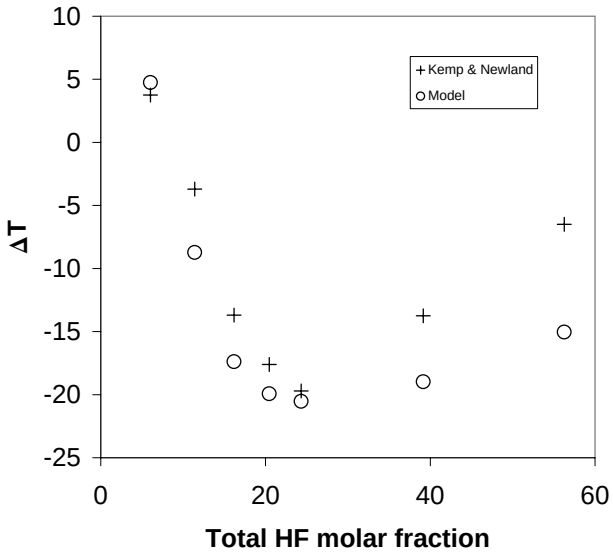

Figure 13. Predicted and measured values of the temperature change in mixtures of HF vapour and humid air vs. total HF molar fraction. Initial temperature $20°C$ *and 80% relative humidity. Data points are from run HF06.*

$\left(\frac{H_{\mathrm{tot}}-H'_{\mathrm{tot}}}{RT}\right)^2 + (\log f'_1/f_1)^2 + (\log f'_2/f_2)^2$. The downhill simplex method of Nelder and Mead (1965) was used for this.

3 The atmospheric surface layer

We lack a general statistical theory of turbulence, but scaling arguments often prove useful. These can be mere dimensional arguments or be more deeply rooted theoretically by reference to scaling properties of a set of governing equations. Surface layer scaling or Monin-Obukhov scaling (Monin and Obukhov 1953) is of the latter type. The governing equations are those based on the Boussinesq approximation. They have time-varying chaotic solutions that are believed to reproduce all essential features of real high Reynolds number turbulence. Therefore the equations are hard to solve and not in themselves useful for dispersion applications. The point is that we may define two fundamental scales: the friction velocity defined as

$$u_* = \sqrt{-\langle uw \rangle} \tag{83}$$

and the Monin-Obukhov length scale

$$L = -\frac{u_*^2 T_0}{\kappa g T_*} \tag{84}$$

where T_0 is a reference temperature (e.g. average absolute temperature near the ground) and

$$T_* = \frac{\langle T'w' \rangle}{u_*} \tag{85}$$

For a stationary flow over uniform terrain the momentum flux $\langle uw \rangle$ and the heat flux $\langle Tw \rangle$ are constant and the values of u_* and L are independent of where they are measured. We may therefore use u_* and L as boundary conditions. The moisture flux is also a boundary condition, but it has little impact on dynamics unless condensation occurs, so we can disregard it. In addition values of the average windspeed and temperature should be specified at a certain reference height.

Furthermore, the equations can be rewritten in non-dimensional form by using $|L|$ as length scale, $|L|/u_*$ as time scale and T_* as temperature scale. This yields two sets of equations, one for $L > 0$ (stable stratification) and one for $L < 0$ (unstable stratification). In non-dimensional form all stable flows therefore obey the same governing equations with the same boundary conditions and similar for all unstable cases. We can therefore imagine that we produce an infinitely long timeseries from the non-dimensional equations. Assuming that the time series is stationary we may let randomly chosen bits of it serve as an ensemble so that time averages of the infinite as ensemble averages (the ergodic hypothesis). This means that relations between non-dimensionalized statistics are universal. The average wind profile, for example, may for be expressed as $u_* f(z/L)$ where f is a universal function, where positive arguments ($z/L > 0$) represent stable conditions and negative arguments represent unstable conditions. It can be shown that due to invariance under Gallilean transformations the profile must be of the form (Monin and Yaglom 1975)

$$\langle U(z) \rangle = u_* \left[\phi(z/L) - \phi_m(z_0/L) \right] \tag{86}$$

The only way that this can remain finite in the limit $|L| \to \infty$ is if ϕ contains a logarithmic term. Singling this out we may therefore write

$$\langle U(z) \rangle = \frac{u_*}{\kappa} (\log(z/z_0) + \Psi_M(z/L) - \Psi_M(z_0/L) \tag{87}$$

where $\kappa \approx 0.4$ is the von Karman constant and $\Psi_M(0) = 0$. This elegantly proves the well known logarithmic wind profile for neutral conditions. In a similar way it can be proved that the average temperature profile is of the form

$$\langle T(z) \rangle = T_0 - \frac{T_*}{\kappa_T}(\log(z/z_0) + \Psi_H(z/L) - \Psi_H(z_0/L) \tag{88}$$

where $\kappa_T \sim 0.4$ is analogous to the von Karman constant and Ψ_H is a universal function. The value of κ_T is less well known than κ. According Bussinger, Wyngaard, Izumi and Bradley (1971) $\kappa/\kappa_T = 0.74$, but they also found $\kappa = 0.35$ where $\kappa = 0.4$ seems to be universally accepted. Others say $\kappa_T = \kappa$. We use $\kappa_T = \kappa = 0.4$.

The assumptions that have to be made in order to derive these results are not strictly fulfilled in reality. The terrain is never completely uniform and the fluxes are not constant in either space or time. The weather changes, in other words, and the analysis of measured time series cannot always be based in the assumption that statistical properties are independent of time (non-stationarity). The influence of the Earth's rotation is another factor which spoils the picture, because we need to neglect the Coriolis force in the governing equations in order to get the desired scaling properties. Therefore surface layer scaling is an approximation. The effect of non-stationarity depends on the statistic in question. Quantities that are correlated over long times are the most difficult because it requires long time series to estimate their mean values and there is a risk that meteorological conditions may change during measurements. Quantities that have short 'memory' are more easy. Unfortunately fluxes, which are used to define u_* and L, are not among the 'easy' ones; experience shows that timeseries should not be shorter than about ten minutes. Fluxes are also notorious as being difficult to measure and experimental errors of u_* and L are therefore large. This contributes to the uncertainty in the determination of universal functions such as Ψ_M and Ψ_H and a large number of different versions have been published. We will use the following due to Bussinger et al. (1971) and Paulson (1970)

Wind speed profile:

$$\Psi_M(\zeta) = \log\frac{(1+\xi)^2(1+\xi^2)}{8} - 2\arctan\xi + \frac{\pi}{2}, \quad \text{where} \quad \xi \equiv (1-16\zeta)^{1/4} \tag{89}$$

for unstable conditions ($L < 0$) and

$$\Psi_M(\zeta) = -4.7\,\zeta \tag{90}$$

for stable conditions ($L > 0$).

Temperature profile:

$$\Psi_H(\zeta) = 2\,\log\frac{1+\sqrt{1-9\zeta}}{2} \tag{91}$$

for unstable conditions and

$$\Psi_H(\zeta) = -5\,\zeta \tag{92}$$

for stable conditions.

It has been suggested to use so-called mixed layer scaling for dispersion in convective conditions ([Nieuwstadt 1980)e.g.]. This involves the boundary layer height and a velocity scale different from u_*. We do not recommend this for dispersion in the lower 10% of the boundary layer as explained in section 4.4.

4 The dispersion model

The model outlined in the following is a traditional integral (or box) model. It resembles e.g. Ooms's (1972) model, but there are many other similar models. Some of these are discussed by Bricard and Friedel (1989), who find that, even if models are based on a common structure, the values of empirical constants are quite different, especially those related to entrainment. The main difference between the model presented here and other integral models is the consequent use of relative diffusion concepts. This has an impact on the interpretation of the model variables and model results and it requires relative diffusion data for parameter tuning. Relative diffusion experiments are difficult to perform, therefore most dispersion data regard absolute diffusion. However, new relative diffusion data are emerging, some of which have been generated during the URAHFREP project. We have therefore decided to use what is available of relative diffusion data as the empirical basis for the model.

4.1 Basic model parameters

An instantaneous release, a puff, is in some ways simpler to discuss than a continuous release. We therefore start with puffs, although plumes will eventually be the main issue. The most rudimentary description of a puff is a specification of the centre coordinates and a parameter describing its size (e.g. a suitably defined diameter) as functions of time. Such a description is fully adequate when concentration profiles are self similar, because the full profile can be obtained by scaling and translating a known standard profile. When buoyancy effects are present the assumption of a self similar profile is not strictly correct, but it may still work well as a first approximation. A plume from a continuous source can be regarded as a series of puffs and the growth of the plume can be inferred from the growth rate a puff traveling along the centreline. In the following we seek equations describing the simple parameters.

The governing equations are as follows: the equation of continuity

$$\frac{\partial \rho}{\partial t} + \nabla \cdot \mathbf{u}\rho = 0 \tag{93}$$

the advection-diffusion equation for contaminant concentration c (mass by mass)

$$\frac{\partial c\rho}{\partial t} + \nabla \cdot \mathbf{u}c\rho = D\nabla^2 c\rho \tag{94}$$

and the Navier-Stokes equation

$$\frac{\partial \rho\mathbf{u}}{\partial t} + \nabla \cdot \mathbf{u}\rho\mathbf{u} = -\nabla P + \rho\mathbf{g} + \rho\nu\nabla^2\mathbf{u} \tag{95}$$

where $\mathbf{g} = (0, 0, -g)$ is the gravitational field vector. In the following equations it is safe to neglect the diffusivity D and the viscosity ν (formally we can say that we study the limit $\nu \to 0$ for fixed D/ν and given boundary conditions).

The released mass is given by

$$m_0 = \int c\rho \mathrm{d}^3 x \tag{96}$$

where the integral is over all space. From (94) it follows that m_0 is a constant equal to the released contaminant mass.

The puff centre $\mathbf{X} = (X, Y, Z)$ is defined as the centre of mass of the contaminant, i.e.

$$\mathbf{X} = \frac{1}{m_0} \int \mathbf{x} c\rho \, \mathrm{d}^3 x \tag{97}$$

The average puff size Σ is defined as

$$\Sigma^2 = \sigma_x^2 + \sigma_y^2 + \sigma_z^2 = \frac{1}{m_0} \left\langle \int (\mathbf{x} - \mathbf{X})^2 c\rho \, \mathrm{d}^3 x \right\rangle \tag{98}$$

where brackets have been used to denote ensemble averaging. The three quantities σ_x, σ_y and σ_z are defined similarly for each direction. For plumes we may use similar definitions if a thin slice is regarded as puff.

4.2 Dynamic equations

Neglecting molecular diffusion the centre velocity is given by

$$\mathbf{U} = \frac{\mathrm{d}\mathbf{X}}{\mathrm{d}t} = \frac{1}{m_0} \int \rho c \mathbf{u} \mathrm{d}^3 x \tag{99}$$

We can go on and use the Navier-Stokes equation to write

$$m_0 \frac{\mathrm{d}\mathbf{U}}{\mathrm{d}t} = -\int \rho c \nabla P \mathrm{d}^3 x + \int \rho c \mathbf{g} \mathrm{d}^3 x + \nu \int c\rho \nabla^2 \mathbf{u} \, \mathrm{d}^3 x \tag{100}$$

The equation is exact, but in fact not very useful. This is because it focuses on the contaminant. The contaminant is entangled with the surrounding air in a highly complex, fractal way that makes it impossible for the cloud to move 'on its own' without taking the air in its neighbourhood with it (and visa versa). Due to the complex shape of the cloud, which locks it to the surrounding air, the pressure term, which mediates the interaction, must be both large and very complicated. On the other hand, the result of the interaction is simply that the contaminant is pushed and pulled at the right places so as to make it follow the air. It is therefore better to include the air in contact with the cloud in the description, and set up an equation for the acceleration of all masses inside a volume B surrounding the cloud. B should not be entangled with the surrounding air in a complicated way, hence it should be a regular shape, e.g. a ball or a rectangular box, not a fractal shape. Inside B the complicated interactions between the HF and the surrounding air are internal forces, which cancel due to the law of action and reaction. B should also be reasonably small, yet large enough to contain essentially all contaminant material. The dimensions of B should of course scale with Σ. The mass m_B inside B is given by

$$m_B = \int_B \rho \, \mathrm{d}^3 x \tag{101}$$

The centre of mass of B should coincide with the puff centre, i.e.

$$\mathbf{X} = \frac{1}{m_B} \int_B \rho \mathbf{x} \mathrm{d}^3 x \tag{102}$$

The centre velocity is estimated as the mean velocity

$$\mathbf{U} \approx \frac{1}{m_B} \int_B \rho \mathbf{u} \mathrm{d}^3 x \tag{103}$$

This can only be approximate when the density varies, but in any case it should be a good approximation.

m_B is an increasing function of time and

$$\frac{\mathrm{d}m_B}{\mathrm{d}t} = \int_{\partial B} \rho \hat{\mathbf{n}} \cdot (\mathbf{u}_s - \mathbf{u}) \, \mathrm{d}A \tag{104}$$

where the integral is over the surface of B, $\mathbf{u}_s$ is the velocity of a surface element and $\hat{\mathbf{n}}$ is a unit vector perpendicular to the surface pointing out of B. The quantity $\hat{\mathbf{n}} \cdot (\mathbf{u}_s - \mathbf{u})$ is the (local) entrainment velocity, which we may assume has a constant value u_e on ∂B. Clearly u_e should scale with $\mathrm{d}\Sigma/\mathrm{d}t$. Moreover, since $\rho = \rho_a$ on the surface, and we may estimate it by the average ambient density profile value $\rho_a(Z)$ evaluated at the height of the centre. These simplifications lead to

$$\frac{\mathrm{d}m_B}{\mathrm{d}t} = u_e \, \rho_a(Z) \, S_B \tag{105}$$

where S_B is the surface area of B. It should be noted that the rate of change of volume of B is only equal to $u_e S_B$ if the processes taking place inside B preserve volume. It is best, therefore, not to have an equation for 'entrained volume', but to determine the volume from m_B and ρ.

Integrating both sides of the Navier-Stokes equation over B and neglecting the viscous term we get the dynamic equation

$$\frac{\mathrm{d}m_B \mathbf{U}}{\mathrm{d}t} = \int_{\partial B} \rho \mathbf{u} \hat{\mathbf{n}} \cdot (\mathbf{u}_s - \mathbf{u}) \, \mathrm{d}A - \int_B \nabla P \mathrm{d}^3 x + \int_B \rho \mathbf{g} \, \mathrm{d}^3 x \tag{106}$$

Assuming uniform entrainment velocity and average ambient values on ∂B the first term on the right hand side becomes equal to $u_e \rho_a u_a S_B$. The pressure can be split into a hydrostatic part and a residual pressure P', i.e. $\nabla P = \nabla P' + \rho_a(Z)\mathbf{g}$. This yields the following equation

$$\frac{\mathrm{d}m_B \mathbf{U}}{\mathrm{d}t} = u_e \rho_a \mathbf{u}_a S_B - \int_{\partial B} \hat{\mathbf{n}} P' \mathrm{d}A + m_B \mathbf{g} (\rho_B - \rho_a) \tag{107}$$

where ρ_B is the average density in B, i.e. $\rho_B = m_B/V_B$ where V_B is the volume of B. Note that the ambient velocity $\mathbf{u}_a$ need not be taken as the average, horizontal velocity. It is possible to draw it from an ensemble e.g. reflecting the probability distribution of the vertical component w. Note that in this way the model simulate the influence of ambient fluctuations compared to HF buoyancy effects. We shall return to this.

We can treat a plume in a similar way as a puff by considering a slice of it as a puff. An envelope containing all the contaminant is placed round the plume. Let s denote the length along the centreline and $\mathbf{k}(s)$ the unit vector tangent to the centreline. By $A(s)$ we denote the area of a cross-section of the plume defined by the envelope and the plane normal to $\mathbf{k}(s)$. B is chosen to be a thin pill-box shaped section between $A(s,t)$ and $A(s+\Delta s, t)$. As time progresses the slice is supposed to move in such a way that there is no net mass transport through the ends $A(s,t)$ and $A(s+\Delta s, t)$. This should ensure little exchange of contaminant through the ends, which can therefore be neglected. Thus entrainment only takes place through the plume edge while internal mixing along the plume is neglected in the model. Following similar lines as above and taking the limit $\Delta s \to 0$ the following equations are obtained. The mass balance equation becomes

$$\frac{\mathrm{d}A\rho}{\mathrm{d}t} = C_A u_e \rho_a \tag{108}$$

where C_A is the circumference of A and ρ is the average density in A. The momentum equation is

$$\frac{\mathrm{d}A\rho\mathbf{U}}{\mathrm{d}t} = C_A u_e \rho_a \mathbf{u}_a - \int_{\partial A} \hat{\mathbf{n}} P' \mathrm{d}l - \frac{\partial}{\partial s} \int_A \mathbf{k} P' dA + A\mathbf{g}(\rho - \rho_a) \tag{109}$$

The terms involving P' represent various kinds of interactions which will be dealt with simple ways. For plumes moving relative to the wind there will be an added mass effect, which we shall return to in section 4.5. The added mass is effective when the plume accelerates. In addition there will be a drag force, which we model as

$$\mathbf{F}_D = \pm C_D C_A \frac{1}{2} \rho_a (\hat{\mathbf{k}} \cdot \mathbf{u}_a)^2 \hat{\mathbf{k}} \tag{110}$$

where $\hat{\mathbf{k}}$ is $\mathbf{k}$ rotated 90 degree (in the x–z plane and minus sign is used for a ascending plumes and + for descending plumes. We use $C_D = 0.3$ as suggested Ooms (1972). Non-hydrostatic forces also play a role when a plume touches down on the ground (or hits the capping inversion). The effect of these is to keep the plume inside boundaries, and we may achieve this simply by stopping the vertical motion of the plume when it hits the ground (or a capping inversion). Moreover, there will be a random contribution which is, at least partly, responsible for the characteristic irregular and meandering plume shape. This could be simulated by a random force, but we will ignore the pressure fluctuations because we believe that the contribution from fluctuations of the momentum of the entrained air is more important.

It can be practical to use the centreline distance s as independent variable instead of the time t. For a stationary plume we have $\partial q/\partial t = 0$ for any quantity q and therefore

$$\frac{\mathrm{d}q}{\mathrm{d}t} = \nabla \cdot \mathbf{u}q = \frac{\mathrm{d}qU}{\mathrm{d}s} \tag{111}$$

Using s instead of t we therefore get conservation equations involving fluxes. Three of these are needed: mass flux $\dot{m}$, momentum flux $\dot{m}\mathbf{u}$ and enthalpy flux $\dot{m}H$. We also have the massflux of HF $c\dot{m}$, but it is constant and equal to the HF release rate $\dot{m}_0$.

The average density ρ in the plume slice A must be determined from the thermodynamics. Note that integration of (108) yields $A\rho$, but we need ρ to determine A and ρ also enters explicitly in the buoyancy term of (109). The density and other useful quantities such as temperature, composition, aerosol content, are given by the thermodynamical state. It is convenient to specify the thermodynamic state by means of the enthalpy H (in J/kg) and the composition in terms of the molar fractions (which can be worked out from c). In real clouds these quantities are complicated functions of time and space, but we shall ignore this and adopt the assumption of homogeneous equilibrium within A. This means that total mixing within A is assumed. The homogeneous equilibrium model is justified as long as the density is a linear function of the concentration, which is the case for buoyancy conserving substances. HF clouds do not conserve buoyancy, and therefore the density will depend on the micro-structure of the concentration field. It is beyond the scope of the present work to take this into account, but it should be emphasized that corrections to the homogeneous equilibrium assumption due to concentration fluctuations could be important. The model may overpredict negative buoyancy because it neglects the effect of regions with low concentrations.

The HF cloud is regarded as consisting of three chemical species, HF, water and dry air, of which the dry air is regarded as inert. Typically the absolute humidity does not vary very much with the height and therefore we may assume that a constant ratio betweeen the molar fractions of water and dry air. Then the cloud

composition is fixed by the ambient humidity and the contaminant concentration c (mass by mass) which is given by

$$c = \frac{\dot{m}_0}{\dot{m}} \tag{112}$$

The enthalpy budget is simplified by the assumption of adiabatic mixing. It is an approximation since heat is generated by the dissipation of turbulent kinetic energy and heat is exchanged by molecular diffusion and radiation, but generally the amount of energy exchanged by these processes is small. According to the entrainment concept the transfer of matter is regarded as a one-way process. In order to be consistent we should model enthalpy transfer in the same way. The transfer of enthalpy across the free surface of the cloud is therefore set equal to the enthalpy of the entrained air. For a grounded cloud the exchange of heat through the ground surface should also be taken into account. The simplest way to model this is to use the ambient heatflux, which is related to the Monin-Obukhov length scale. This leads to the following enthalpy budget equation

$$\frac{\mathrm{d}\rho AH}{\mathrm{d}t} = C_A u_e \rho_a H_a + Q_s + A\frac{\mathrm{d}P}{\mathrm{d}t} \tag{113}$$

where H_a is the enthalpy (in J/kg) of the entrained air, Q_s is the heat transfer from the ground, which we estimate by the ambient value

$$Q_s = \langle Tw \rangle C_{pa} b - \frac{C_{pa}\rho_a u_*^3 T_a}{gL\kappa} b \tag{114}$$

where b is the plume width. In case of very large temperature differences additional terms could be considered. The last term on the right hand side of (113) accounts for adiabatic cooling of a rising plume due to pressure changes. The easiest way to deal with this is to assume constant pressure (i.e. drop the term) and instead correct the ambient temperature profiles for the adiabatic lapse rate.

The shape of A is assumed to be circular for elevated plumes. Ground contact is modelled in the simplest possible way. When Z is shorter than the radius $r = \sqrt{A/\pi}$ the plume has ground contact and A is modelled as a circle with the bit under the surface cut off. No particular influence on the plume dynamics is assumed except that the radius and the circumference are calculated differently. The lowest value of Z is determined by the centre of mass of a semi-circle with centre at ground level and area equal to A. When Z gets below this value in the computation it is simply stopped and W is set equal to zero if it is negative.

Finally we must decide the relation between A and Σ. In the model A is determined by the way we model the entrainment velocity. When the density is constant and $A = \pi r^2$ is circular the entrainment velocity is simply $u_e \mathrm{d}r/\mathrm{d}t$, so the definition of r is coupled to the definition of u_e. The measurable quantities are σ_y and σ_z and a we must choose a relation like $A = a\pi(\sigma_y^2 + \sigma_z^2)$ (or e.g. $A = a\pi\sigma_y\sigma_z$), where a is a constant, in order to relate A to something measurable. The values of a used in models are typically between 1 and 3. Somewhat arbitrarily we choose $a = 1$ so that

$$A = \pi(\sigma_y^2 + \sigma_z^2) \tag{115}$$

With this choice a Gaussian concentration profile should have c as the centre (maximum) concentration.

4.3 Relative vs. absolute diffusion

It is instructive to rewrite equation (98) in the form

$$2\Sigma^2 = \frac{1}{{m_0}^2} \int \mathrm{d}^3x \int \mathrm{d}^3x' \, \langle \chi(\mathbf{x},t)\, \chi(\mathbf{x}',t) \rangle \, (\mathbf{x}-\mathbf{x}')^2 \tag{116}$$

where $\chi = \rho c$ is the mass-by-volume concentration. $\langle \chi(\mathbf{x},t)/m_0 \rangle$ can be regarded as the probability density of a randomly chosen contaminant particle. Likewise the correlation $1/(m_0^2)\, \langle \chi(\mathbf{x},t)\chi(\mathbf{x}',t) \rangle$ is the joint probability density for a randomly chosen particle pair. The right hand side can therefore be interpreted as the mean square separation of particle pairs in the puff. Σ is therefore a two-particle statistic which must be determined from repeated experiments involving measurements of two (or more) particles. In order to measure the two-point correlation function $\langle \chi(\mathbf{x},t)\, \chi(\mathbf{x}',t) \rangle$ simultaneous concentration time series must be available for many spatial positions. The situation is analogous for measurements of the plume width for continuous releases, which is also a two-particle statistic. Unfortunately this prescription is seldom followed in experiments, since the vast majority of dispersion experiments are devoted to measurements of $\langle \chi \rangle$. From these experiments one can calculate a width using the correlation of the average concentration in (98), i.e.

$$\Sigma_f^2 = \frac{1}{2{m_0}^2} \int \mathrm{d}^3x \int \mathrm{d}^3x' \, \langle \chi(\mathbf{x}',t) \rangle \, (\mathbf{x}-\mathbf{x}')^2 \tag{117}$$

which is equivalent to

$$\Sigma_f^2 = \sigma_{xf}^2 + \sigma_{yf}^2 + \sigma_{zf}^2 = \frac{1}{m_0} \left\langle \int (\mathbf{x} - \langle \mathbf{X} \rangle)^2 c\rho \, \mathrm{d}^3x \right\rangle \tag{118}$$

Σ_f can be interpreted in terms of the rms distance between two particles randomly chosen from two *different* puffs realizations. We can also interpret Σ_f as the size of the volume where contaminant particles are likely to be found for an ensemble of repeated experiments. In the same way Σ is the average size of the instantaneous puff volume, regardless of where its centre may be located. Σ_f is always larger than Σ, in fact

$$\Sigma_f^2 = \Sigma^2 + \Sigma_c^2 \tag{119}$$

where Σ_c^2 is the (ensemble) variance of the centre position $\mathbf{X}$. Usually Σ_f^2 and Σ_c^2 are of the same order of magnitude while Σ^2 is considerably smaller. From the URAHFREP field experiments (Ott and Jørgensen 2001) detailed information on the concentration field was obtained by cross-plume lidar scanning. Both σ_y (i.e. the plume width based on two-particle statistics) and σ_{yf} (width based one-particle statistics with 3 minute averaging) were derived and typically $\sigma_{yf}^2/\sigma_y^2 \sim 3$. It therefore makes a considerable difference whether Σ of Σ_f is used to estimate concentrations, especially for long averaging times. We have found that Nieuwstadt's (1980) tabulated values of σ_{yf} for the Prairie Grass experiment (ten minute averages) are well represented by the simple relation $\sigma_{yf} = 3u_*t$. In the field experiments we find $\sigma_y = 0.7u_*t$, which gives an even larger ratio $\Sigma_{yf}^2/\Sigma_y^2 \sim 18$. Since concentrations are inversely proportional to Σ^2, the definition of the plume width is of

Even if two-particle statistics is more difficult to obtain experimentally than one-particle statistics, there are several reasons for preferring Σ for Σ_f. The instantaneous size is more relevant in modelling for example plume rise and explosion risks. Σ_f merely indicates the size of the volume where puffs may be found, and there are of course situations where this can be relevant, e.g. determination of a safe area. For plumes Σ_f also usually involves a time average rather than an ensemble average and the averaging time is significant. In the atmosphere Σ_f increases with averaging time. In some experiments a steady value is reached for long averaging times, in others there is no convergence since Σ_f just continues to

increase. It is therefore necessary to specify an averaging time. The problem is that the meandering of the centre Σ_c becomes a measure of the uncertainty of the wind direction for averaging times larger than about one minute. The dependence on meandering (through the dependence on averaging time) is awkward because meandering has little influence on the growth of a puff. Since Σ_c is governed by time large scales of the wind field it is also not well correlated with meteorological surface layer parameters, which probably explains the poor reproducibility of one-particle statistics. The reproducibility of Σ, and other Gallilei invariant two-particle statistics, is much better.

Deterministic models produce non-random trajectories reflecting a mean behaviour, and effects of meandering should be kept in mind when interpreting the results. The fact that the model plume trajectory is located strictly in the $x - z$ should therefore be taken with a grain of salt. Horizontal meandering effectively broadens the sector which is affected by the plume. In nature the plume is located somewhere within the affected sector, and its presence is intermittent. The determination of the width of the affected sector, and the concentration averaged over the sector, is the goal for the majority of dispersion experiments and models (σ curves). The aim of the present model is to represent the physical characteristics of the plume relative to its instantaneous, random position. This should make the model suited for assessment of instantaneous concentrations (relevant e.g. for explosion risks). If time averaged concentrations are needed, these can be obtained by smearing out the concentration over the width of the wider affected sector. This is a simple matter of convoluting the output concentration with the wind direction probability corresponding to the observation time, which can be done in post-processing. Vertical meandering can be treated in a similar way, but is could also be accounted for by adding randomness to the entrained air and/or by the introduction of random forces. In convective air the ground concentration is intermittent because parts of the plume are on the ground while others have lifted off. This is caused by alternating regions of up-draught and down-draught, which are generally larger in size than the plume. These are quit persistent, and it is a characteristic feature that plume elements tend to follow fairly straight lines. Plume elements on their way up are therefore likely to continue moving upwards, while elevate plume elements with a downward velocity are likely to hit the ground. The meandres are therefore mostly a result of individual plume elements following different directions. Meandres therefore tend to grow in size while keeping their proportions (this is difficult to measure, but visual observations leave this impression). Up-draughts are more rare than down-draughts and therefore also more intense, since $\langle w \rangle = 0$ by mass conservation. In the surface layer the typical width of an up-draught structure scales with the height above the ground. In the mixed layer up-draughts grow to large convection cells comparable in size to the boundary layer height z_i. The intensity of vertical motion also grows with the height, and near the ground the large convection cells in the mixed layer above have little effect.

These considerations suggest that the vertical component of the ambient velocity w_a should be included for convective conditions. It should be constant in each model run, and the value should be drawn from an ensemble. The pdf of w_a can be found from anemometer measurements. Adding randomness to the model input in this way can be anadvantage, in particular in the convective case. Here the trajectories of a passive contaminant are unstable, in nature as well as in models. Whether a plume goes up or down may therefore depend on the detailed initial conditions or even on numerical errors. This difficulty is overcome when the deterministic model is run with representative random values of w_a. The approach also circumvent another problem, namely that an envelope which is wide enough to always contain the plume would have an unrealistically large inertia and (109)

would not be valid. We therefore choose to interpret the diameter of envelope as being sufficiently large to contain the instantaneous cloud with its particular meandres, but too small to contain meandres at any time.

Finally, we note some recent experimental results for relative diffusion. They regard the so-called distance-neighbour function $\mathcal{D}$ which is defined as follows

$$\mathcal{D}(\mathbf{x}',t) = \frac{1}{{m_0}^2} \int \langle \chi(\mathbf{x}+\mathbf{x}',t)\chi(\mathbf{x},t)\rangle \, \mathrm{d}^3x \tag{120}$$

$\mathcal{D}(x',t)$ can be interpreted as the pdf at time t of the separation between two randomly chosen contaminant particles. We may also interpret $m_0\mathcal{D}(\mathbf{x}')$ as the mean concentration in the surroundings of a randomly chosen particle. We note that

$$2\Sigma^2 = \int |\mathbf{x}'|^2 \, \mathcal{D}(\mathbf{x}',t) \, \mathrm{d}^3x' \tag{121}$$

The distance-neighbour function was introduced by Richardson (1926), who also offered a simple model for inertial range turbulence. Richardson proposed to use a diffusion equation with a diffusivity $K(|\mathbf{x}'|)$ depending on the separation $|\mathbf{x}'|$, but independent of time. In inertial range turbulence the energy dissipation ε is the only scaling parameter, hence K must be of the form $K = C'\varepsilon^{1/3}|\mathbf{x}'|^{4/3}$, where C' is a numerical constant, and

$$\frac{\partial \mathcal{D}(r,t)}{\partial t} = \frac{1}{r^2}\frac{\partial}{\partial r} C'\varepsilon^{1/3} r^{10/3} \frac{\partial \mathcal{D}(r,t)}{\partial r} \tag{122}$$

Recent direct measurements made by Ott and Mann (2000) show that $\mathcal{D}$ closely follows the solution to (122), see figure 14.

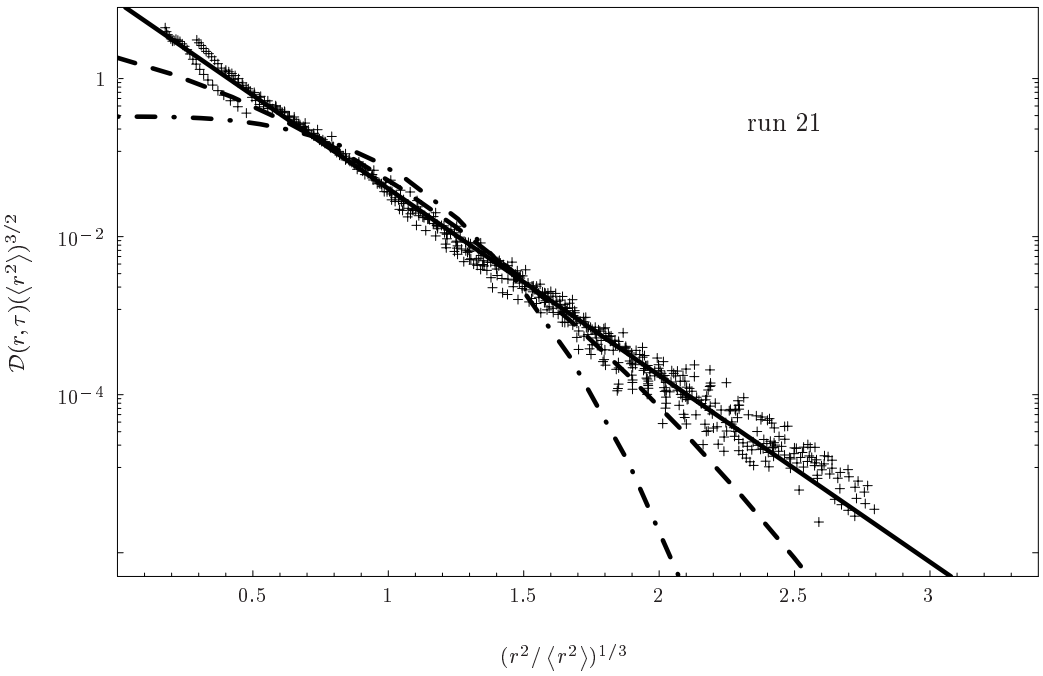

Figure 14. Distance neighbour function (points) compared to the predictions of Richardson (solid), Kraichnan (dashed), and Batchelor (dot-dashed).

In plumes a distance-neighbour function $\mathcal{D}(y,t)$ can be defined by means of the concentration on a line across the plume; t is the travel time x/U. Such measurements can be made with a lidar. In the neutral surface layer the friction velocity u_* is the only scaling parameter, hence we may copy Richardson's approach and

postulate a diffusion equation for $\mathcal{D}(y,t)$ with $K = \gamma\, u * |y|$, where γ is a numerical constant, viz.

$$\frac{\partial \mathcal{D}(y,t)}{\partial t} = \frac{\partial}{\partial y}\gamma u_* |y| \frac{\partial \mathcal{D}(y,t)}{\partial y} \tag{123}$$

The solution to this equation is

$$\mathcal{D}(y,t) = \frac{\exp\left(-\frac{|y|}{\sigma_y}\right)}{2\sigma_y} \tag{124}$$

where

$$\sigma_y = \gamma u_* t \tag{125}$$

Figure 15 shows an example of $\mathcal{D}$ measured in the Borex experiment (Jørgensen and Mikkelsen 1993). It is extremely close to an exponential (note the logarithmic scale). A linear growth of σ_y with travel time was also observed. The experimental results show a remarkable reproducibility of the distance-neighbour function.

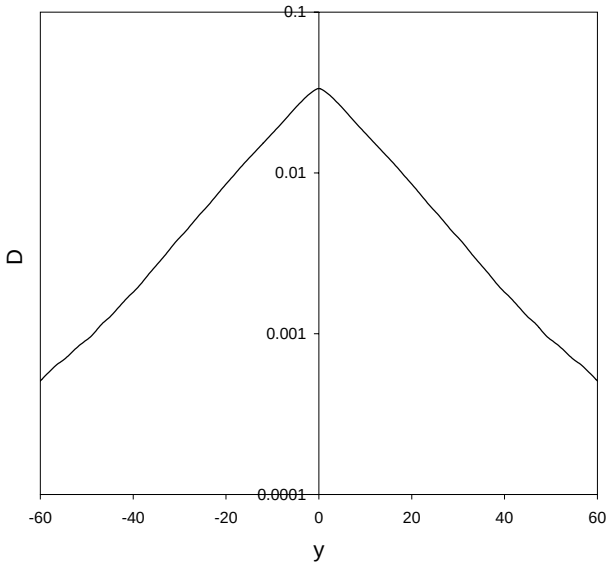

Figure 15. Distance neighbour function obtained from lidar measurements (Borex8a).

4.4 Cloud growth

Passive clouds

The growth of a passive puff can be divided into several regimes each characterized by a different behaviour. Very tiny puffs depend on molecular diffusion and viscosity, but they are not relevant in this context because of the small size of the microscale of atmospheric turbulence (a few millimeters). For puffs much larger than the microscale, but still much smaller than the integral length scale, the growth is governed by inertial range turbulence. Inertial range turbulence is approximately isotropic and characterized by a single parameter, the turbulent kinetic energy dissipation rate ε. We will call this the Richardson diffusion regime. For this we have

$$\left\langle (\Delta \mathbf{x})^2 \right\rangle = C\,\varepsilon\,t^3 \tag{126}$$

where $\Delta\mathbf{x}$ is the vector between two randomly chosen particles in the puff and C is a numerical constant. Since $\Sigma^2 = \frac{1}{2}\left\langle (\Delta \mathbf{x})^2 \right\rangle$ we have

$$\Sigma^2 = \frac{1}{2}\,C\,\varepsilon\,t^3 \tag{127}$$

The value of the constant C, which is related to C' in (122), was measured by Ott and Mann (2000) who found $C = 0.4 - 0.6$. This regime is relevant for elevated releases that are well above the ground. In this regime puffs grow rapidly.

Puffs that are much larger than the integral length scale of the turbulence, l, should theoretically grow as

$$\Sigma^2 = 2\left\langle (\mathbf{u}')^2 \right\rangle T_L\,t \tag{128}$$

where $\left\langle (\mathbf{u}')^2 \right\rangle$ is the turbulent kinetic energy and T_L is the Lagrangian time scale, which is proportional to $\frac{\left\langle (\mathbf{u}')^2 \right\rangle}{\varepsilon}$. In this limit the growth is governed by a normal diffusion equation with constant eddy diffusivity which produces Gaussian puffs. This is the only regime where the analogy between molecular diffusion and turbulent diffusion truly holds. However, a condition for a normal diffusion regime is that the turbulence is homogeneous in the volume under consideration. Therefore $\left\langle (\mathbf{u}')^2 \right\rangle$ and ε must be constant, and this condition is seldom fulfilled. In the neutral atmospheric surface layer we have $\varepsilon = \frac{u_*^3}{\kappa z}$, hence ε is profoundly non-constant near the ground. Moreover, l is proportional to z so the surface layer is not homogeneous at all. When an elevated puff has grown out of the Richardson regime, it will therefore not enter a normal diffusion regime as is often said. The Richardson regime ends when $\Sigma \sim l \sim z$, which is approximately when the puff has grown large enough to touch the ground. From then on the puff therefore becomes ground based, limited to grow upwards only. Since the centre climbs upwards, both l and Σ grow and the condition $\Sigma \sim l \sim z$ continues to be valid. Consequently, a normal regime with $\Sigma \gg l$ is never reached. Instead the diffusion enters yet another regime valid for grounded clouds in the surface layer. Since the surface layer is characterized by the friction velocity u_* and the Monin-Obukhov length scale L, the puff size is determined by these two parameters and time. For dimensional reasons we therefore have

$$\frac{\Sigma}{u_* t} = \mathcal{F}_\Sigma\left(u_* t/L\right) \tag{129}$$

where $\mathcal{F}_\Sigma$ is a universal function. In the neutral atmosphere, where $L \to \pm\infty$, we simply get

$$\Sigma^2 = (\lambda u_* t)^2 \tag{130}$$

where λ is a numerical constant. By analogy a similar result holds for plumes if Σ is a cross-plume length scale (width, height or thickness) and t is interpreted as the travel time $t = X/U$. In the URAHFREP field experiments we found that the plume width grows as $\sigma_y \approx 0.8 u_* t$, and this correlation is in fact valid even for unstable conditions. It also fits data from the Madona and the Borex experiments. This experimental result is quite remarkable, because in conventional Gaussian plume models there is a strong dependence of the plume width on stability. These models are based on one time averaged plumes and therefore include meandering in the plume width.

From the field experiment we also find that the centroid height of the plume, Z, is well represented by the relation $Z \approx 0.6 u_* t$ for $-u_* t/L < 0.2$. For $-u_* t/L > 0.2$

data are sparse and scattered, but the growth is clearly faster for more unstable conditions. A similar stability dependence is seen for the plume thickness. One could expect thermal convection to affect the vertical growth, so the apparent lack of coupling to the lateral growth is surprising.

It must be kept in mind that the ratio z/L is the proper measure of atmospheric stability, and therefore the height above the ground (or cloud height) determines the impact of stability. For $z < -0.1L$ mechanical friction dominates the effects of convection and the atmosphere can be considered is neutral. Above, for $z > -0.1L$, free condition prevails, and the transition between the two regions is fairly sharp. In free convection the ground friction is unimportant and the wind profile is flat. The wind field therefore merely represents a uniform translation, and u_* becomes unimportant. In free convection we can therefore eliminate u_*, so that we only have one scaling parameter, e.g. the vertical buoyancy flux $B = \frac{\langle Tw \rangle g}{T} = -\frac{{u*}^3}{\kappa L}$. For dimensional reasons we must have

$$\Sigma^2 = C_\Sigma \frac{g \langle Tw \rangle t^3}{T} = -C_\Sigma \frac{(u_* t)^3}{\kappa L} \tag{131}$$

where C_Σ is a constant (which depends on the exact definition of Σ). Note that $-\frac{u_*^3}{L\kappa}$ is the mechanical energy production caused by convection, which is always smaller than ε and comparable to ε for strong convection. Thus (131) and (127) have similar structures. This type of growth can continue until the final depth of the boundary layer z_i becomes important. The region where (131) applies is roughly limited to the lower tenth of the boundary layer, hence $-L$ must be less than about $0.1 z_i$ for this regime to exist. The condition $-L < 0.1 z_i$ is often satisfied in the atmosphere, but it is difficult to study in a wind tunnel, because $0.1 z_i$ will only amount to a few centimeters. Therefore there are few data to build on, and very few involve relative diffusion.

The Prairie Grass experiment contains many unstable trials, also in the free convection regime. The data was analyzed by Nieuwstadt (1980), Briggs (1982) and Venkatram and Du (1996). Direct measurements of the plume centroid are not available (most samplers were placed close to the ground) so a surrogate plume thickness Z_{ps} was used. Z_{ps} is based on integrals of the ground level concentration across the plume, i.e. $Z_{\mathrm{ps}} = \frac{m_0}{u_a \int \langle \rho c(x,y,0) \rangle \, \mathrm{d}y}$. One can expect Z_{ps} to be a good estimate for Z when the maximum concentration in the plume is on the ground and the profile is approximately self similar. For $-Z/L$ larger than about 1 plume become elevated and Z_{ps} will tend to overestimate Z. In the URAHFREP experiments both Z_{ps} and the centroid elevation Z were measured. For grounded plumes the values are well correlated so that

$$Z_{\mathrm{ps}}/Z = 1.4 \pm 0.1 \tag{132}$$

This is based on all experiments except trial 12, where the the plumes showed signs of lift-off. Z_{ps} is based on measurements taken on the ground, where convection is dominated by shear, so even for strong convection the ground concentration cannot be fully determined by pure convection. Therefore (132) is restricted to $-u * t/L$ less than about 1, where plumes exhibit neutral behaviour. The trend in the URAHFREP data is that the ratio Z_{ps}/Z increases when $-u * t/L > 1$. Combining (132) with Nieuwstadt's data analysis we find

$$Z^2 = -1.0 \frac{u_*^3}{L} t^3 \tag{133}$$

So-called mixed layer scaling is sometimes assumed for the upper 90% of the convective boundary layer. This means using z_i and $w_* = (g z_i \langle Tw \rangle / T)^{1/3}$ as

scaling parameters instead of L and u_*. It should be noted that (131) is consistent with mixed layer scaling because it can be rewritten as

$$(\Sigma/z_i)^2 = C_\Sigma (w_* t/z_i)^3 \tag{134}$$

In this equation the z_is are dummy because they cancel out when $w_* = (g z_i \langle Tw \rangle / T)^{1/3}$ is inserted. Nieuwstadt actually used mixed layer scaling so his correlation for $Z_{\rm ps}$ is $Z_{\rm ps}/z_i = 0.9(w_* t/z_i)^{3/2}$ and observed a very nice collapse by plotting $Z_{\rm ps}/z_i$ against $w_* t/z_i$. However, this may simply be due to the correlation through the common factor z_i. Therefore (134) would appear to be justified by such a plot even if the z_is were completely random (the more random the better!). Plotting $-Z_{\rm ps}/L$ vs. $-u_* t/L$ also produces a nice curve, but here L plays a similar role as a common factor. Better plots are obtained when $Z_{\rm ps}$ is scaled with the downwind distance x, since this to a large extent eliminates build in correlations (though not completely since $t = x/U$). Mixed layer scaling predicts that $x/(w_* t)$ is a function of $w_* t/z_i$, while surface layer scaling predicts that $x/(u_* t)$ is a function of $-u_* t/L$. Hence $Z_{\rm ps}/x$ vs. $w_* t/z_i$ should collapse according to mixed layer scaling, while $Z_{\rm ps}/x$ vs. $-u_* t/L$ should collapse according to surface layer scaling. Comparing the two graphs (figure 16) it is evident that surface layer scaling performs best. Therefore there does not seem to be a need for z_i.

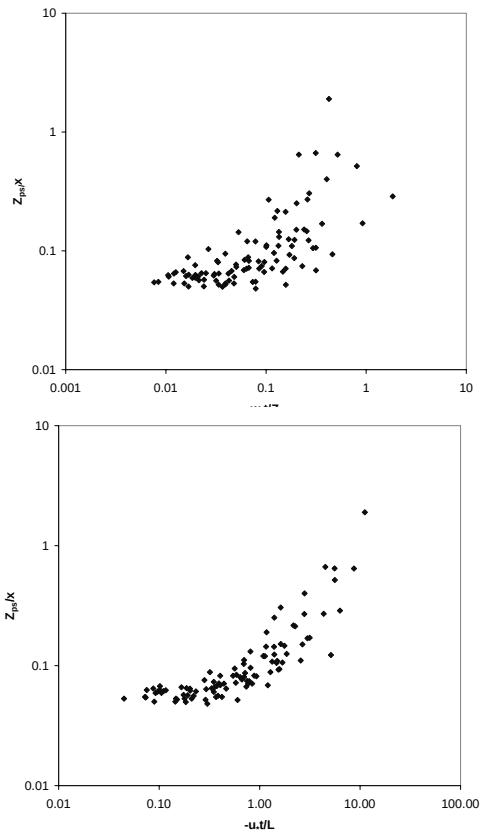

Figure 16. Top:$Z_{\rm ps}/x$ vs. $w_* t/z_i$ (Mixed layer scaling). Buttom: $Z_{\rm ps}/x$ vs. $-u_* t/L$ (Surface layer scaling).

Nieuwstadt also analysed the plume width σ_{yf}, based on ten minute averages, and found that $\sigma_{yf}/z_i = 0.6 w_* t/z_i$ is in good agreement with data. In this relation the z_is do not cancel, hence there seem to be a genuine dependence on the boundary layer height. Re-analysing the data we find that $\sigma_{yf}/(w_* t) = 0.7 \pm 0.24$.

Applying the same exercise to $\sigma_{yf}/(u_* t)$ we find $\sigma_{yf}/(u_* t) = 2.95 \pm 0.97$, which is in fact a slightly better fit. This result indicates that the behaviour of plumes on the ground is governed by local turbulence quantities and local fluxes rather than effects caused by the value of z_i. It should be noted that the measured σ_{yf} is for the time averaged plume, where we are interested in the relative diffusion plume width σ_y. As already noted the URAHFREP trials yielded $\sigma_y = 0.8 u_* t$, with is considerably smaller coefficient. There was also no apparent dependence on stability. Surface layer scaling will break down eventually at plume elevations comparable to z_i, but these results indicate that surface layer scaling still is a good approximation not only in the surface layer but also in the free convection zone above it. Mixed layer scaling is therefore only relevant when the plume reaches far into the boundary layer. When this happens the plume will soon be spread to fill the whole boundary layer and the vertical growth stops.

Stable stratification is generally a result of hot air entering over cold land. It is found at night or when a dense cloud cover shields out the sun. The temperature profile is inversed with cold, dense air below, and the heat flux is directed from the air down to the ground (L positive). The downward heat flux acts as a turbulent kinetic energy sink. The turbulence is therefore reduced compared to neutral or convective conditions and the integral length scale of the turbulence is also reduced. The stable boundary layer is therefore less able to mix and dilute a contaminant cloud. Elevated plume trajectories tend to be strictly horizontal even if the terrain is not completely flat. An elevated plume may therefore bounce into an isolated hill or a building.

The depth of the boundary layer is also small, 100m is often quoted as a typical value, but in strong stability it can be an order of magnitude smaller. Material emitted into the boundary layer tends to stay there, so the effect of the final depth of the boundary layer can be large even close to the source. Above the boundary layer the air is neutrally stratified and there is very little turbulence. Due to the shallow depth of the boundary layer, elevated sources (stack, vent on a roof) are likely to be outside the boundary layer. In that case the vertical growth is essentially controlled by the turbulence induced at the source, the thickness will approach a final value and contaminant is not likely to reach the ground over flat terrain.

In strong stability ($L \sim +0$) the turbulence structure is dominated by the dynamic decoupling of strata (layers), which tend to slide almost frictionless on each other. Surface layer scaling does not work for lateral wind components. The lateral dispersion of a plume is much larger than the vertical, and is very hard to predict because it may depend on a number of factors that are not covered by the usual micro-meteorological parameters.

Very stable conditions are found in open terrain at nights with little wind and few clouds, which is not unusual. These conditions define worst case dispersion scenarios, yet they are not well understood. The stable stratification tends to inhibit the turbulence, and turbulent diffusion drastically reduced, and the boundary layer can be very shallow, perhaps only ten metres. The turbulent length scale is reduced so that $l \propto L$, except close to the ground, and the conditions are independent of z (z-less scaling regime). In other words the conditions are homogeneous and the growth of a puff should follow

$$\Sigma^2 = C_s \, u_* L \, t \tag{135}$$

Such a behaviour was observed by Bennett, Jørgensen, Lyck, Løfstrøm, Mikkelsen and Ott (1999) for the vertical growth. However, the lateral growth is much larger than the vertical growth so (135) can only be expected to hold for the vertical spread σ_z. The lateral spread is dominated by large fluctuations generated by

layers in the stratified air sliding on each other in different directions. Such motion can be induced by local terrain effects (drainage flows), meso-scale effects and perhaps even by gravity waves. In addition the stable boundary layer is unsteady. During the night the air is cooled by the cold surface and by direct radiation to the universe. As the density gradient develops the turbulence dies out and the friction between layers is reduced. As a result $\mathrm{d}u/\mathrm{d}z$ increases, and eventually the profile contains enough energy to mix the layers. At that point the stratification breaks down in a burst of turbulent mixing, which evens out the temperature and velocity profiles and the process starts all over again. A cycle may take about one or two hours. Unfortunately there are very few dispersion data for this situation. The processes involved are not fully understood and the implications for dispersion modelling are unclear. Further research is needed on dispersion in the nocturnal boundary layer.

Entrainment model

The entrainment rate is a central feature of a dispersion model. For an elevated plume the radius is $r = \sqrt{A/\pi} = \sqrt{2}\sigma$, where is defined by the y–component, say, so that $\sigma_y^2 = \Sigma^2/3$. For a passive (volume preserving) plume we have

$$u_e = \frac{\mathrm{d}r}{\mathrm{d}t} = \sqrt{2}\,\frac{\mathrm{d}\sigma}{\mathrm{d}t} \tag{136}$$

For a plume on the ground the cross-section is regarded as a semi-disk, with $A = \pi\sigma^2$ and $r = \sqrt{2A/\pi}$, so (136) is still valid. The simplest situation is for an elevated cloud where shear plays a minor role, in other words the Richardson regime. From (127) it follows that

$$u_e = \sqrt{(2)}\frac{\mathrm{d}\sigma_y}{\mathrm{d}t} = \left(\frac{9C\varepsilon\sigma_y}{16}\right)^{\frac{1}{3}} \tag{137}$$

For elevated plumes may substitute $\varepsilon = u_*^2\frac{\mathrm{d}U(Z)}{\mathrm{d}Z} + \frac{g\langle wT\rangle}{T}$, which simplifies to $\varepsilon = \frac{u_*^3}{\kappa Z}$ in neutral conditions.

We will make the assumption that (137) holds even when Z, and thereby ϵ, varies. This neglects 'memory' to a certain extent, which may not be permissible if ε varies too rapidly. Taking such memory effects into account would be extremely difficult, since it would require the development of a general, rigorous theory of turbulent diffusion.

For ground based plumes we shall stretch the arguments even further. A ground based plume is constrained by the presence of the ground, which also modifies the turbulent wind field considerably. Nevertheless, we still use (137) with a suitable value of ε. Thus a plume on the ground is considered as the upper half of a hypothetical axi-symmetric free plume which extends below the ground surface. In (137) we evaluate ε by its ambient value the height $\beta_\varepsilon\sigma_y$. The assumed axi-symmetry means that $\sigma_y = \sigma_z$. For a mirrored plume on the ground the centre is on the surface and we should define σ_z as the mean of z^2 rather than $(z-Z)^2$. For near neutral conditions we have $\varepsilon(\beta_\varepsilon\sigma_y)) = \frac{u_*^3}{\kappa\beta_\varepsilon\sigma_y}$ and (137) reduces to

$$\frac{\mathrm{d}\sigma_y}{\mathrm{d}t} = \lambda u_* \tag{138}$$

with

$$\lambda = \left(\frac{9C}{16\kappa\beta_\varepsilon}\right)^{\frac{1}{3}} \tag{139}$$

The linear growth of σ_y with time for a grounded plume is consistent with surface layer scaling and observations. Moreover, the value of λ is very reasonable. The URAHFREP data give $\sigma_y = (0.69 \pm 0.11)u_*t$ and $\sigma_z = (0.82 \pm 0.13)u_*t$. The Borex experiments give $\sigma_y = 0.75u_*t$. These correlations are for near neutral conditions ($0 > u_*t/L > -0.5$). Assuming the 'natural' value $\beta_\varepsilon = 1$ and the measured $C = 0.5$ (Ott and Mann 2000), equation (139) yields $\sigma_y = 0.89u_*t$ in good agreement with the observations.

Thus (137) works both for grounded and for elevated plumes. In the intermediate case we still apply (137) with $\sigma = r/\sqrt{(2)}$ where r is the radius of a disk with a section cut off.

This procedure is convenient because it could bring down the number of model parameters and we shall use it even for non-neutral conditions (where there are correction terms to ε). In URAHFREP data σ_y grows linearly with time even in convective conditions, while there are indications that σ_z (with the plume centre on the ground) grows faster than linear for $-u_*t/L$ larger than about 0.4. A plausible explanation for this is that the plume starts to rise because of heating, and this view is supported by the fact that the centroid Z also seems to grow with a faster than linear rate for $-u_*t/L > 0.4$.

For a grounded plume in convective conditions we may evaluate ε by the simplified expression

$$\varepsilon(z) = u_*^2 \frac{\mathrm{d}U}{\mathrm{d}z} + \frac{\langle Tw \rangle\, g}{T} \approx \frac{u_*^3}{\kappa z}\left(1 - \frac{z}{L}\right) \tag{140}$$

This equation is a simplified kinetic energy balance. McBean and Elliott (1975) argues that the divergence of the energy flux and the pressure transport term can be neglected since they are small and tend to cancel. We have also assumed a logarithmic wind profile without Monin-Obukhov corrections (they are of course included in the code). This leads to an overestimate of the mechanical production, but it is small compared to the buoyancy production term. Inserting this $\varepsilon(\sigma_y)$ into (137) we get

$$\frac{\mathrm{d}\sigma_y}{\mathrm{d}t} = \lambda u_* \left(1 - \frac{\sigma_y}{L}\right)^{\frac{1}{3}} \tag{141}$$

which has the analytic solution

$$\sigma_y = -L\left[\left(1 - \frac{2\lambda u_* t}{3L}\right)^{\frac{3}{2}} - 1\right] \tag{142}$$

The right hand side does not deviate appreciably from $\lambda u_* t$ unless $-u_*t/L$ is as large as about 10. At that point the plume is no longer grounded which was assumed in the calculation. In other words, there should not be an enhanced growth of the plume at the point where the plume begins to lift off from the ground. This is consistent with the linear behaviour of σ_y that was observed in the URAHFREP field trials.

Experimental studies of rising line thermals have revealed a characteristic structure, Richards (1963). The positive buoyancy pulls up the mid section of the plume and creates a double vortex. The material is concentrated in two cores instead of one as for a passive plume. It is natural to expect an entrainment velocity roughly equal to the vertical velocity of the thermal. In rising buoyant plumes buoyancy forces therefore induce additional mixing, which is often the largest contribution to the plume growth. Hoult, Fay and Forney (1969) suggested to model the entrainment velocity as a sum of two separate contributions for the longitudinal and the transverse components of the velocity difference. For each of these we may define an entrainment velocity

$$u_{e\parallel} = \beta_{\parallel}|(\mathbf{u} - \mathbf{u}_a) \cdot \mathbf{k} \tag{143}$$

$$u_{e\perp} = \beta_{\perp}|(\mathbf{u} - \mathbf{u}_a) \cdot \hat{\mathbf{k}}| \tag{144}$$

This approach is followed my most modellers, but the values of the numerical constants $\beta_{\parallel}$ and $\beta_{\perp}$ vary somewhat, Bricard and Friedel (1989) gives a list of values used in various models. The value is of course linked to the definition of the cloud envelope or area A. We choose $\beta_{\parallel} = 0.08$ and $\beta_{\perp} = 0.5$.

The two entrainment coefficients are relevant in different situations. $\beta_{\parallel}$ is relatively unimportant except close to the source where the plume/jet is influenced by source induced momentum. $\beta_{\perp}$ is important only during plume rise (and descent). The effect of a large value of $\beta_{\perp}$ is not only to make the plume grow faster during plume rise, but also to slow down the ascent. The 'ballistic' type of models we are discussing here tend to overestimate plume rise when forces counteracting buoyancy are not properly accounted for and may therefore need a too large of $\beta_{\perp}$ in order to reproduce the plume rise. We use added mass as a more appropriate way to slow down the rise.

Including the contribution u_{ea} from the ambient turbulence as discussed in the previous section we have three contributions to the entrainment velocity. We choose to calculate the total entrainment rate as the rms value of these three contributions. The processes rarely compete so it would make little difference if we choose the largest value or the sum as some modellers prefer it.

4.5 Added mass

We now return to the momentum equation (109) to discuss the residual pressure P', which was defined as the difference between P and the hydrostatic pressure corresponding to the mean density profile. The term $\int_{\partial B} P'\hat{\mathbf{n}}\mathrm{d}A$ contains the interaction of the cloud with the surrounding air. This has already been taken into account by the inclusion of a drag force, but there is more.

Meandering is a well known feature, which has considerable impact on real plumes, but such randomness has been removed in the model trajectory. The justification for the removal of meandering is that it has little influence on the growth rate of the cloud since this is driven by turbulent mixing on relatively small length scales. The regular model trajectories should be interpreted with some allowance for irregularities caused by meandering and random up- and down-draughts. Models based on one-particle diffusion incorporate meandering in the definition of the plume cross-section A, which is made big enough to envelope the meandering cloud. This is unfortunate because it leads to artificially low concentrations and too high inertia of the cloud. When buoyancy effects are involved it is important to keep A at a right size which reflects the actual dimensions of an instantaneous cloud. For thermodynamic calculations it may even be an advantage to choose A so small that the concentration is non-zero at the surface, and not all contaminant material is contained inside, because this may produce a representative average concentration. This, on the other hand, is awkward since it would be necessary to consider *de*-trainment, which would be difficult to model in a realistic way. For dynamic calculations a somewhat larger A is preferable because the plume may disturb the flow beyond also where there is no contaminant. Below we attempt to model this disturbance of the flow outside A in a simple way, which makes it possible to incorporate it into the equations of an integral model.

A rising plume is an injection into to the wind field. Although a rising plume is completely flexible it still represents a volume which the ambient air must find its way around. In this way it acts as if it were a solid object. We will therefore

model the flow around a rising plume by considering the plume as a solid cylinder. In order to simplify matters we will disregard entrainment in this connection and consider the plume surface as impenetrable. We will also regard the plume surface to be ideally smooth since this seems more appropriate than the usual no-slip boundary conditions for solid surfaces. The plume is modeled as a horizontal infinite cylinder aligned in parallel with a uniform wind field. Motion along the horizontal plume axis is assumed not to affect the ambient flow, hence may use a reference frame at rest with respect to the wind field, which is therefore zero. This eliminates flow along the cylinder axis and reduces the flow to two dimension. With all these simplifications the problem has a solution in terms of an irrotational potential flow, i.e. a flow of the form $\mathbf{u} = \nabla\phi$.

We recall that 2D potential flow fields $\mathbf{u}(x, y) = (u(x, y), v(x, y))$ are linked to complex analytic functions in the following way. The xy plane is identified with a complex z-plane through $z = x + iy$, and the flow field is represented by the complex function $w(z) = u(x, y) - iv(x, y)$. If the flow is irrotational and incompressible then w is analytic, and visa versa. Furthermore, if $w = \frac{\mathrm{d}\lambda}{\mathrm{d}z}$ where $\lambda(z)$ is a (time dependent) complex analytic function then Navier-Stokes equation is satisfied. The potential ϕ is the real part of λ while $\psi \equiv \mathrm{Re}\lambda$ is constant along stream lines.

Consider flow around a disk of radius a moving along the x-axis, so that centre coordinates are $(0, c(t))$. This problem has the simple solution

$$\lambda(z) = -\dot{c}\frac{a^2}{z - c} \tag{145}$$

where $\dot{c} = \frac{\mathrm{d}c}{\mathrm{d}t}$ is the velocity of the disc. The kinetic energy is $\frac{1}{2}\rho_a \mathbf{u}^2 = \frac{1}{2}\rho_a |w|^2 = \frac{1}{2}\rho_a \frac{\dot{c}^2 a^4}{|z-c|^4}$, hence total kinetic energy of the fluid is given by

$$E_{\mathrm{kin,fluid}} = \int_a^\infty \frac{1}{2}\rho_a \frac{a^4\dot{c}^2}{r^4}\, 4\pi r^2\, \mathrm{d}r = \frac{1}{2}\rho_a \pi a^2 \dot{c}^2 \tag{146}$$

If we place the disc in a conservative force field, the external force on it is equal to $F = -\nabla\, E_{\mathrm{pot}}(c)$, where $E_{\mathrm{pot}}(c)$ is the potential energy. The Lagrangian of the system consisting of both the disc and the fluid is then given by

$$\mathcal{L}(\dot{c}, c) = E_{kin} - E_{pot} = \frac{1}{2}(\rho + \rho_a)\pi a^2\, \dot{c}^2 - E_{pot}(c) \tag{147}$$

The equation of motion is given by the general Euler-Lagrange equation

$$\frac{\mathrm{d}}{\mathrm{d}t}\frac{\delta\mathcal{L}}{\delta\dot{c}} - \frac{\delta\mathcal{L}}{\delta c} = 0 \tag{148}$$

which in this case becomes

$$\pi a^2(\rho + \rho_a)\frac{\mathrm{d}^2 c}{\mathrm{d}t^2} = -F(c) \tag{149}$$

This equation is the same as it would have been in vacuum except that the density of the disc ρ has been replaced by $\rho + \rho_a$. This demonstrates the added mass effect which was introduced into the problem of rising thermals by Escuder and Maxworthy (1973). For a rising plume, where $\rho < \rho_a$, it means that more than half of the buoyancy forces are transferred to the ambient flow, so it is not a small effect. The simplest way to include added mass is to substitute $(\rho + \rho_a)W$ for ρW in the momentum equation, but leave the horizontal component ρU unchanged. This is the approach also followed by Weil (1988). The plume axis is not strictly horizontal so it is an approximation. A more general, and also more complicated, set of the equations is developed in appendix A where we also discuss added mass effects at boundaries.

4.6 Heat budget for a grounded plume

The water tank experiments of Willis and Deardorff (1976) show that passive plumes from a ground sources lift off in convective conditions. A model that pretends to cope with lift-off buoyancy effects must be able to reproduce this behaviour. The turbulence of the convective boundary layer is dominated by thermals that start at the ground and merge into still larger structures as they ascend. Imagine that we passively mark the air that passes a spot on the ground. The plume of marked air is of course as good as any passive plume, and we may apply the model to it. As long as the plume is close to the ground we are in the near neutral regime, where the temperature profile is logarithmic, viz.

$$T_a(z) = T_0 - \frac{\langle Tw \rangle}{\kappa_T u_*} \log\left(\frac{z}{z_0}\right) \tag{150}$$

In this regime plume dimensions grow linearly in time. Setting the cross-plume area $A = hb$, where H is the plume height and b is the plume width we may write the enthalpy budget equation as

$$\frac{\mathrm{d}hbT}{\mathrm{d}t} = \langle Tw \rangle\, b + T_a(\beta h)\, \frac{\mathrm{d}hb}{\mathrm{d}t} \tag{151}$$

where β is a suitable constant so that $T_a(\beta h)$ represents temperature of the entrained air, which, in the model, is taken from the average profile. The first term on the right hand side represents the heat transfer from the ground, and the equation holds as long as the plume is on the ground. There is no loss term corresponding to heat transfer upward from the plume, because it is assumed that hb grows fast enough to avoid hot air from escaping from the plume, at least for a period until the plume lifts off. At that point the heat transfer from the ground ceases and heat stored in the plume is transported upwards by plume rise. Using the logarithmic temperature profile and the fact that h and b are proportional to t we get the simple result

$$T - T_a(\beta h) = \frac{1}{2} \frac{\langle TW \rangle}{u_*} \left(\frac{1}{\lambda_h} + \frac{1}{\kappa_T}\right) \tag{152}$$

where $\lambda_h = h/(u_* t)$. Thus the heating of the plume by the ground is compensated by mixing with ambient air that tends to cool it, and, as a compromise, $T - T_a$ ends up being constant. This makes the equation for the vertical momentum simple, i.e.

$$\frac{\mathrm{d}hbW}{\mathrm{d}t} = hb\frac{(T - T_a)g}{T_0} = -hb\frac{(\lambda_h + \kappa_T)u_*^2}{2\kappa\kappa_T \Lambda_h L} \tag{153}$$

The equation is easy to integrate with the result

$$Z = -\frac{(\lambda_h + \kappa_T)}{12\kappa\kappa_T \Lambda_h L} \frac{(u_* t)^2}{L} \tag{154}$$

We may define lift-off by the condition that the centroid height is equal to h so that the time to lift-off is given by

$$-\frac{u_* t_{\mathrm{lift-off}}}{L} = \frac{12\lambda_h^2 \kappa\kappa_T}{\kappa_T + \lambda_h} \sim 1.2 \tag{155}$$

where $\kappa = \kappa_T = 0.4$ and $\lambda_h = 0.9$ has been used. The URAHFREP data show deviations from the linear growth of Z at $-u_* t/L \sim 0.4$. Above this value the data are very scattered, so all we can say is that 1.2 is consistent with the data since it is higher than 0.4. The Prairie Grass data cover a wider range of stabilities, and here $-u_* t/L \sim 1.2$ agrees well with the point where $Z_{\mathrm{ps}}/(u_* t)$ is equal to twice the value in the neutral limit.

Of course this calculation depends on the assumed temperature of the entrained air. Using the mean profile temperature means that we assume that the entrained air is just a random sample. If we assume that the entrained air has a similar history as the marked plume then it should also have the same temperature. This would lead to a logarithmic increase of T with time instead. However, adjacent air parcels do not generally share a long history unless they are closer together than the Kolmogorov microscale, which is typically only a few millimetre, but a correlation could exist if the marked plume is part of a larger hot plume. In that case we should consider the larger plume instead and adjust $t = 0$ to the time where the larger plume emerged. Despite these uncertainties we interpret the finite value of the temperature difference $T - T_a \sim 1.8 \langle Tw \rangle / u_*$ as indicating a characteristic temperature rise for naturally occurring hot spot near the ground. On a sunny day $\langle Tw \rangle / u_*$ can be as large as 1K. According to this $\rho_a 1.8 \langle Tw \rangle / (Tu_*)$ is a typical naturally occurring density difference. A plume from a buoyant release must exhibit larger density differences in order to have a definite influence on the plume behaviour. In the same way $t_{\mathrm{lift-off}}$ can be interpreted as a typical time scale for air staying on the ground in a convective atmosphere.

We also note that Briggs's (1973) lift-off parameter $L_p = \frac{\Delta\rho h g}{\rho u_*^2}$ is equal to 5 at $t = t_{\mathrm{lift-off}}$. Briggs originally proposed $L_p \sim 2$ as a lift-off criterion (with an uncertainty of about a factor 4). In a later unpublished analysis of the experiments of Meroney (1979), Briggs raised the critical value to 29. As pointed out by Meroney, L_p decreases with distance for constant buoyancy point sources while it is constant for a transverse line source. L_p is an increasing function of t (or x) for the case considered in this section, as it would be for an HF cloud turning positively buoyant. Therefore the local criterion for lift-off, if there is such a thing, is that $L_p < 29$ or $L_p > 29$ as the case may be. The observed L_p values at lift-off differed by almost three orders of magnitude, and Meroney concludes that 'such wide variations of L_p at lift off precludes specification of a single critical value'. Ramsdale and Tickle (1998) reviewed lift-off models and experiments as part of the URAHFREP project. They point out that existing lift-off criteria are based on buoyancy conserving releases, and cannot immediately be generalized to flows where buoyancy varies without a better understanding of the necessary *local* conditions. They also conclude, based on the experimental evidence, that it is inadequate to assume that plumes simply lift off as soon as they become positively buoyant. The present model does this and although it seems to work for rising thermals, but we agree that this may not be adequate. The added mass effect included in the model is a step slows down the rise by a factor of two, there could be other factors inhibiting plume rise. In Appendix A we speculate on a possible enhanced added mass effect in the proximity of the ground which could make buoyant clouds stay on the ground. It is possible that this could improve the model without complicating the mathematical framework.

4.7 Concentration profiles

The model provides the plume cross-section area A, a mean concentration C and the height of the centroid Z. We also have decided the relation between A, Z and σ. Additional assumptions are necessary in order to construct the concentration profile $C(y, z)$ from these quantities. The concentration profile of a plumes close to the ground is conventionally modelled as a superposition of two profiles located symmetrically with respect to the ground, i.e.

$$C(x, y, z) = C_0 \phi(x, y, z - Z_c) + \phi(x, y, z + Z_c) \tag{156}$$

where

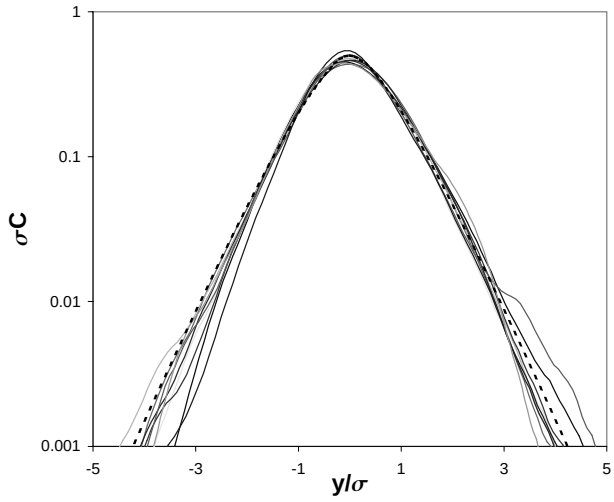

Figure 17. Thin lines: normalized moving frame depth integrated concentration obtained in the UHRAFREP trials. Dashed line: $(1/2 + |y|/\sigma)\mathrm{e}^{-2|y|/\sigma}$

$$C_0 = \frac{AC}{\int\int \phi(x,y,z)\,\mathrm{d}y\,\mathrm{d}z} \tag{157}$$

Z_c must be adjusted so that the centroid height is equal to Z. Gaussian profiles are by far the most popular, i.e.

$$\phi(x,y,z) = \exp\left[-\frac{y^2+z^2}{2\sigma^2}\right] \tag{158}$$

and $C_0 = C$.

Two-dimensional LIDAR profiles obtained during the UHRAFREP trials are shown in figure 17. The profiles were normalized and integrated in the vertical direction so the plot shows $\sigma_y \frac{\int \mathrm{d}z c(x,y,z)}{\int \mathrm{d}z\mathrm{d}y c(x,y,z)}$ versus y/σ_y for $x = 100$m. Moreover the y-axis was alligned for each LIDAR scan so that $y = 0$ corresponds to the plume centre. Only smoke data is shown, but the HF data are not different. The plot is remarkably reproducible, and similar plot from other experiments with different downwind distances look the same. The dotted curve is the function $\frac{1}{2}(1+2|y|/\sigma_y)\mathrm{e}^{-2|y|/\sigma_y}$ which makes a good fit to the data. It is noteworthy that the tails are exponential rather than Gaussian. Exponential tails have been observed also in other smoke experiments (Borex, Madona) and seem to be a characteristic feature. We propose to use the following two dimensional analog to the depth integrated profile

$$\phi(y,z) = (1+\sqrt{5}\frac{\sqrt{y^2+z^2}}{\sigma})\exp\left(-\sqrt{5}\frac{\sqrt{y^2+z^2}}{\sigma}\right) \tag{159}$$

The depth integrated concentration corresponding to this profile is not much different from $\frac{1}{2}(1+2|y|/\sigma)\mathrm{e}^{-2|y|/\sigma}$. With this profile the centre concentration becomes

$$C_0 = \frac{AC}{\int\int \phi(x,y,z)\,\mathrm{d}y\,\mathrm{d}z} = \frac{5}{3}C \tag{160}$$

For an elevated plume, where $A = \pi(\sigma_z^2+\sigma_y^2) = 2\pi\sigma^2$, the non-Gaussian profile has 89% of the contaminant is inside A, which should make A 'reasonably small, yet large enough to contain essentially all contaminant material' as previously stated. For comparison the Gaussian profile only contains 63% inside A. The

concentration at the centre is almost twice as high as for the Gaussian profile. It therefore matters a great deal which profile is choosen.

5 Comparison with field measurements

The URAHFREP field campaign is described in Ott and Jørgensen (2001). The experiments were designed as down-scaled releases because of limitations on release rates imposed by environmental and safety considerations. Hall (1997) and Hall and Walker (1997) show that so-called Froud scaling applies. This means that if lengths are scaled by the factor S then times should be scaled by $S^{\frac{1}{2}}$ while densities, temperature and humidity should be the same. Thus the release rate is scaled by $S^{\frac{5}{2}}$ and wind speed by $S^{\frac{1}{2}}$. The Monin-Obukhov length scale gets a factor S, i.e. the stability is scaled towards neutral. Low wind speeds combined with high relative humidities were preferred.

Each of the HF releases was followed by one or more passive smoke releases. This was done in order to highlight the influence of HF on the plume. A vertical cross–section of the plume 100m downwind of the source was scanned at intervals of about 1.5 seconds with lidar. In addition arrays of filter samplers, light-path instruments (fast concentration sensors), electrochemical sensors and thermocouples were placed at various distances and meteorology was monitored by fully instrumented meteorological mast.

There was generally no observable difference between HF and smoke at 100m. The exception was Trial 12 which was made under a combination of high relative humidity and very low windspeed. In this case the plume centre was raised above ground and maximum concentrations were not found above the ground. It should be noted that this behaviour was observed both for the HF plume and for the smoke plume made immediately after, although the riser of the plume centre was less for the smoke than for the HF. It is therefore not quite clear whether to what extent the behaviour was induced by HF or caused by the unstable atmosphere. It is likely that both factors contributed to the rise of the HF plume in Trial 12.

Model runs were made for all HF releases. Typical examples of output are shown in figures 18 and 19.

Plume geometry

Table 1. Comparison of predicted and observed centroid elevations and plume widths.

Trial	Z model m	Z observed m	σ_y model m	σ_y observed m
HF003	4.8	6.5	8.2	6.8
HF004	5.1	4.9	8.7	8.8
HF005	4.6	5.3	7.8	7.5
HF006	4.8	6.1	8.1	6.6
HF007	5.1	7.0	8.8	6.7
HF008	6.3	8.2	10.9	6.9
HF009	4.8	4.3	8.2	6.1
HF010	5.0	6.1	8.2	7.6
HF011	4.7	6.0	8.0	7.4
HF012	25.1	19.3	10.5	8.4

Plume dimensions at 100m were measured by the lidar and the centroid elevation Z and (moving frame) σ_y have been extracted from the data deduced. The results

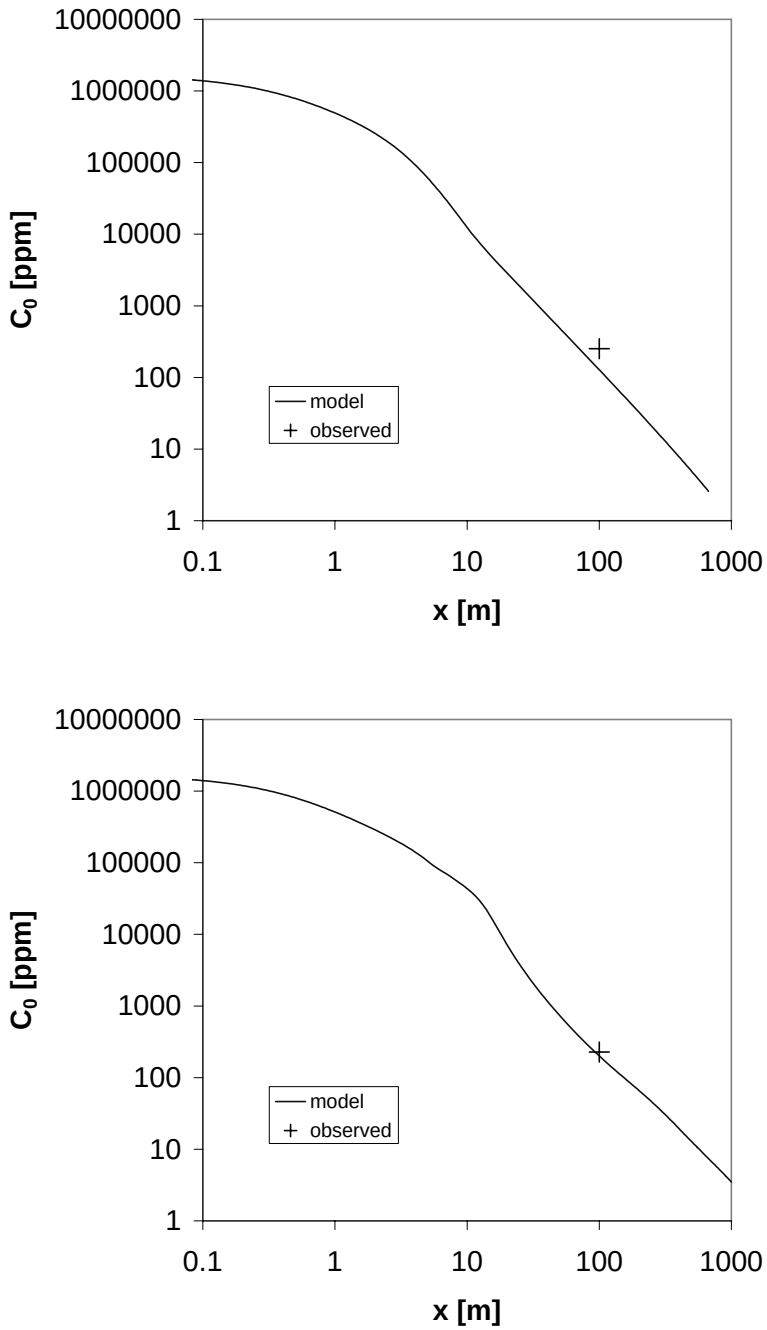

Figure 18. Model predictions of C_0 for Trial 4 (top) and Trial 12 (bottom).

are compared with the model predictions in table 1. The entrainment rate has been modeled so as to reproduce passive cloud results which are similar to these releases, so it is not surprising that the works well. The plume width is generally slightly larger than the observed values. Except for Trial 12 the HF plumes were not more elevated than the accompanying smoke plumes. The model reflects this behaviour and it does not predict rise of the centroid for these releases. In Trial 12 the centroid was observed to be elevated and the plume centre (maximum concentration) was raised above the ground. The model predictions is in agreement with this even if the rise is somewhat larger than observed.

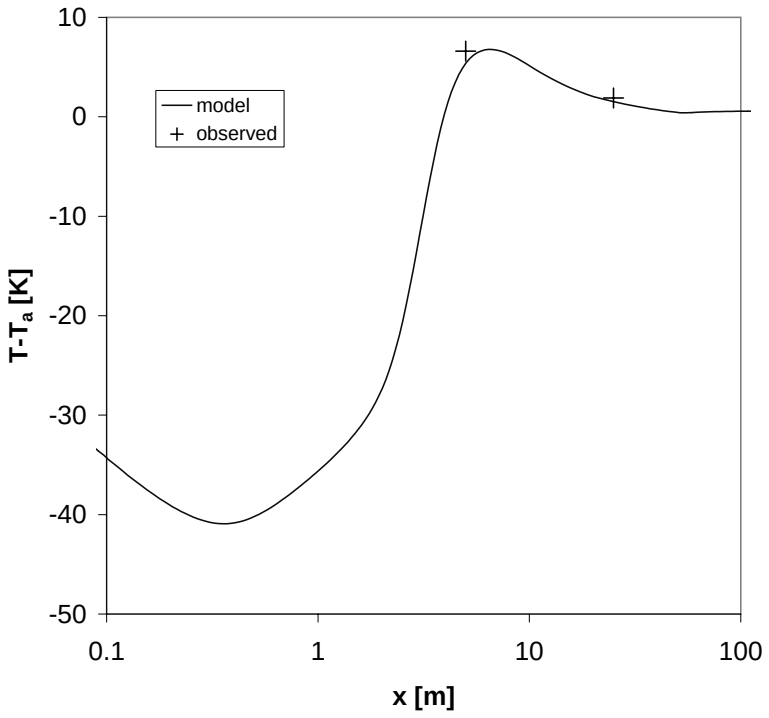

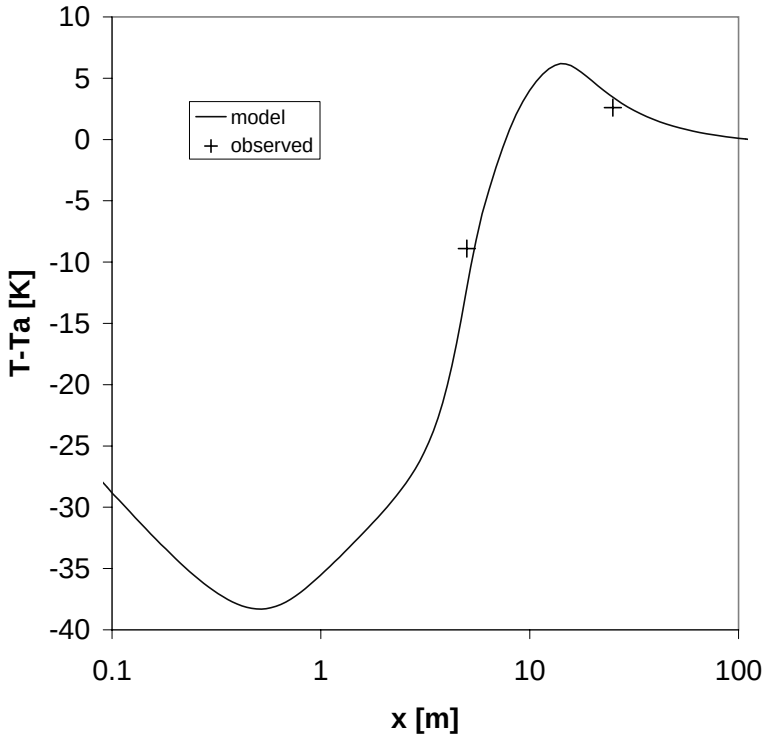

Figure 19. Model predictions of $T - T_a$ for Trial 4 (left) and Trial 12 (right).

Concentrations

Concentrations can be deduced from the lidar measurements using a mass balance (Ott and Jørgensen 2001). The data analysis does not take HF deposition on the ground into account, but a comparison with the absolute measurements made by

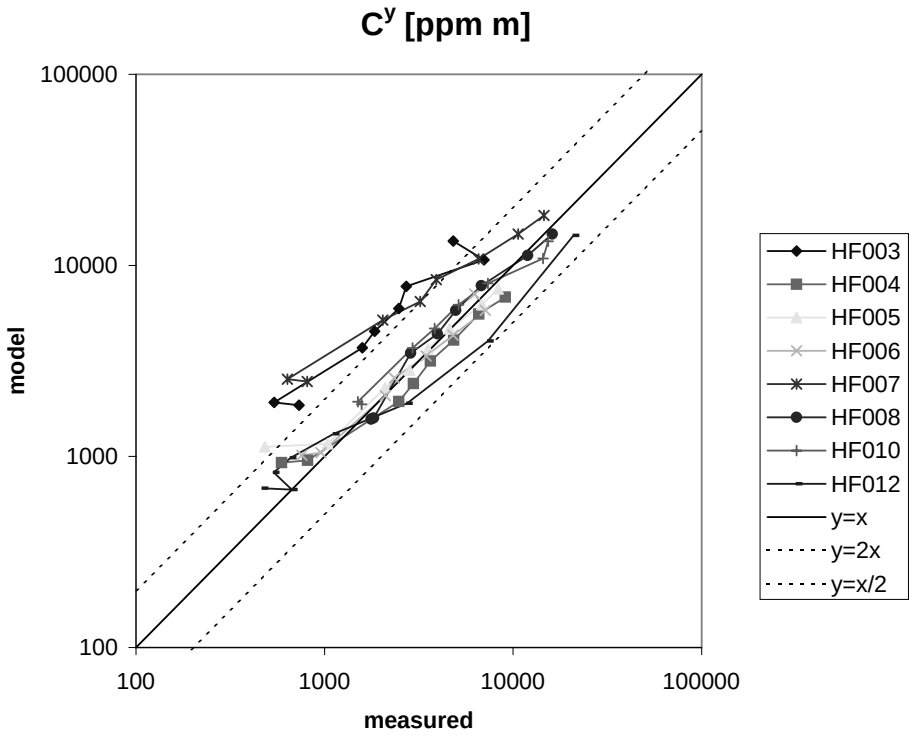

Figure 20. Comparison of measured and predicted values of $C^y = \int C(y,z,x)\mathrm{d}y$. *Measurements were made at height* $z = 1.5$m *and sensor arcs at* $x = 20$, *30, 45, 60, 100 and 200*m.

Table 2. Comparison of predicted and observed centre concentrations.

Trial	C_0(100m) model ppm	C_0(100m) observed ppm
HF003	260	253
HF004	128	133
HF005	170	144
HF006	148	111
HF007	339	240
HF008	181	188
HF010	259	240
HF012	201	227

filter samplers shows good agreement and therefore HF deposition cannot have led to major reductions of concentrations. The centre concentration C_0 has been calculated from data.

Model concentrations were calculated using the profile suggested in section 4.7, i.e. $C_0 = \frac{5}{3}C$ is taken as the model prediction for a grounded plume. The measurements and the corresponding model results are shown in Table 2. Trials 9 and 11 were mixed HF and iso-butane releases which the model cannot handle in its present form. For the remaining pure HF releases the model results are in excellent agreement with the observations.

The filter sampler data are more difficult to relate one-by-one to the model results because of the influence of the sampling time. The samplers had been placed in arcs which enables us to make the average cross–plume integrated concentration

$C^y = \int C(x, y, z = 0)\,\mathrm{d}y$. C^y is independent of meandering and can therefore be compared to model results. This has been done in figure 20. C^y is a decreasing function of distance. The model overpredicts by more than a factor of two for Trial 3 and Trial 7 and it underpredicts the near distance values for Trial 12. Otherwise the predicted values are in reasonable agreement with measurements, in particular the model captures the reduced values in Trial 12 reasonably well.

Temperatures

Table 3. Comparison of predicted and observed temperature deviations in the plume core.

Trial	$T - T_a$ @5m model K	$T - T_a$ @5m observed K	$T - T_a$ @25m model K	$T - T_a$ @25m observed K
HF004	5.4	6.6	1.5	1.9
HF005	2.7	5.9	1.0	1.2
HF006	2.4	5.2	0.1	0.8
HF007	-18.3	-21.1	-0.6	-0.5
HF008	-4.0	-27.9	1.6	3.1
HF010	-8.1	-19.4	2.6	2.8
HF012	-12.1	-8.9	3.5	2.6

Table 4. Comparison of global maxima and minima of the temperature deviation.

Trial	$T - T_a$ min. model K	$T - T_a$ min. observed K	$T - T_a$ max. model K	$T - T_a$ max. observed K
HF004	-40.9	-6.7	6.8	8.0
HF005	-41.2	-6.8	5.9	7.2
HF006	-42.1	-1.5	4.9	7.0
HF007	-44.2	-48.2	1.1	3.2
HF008	-41.6	-44.6	4.2	6.3
HF010	-39.7	-39.2	5.4	7.3
HF012	-38.3	-18.9	6.2	6.3

Figure 19 shows predicted centre temperatures. The 'raw' model temperature T is shown with no attempt to augment it with a profile. The temperature measurements are very detailed with sensors (thermocouples) arranged in two–dimensional cross-plume arrays. Certain interpretations have to be made in order to compare the thermocouple data with the model. First, the thermocouples basically measure their own temperature which may differ from the cloud temperature. Several factors influence the readings such as solar radiation and the fact that the sensors get wet. The solar radiation was probably not a problem because the probes were fairly small and because the cloud shielded the sunshine to some extent. More uncertain is the effect of hydrofluoric acid on the probes. For a probe permanently inside the cloud we may assume thermal equilibrium, but in reality the probes moves in and out of the cloud, because of meandering. When the probe is outside the cloud the hydrofluoric acid may evaporate and cause a temperature drop in the probe. It could also happen that more moisture condenses on it, which would raise

the temperature. However, the measured temperature differences are so large that these instrumental errors are insignificant. Secondly, the model variable T must be given an interpretation before it can be compared to measurements. Somehow T should represent an average temperature in the core of the plume, but it is difficult to determine where the core is because of the substantial variations of the measured temperatures across the plume. The relation between concentration and temperature is highly non-linear. This means that the core can be either hot or cold depending on the concentration range, and a cold core will be surrounded by a hot rim. A simple procedure was followed. The measured temperatures had been turned into temperature differences $T - T_a$ by comparing with readings taken before the HF was released. For each of the sensor arrays two time series were made containing the highest and the lowest values of the simultaneously observed temperature differences. In each case it was decided by inspection which of the two corresponded to temperatures in the plume core and that time series was time averaged and compared to $T-T_a$ predicted by the model. The results of this analysis is shown in table 3. There is general agreement between model and observation with respect to the sign (hot/cold core) and some apparant quantitative disagreements (e.g. Trial 8). However, the predicted temperature variations over the first few metres are so large that the model is not wrong by a large distance. This is also reflected in the very large variations of the observed temperature across the plume (30K or more for the cold core plumes).

An alternative analysis is given in table 4, where the highest and lowest temperature differences are compared. The model yields a highest and a lowest temperature which occur at certain concentrations determined by thermodynamics. The range of measured temperatures should lie within the limits, and because thermocouples were spread over a wide range of positions and exposed to a wide range of concentrations, there should be a fair chance for the measured temperatures to fill the range predicted by the model. According to table 4 the agreement is relatively good for the maxima. The minima are in good agreement for the cold–core cases (Trials 7, 8, 10 and 12), but not for the hot–core cases. This must because the temperature minima were attained at distances shorter than 5m, where there were no sensors to record them. This is can be regarded as a test of the assumption of homogeneous equilibrium.

6 A case study

In this section we make a case study which could represent considerations entering a risk assessment of an HF release. The study has been inspired by a similar study made by Chhibber and Kaiser (1996). The question is to what extent HF thermodynamics reduce ground level concentrations and which meteorological conditions are required.

In order to simplify things we shall limit the discussion to a continuous release of 10 kg/s of HF through a 2cm diameter horizontal nozzle located 1m above the ground. The surface roughness is 1 cm in all cases. We take the following input as the 'standard case': $L = -1000$m (near neutral stability), ambient temperature $T_a = 20°$C and windspeed $U = 5$m/s. This can be recognized as the standard D5 case. Figure 21 shows calculated ground level concentrations (C_0) for five different relative humidities. At 50% relative humidity there are no buoyancy effects. At higher humidities the calculations show progressively larger reductions of the concentration reaching one order of magnitude at 95% relative humidity. The reduced concentrations are found in a range of concentrations limited lift-off and touch-down. Near lift-off the curves bend slightly upwards. This is an artifact of the model caused by the way the plume radius is calculated when the plume has partial contact with the ground. A more cosmetic procedure could have been used, but it would not change the results very much.

Figure 22 is similar to figure 21 except that the ambient temperature is 10°C. Interestingly the effects are higher at the lower temperature. The plume rise sets in at slightly larger distances, but it is more persistent. The absolute humidity is much lower at 10°C than at 20°C, so less water vapour is available and one could therefore expect a smaller effect. However, the hydrofluoric acid droplets are more stable because of the lower vapour pressure and they are so hygroscopic that they essentially drain the air for all its moisture. This continues until the HF concentration in the droplets reach about 30–40%, and then the the water vapour fraction in the gas phase begins to rise. With less water available it takes longer time to form stable droplets, but once they have formed the contribution to the enthalpy budget is about the same for any ambient temperature. The volatility, on the other hand, depends on ambient temperature and the droplets evaporate more slowly the colder they are.

Raising T_a to 30°c (figure 23) eliminates effects even at 70% relative humidity. This explains the lack of effects in the Goldfish experiments where temperatures were high and relative humidities low.

The effect of lowering the windspeed to 2m/s (and otherwise keeping the standard case) is shown in figure 24. In this case concentrations are reduced considerably, up to about two orders of magnitude for 95% relative humidity and up to about one order of magnitude for 70% relative humidity.

Raising the windspeed to 10m/s has a large effect as can be seen in figure 25. Hardly any reduction is seen and a closer inspection reveals that the centroid elevation is comparable to the plume width, or smaller, so the plume rise could be insufficient to lift the plume over e.g. a tall building.

Finally figure 26 shows the results for $U = 2$m/s, $T_a = 20^circ$C and $L = 30$m. This corresponds to stable conditions (class E to F, say), encountered for example during a night with light winds and not too many clouds. In this case the rise is impeded by the stable density gradient, but the reductions are still large.

The ground level concentration have been calculated using the proposed exponentially tailed profile, but it should not change the result dramatically if a Gaussian profile is used instead. It should be emphasized that use the assumed profile is one of the least certain aspects of the model, in particular for rising

plumes, where we have little experimental results to build on. It is possible that the model is overly optimistic with respect to reductions of the concentrations under a rising plume since there might be a *de*-trainment mechanism that pulls material out of the plume, into the ambient flow and sweeps along the ground. The Coanda effect could also be mentioned. The cases where there is no or little effect of HF are more certain, since the onset of buoyancy effects depends on the thermodynamic part of the model rather than the dispersion part.

The calculations basically confirm the conclusions drawn by applying scaling laws to the results of the field experiments, namely that relative humidities higher than about 90% and wind speeds below 5m/s are required in order to get an appreciable plume rise for a 10 kg/s release in near neutral conditions. They also show that plume rise is eliminated by stable stratification.

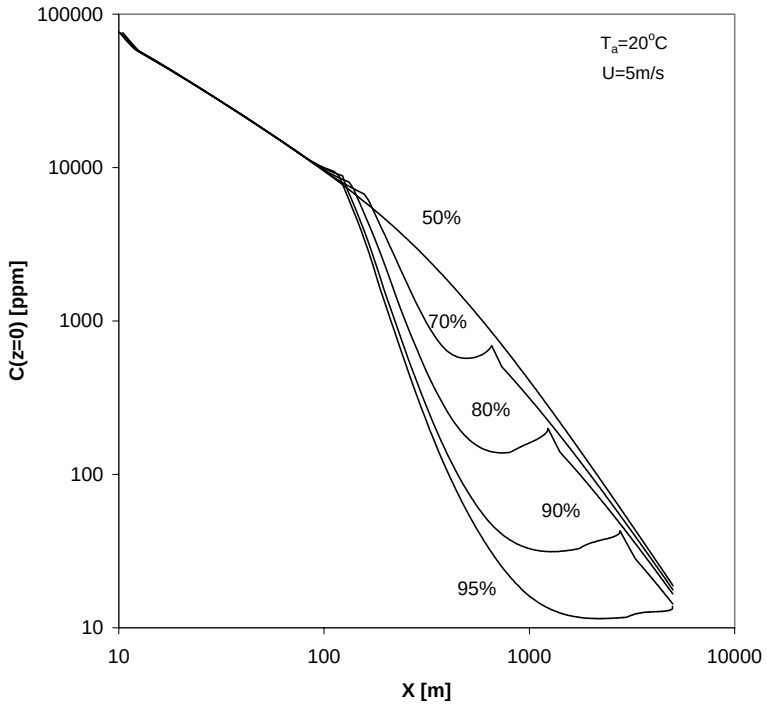

Figure 21. Predicted ground level concentrations. Ambient wind speed is 5m/s and ambient temperature is 20°C

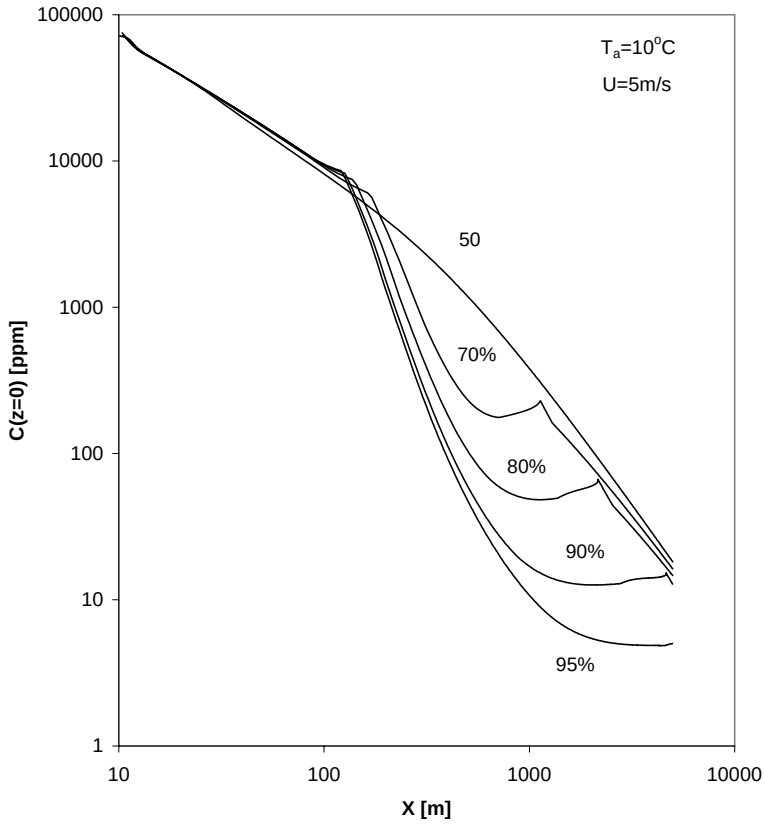

Figure 22. Predicted ground level concentrations. Ambient wind speed is 5m/s and ambient temperature is 10°C

.

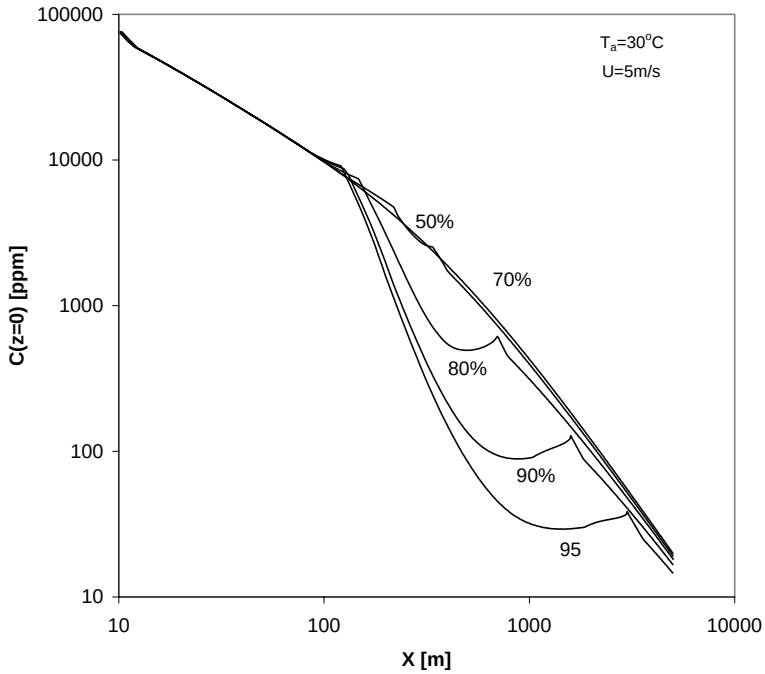

Figure 23. Predicted ground level concentrations. Ambient wind speed is 5m/s and ambient temperature is 30°C

.

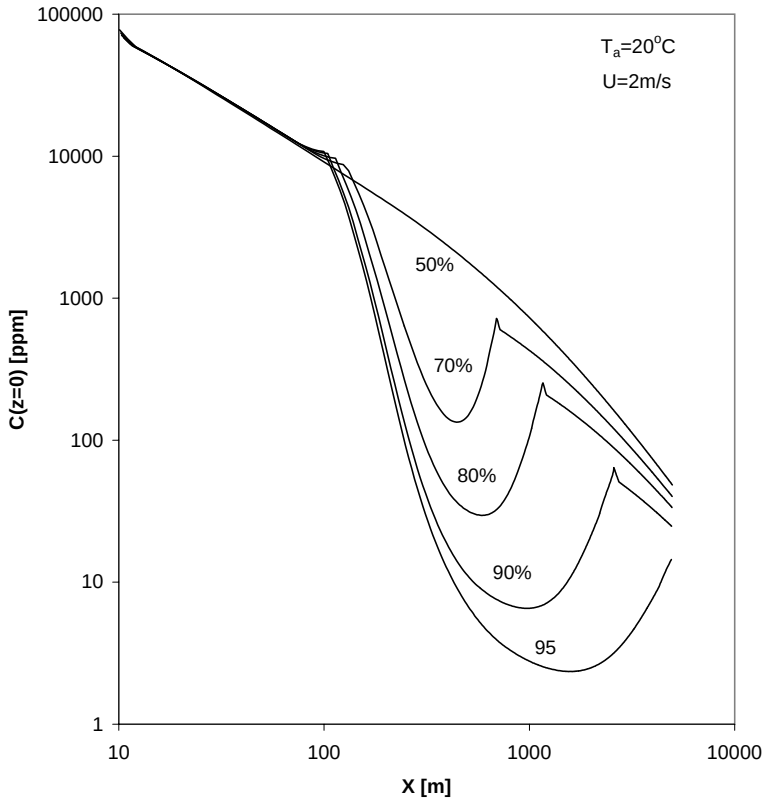

Figure 24. Predicted ground level concentrations. Ambient wind speed is 2m/s and ambient temperature is 20°C

.

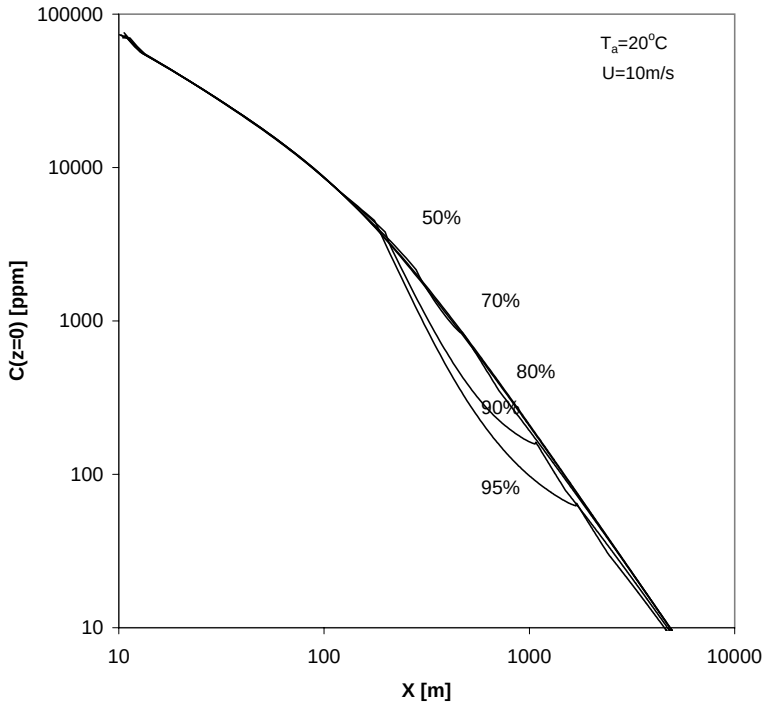

Figure 25. Predicted ground level concentrations. Ambient wind speed is 10m/s and ambient temperature is 20°C

.

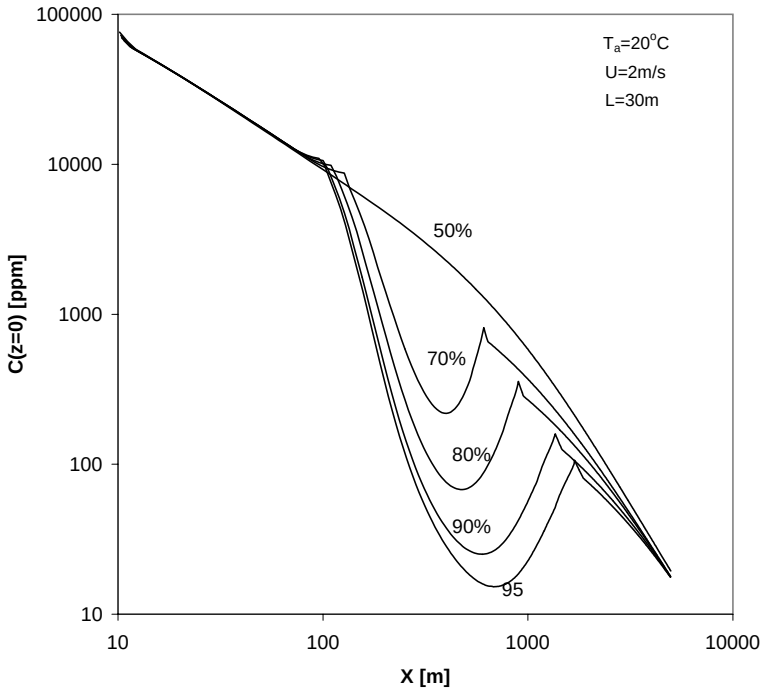

Figure 26. Predicted ground level concentrations. Ambient wind speed is 2m/s and ambient temperature is $20°\mathrm{C}$ *and* $L = 30\mathrm{m}$ *(stable).*

7 Conclusions

An integral model describing the dispersion of continuous releases of HF has been developed. The work naturally falls into two separate parts: thermodynamics and dispersion.

A new thermodynamic model has been developed on the basis of a review of existing data and models. Very few experimental investigations of HF thermodynamics have been conducted in the past fifty years, and in particular high quality P–T–V data are scarce. We show how P–V–T data can be used to determine thermodynamic properties of a real gas via the function $P(f,T)$, the pressure as a function of temperature and fugacity. A simple rings–and–chains model has been proposed. The model is validated against the results of several independent experiments.

The phase equilibria of the HF–water–air system is described by means of exact relations involving fugacities. This aspect of the model has also been validated against experiments, including those generated in this project. The level of accuracy of the thermodynamical model seems to be more than adequate for dispersion calculations.

The model has been used to calculate the buoyancy of adiabatic mixtures of HF and humid air at a number of temperatures and values of the relative humidity. Positive buoyancy is associated by the formation of a fog of hydrofluoric acid droplets and we find find that this is governed by more the relative humidity than absolute humidity. The explanation for this is that the water vapour pressure of the droplets is low compared to water vapour pressures of even in the dryest atmosphere. Small concentrations of HF are therefore able to condense nearly all the water vapour in the air. For a range of different ambient temperatures, humudities and HF concentrations, one mol of HF causes about one mol of water vapour to condense. The maximum cloud temperature is reached as soon as this amount of water is available, and at that point the released enthalpy of condensation, which is what heats the cloud, is therefore always about the same. The temperature rise is faster at larger humidities simply because there is less dry air to heat. When the concentration gets low enough, the droplets begin to evaporate. The HF evaporates faster than the water so that the droplets gradually change composition. Since vapour pressures are generally lower at lower temperatures, the droplets are more stable at low temperatures and high relative humidity and the period of positive buoyancy is therefore longer than at high temperatures, and this tends to more than compensate the slower temperature rise in the period where there is condensation.

The dispersion has been modelled in simple ways using an integral model. Although this type of model has a foundation in the Navier-Stokes equations, the dispersion process is basically put in 'by hand'. The final set of equations is derived from a series of approximations and interpretations which, to a large extend, are based on a phenomenological understanding. This is described in some length. The concept of relative diffusion is a basis for these arguments, and the resulting model is relative dispersion model, and relative diffusion data has been used to tune it.

In the UHRAFREP project the plan was to supplement field experiments with model development in order to understand and generalize experimental findings and to produce a tool for the prediction of HF dispersion. The model has been tested against the field measurements, and the comparison shows reasonable agreement. In all except one the experiments there were no signs of buoyancy effects, and the model agrees. In Trial 12 reduced ground level concentrations were observed as well as an elevation of the cloud centroid. This behaviour is captured

by the model. The predicted concentrations are very close to those deduced from lidar data, while the plume widths are slightly larger than the observations.

Since there are indications that Trial 12 is a limiting case, it seems that the model is capable of predicting the onset of HF induced effects. More doubt can be cast on the models ability to predict the behaviour of a rising HF plume. This has never been observed and hence there are no data to compare the model with. Reduced ground level concentrations were observed for passive plumes in the Prairie Grass experiment. We have interpreted this as a result of the creation of thermals, although deposition on the ground also may have contributed. The model should be able to reproduce this behaviour until the point where the plume/thermal begins to rise from the ground. The subsequent rise is difficult with this type of model because the thermal may extend wider than the plume. In the same way a buoyant HF plume may be the seed of a thermal which may extend wider than the plume. The model does not take such a collective motion of the surrounding air into account and may therefore underpredict plume rise in these situations. The model simply turns off the heating when the plume looses contact with the ground, where in reality heating may continue to generate hot rising air below it. The effects of up-drafts and down-drafts may also add considerable randomness to the plume trajectories, but probably only very strong convection would be able to send a rising HF plume down again. We have indicated some simple ways to take this into account. Thus the introduction of a random vertical velocity component of the entrained air could be considered. An analysis of the enthalpy ballance for a grounded plume also indicates that temperature differences in the plume somewhat larger than $\langle Tw \rangle / u_*$ are required in order to compete with the ambient convection. However, due to the deterministic nature of the model, it not well suited for strong convection. In near neutral or moderately stable conditions there should be less concern.

A case study of a 10kg/s release has been made in order to determine the conditions necessary for HF induced buoyancy to have an effects on ground level concentrations. We find that effects increase with decreasing ambient temperature, but the variations are relatively small. Buoyancy effects decrease with increasing windspeed, as expected. The model predicts considerable reductions of the ground level concentrations for high humidities and 2m/s windspeed, while there is very little plume rise at a windspeed of 10m/s. Plume rise is somewhat impeded by stable stratification but not eliminated. It should be noted that the predicted ground level concentrations rely heavily on the assumed profile, which is not a well tested aspects of the model.

Buoyancy is the driving force in plume rise and all other forces acting on the plume will tend to oppose it. In case the model has not taken all of these into account, it is deemed to overpredict plume rise. Conversely, there is no reason to expect plume rise if equilibrium thermodynamics forbids it, and therefore the model should be trustworthy in cases where plume rise is not predicted.

A More on added mass

In this appendix we speculate further on added mass. Some of the considerations are somewhat speculative and have not been implemented in the model, mainly because we wish to keep it as simple as possible.

In the simple example in section 4.5 the ground was neglected. Below we will try to incorporate the effect of the ground in an approximate way. For simplicity we keep the ambient flow field uniform and thus assume that the ground is ideally smooth. We use the y-axis as ground so that the disk moves in the half-plane $x > 0$.

As a first approximation we take (145) and then make successive 'repair'. The free solution (145) respects the boundary conditions on the surface of the disk, but not on the y-axis. The first repair is to make λ antisymmetric with respect to the y-axis by adding a mirrored pole located at $-c$. This leads to

$$\lambda \approx a^2 \dot{c} \left(-\frac{1}{z-c} + \frac{1}{z+c} \right) \tag{A.161}$$

This unfortunately spoils the boundary condition on the disk, hence the second repair consists of adding a pole at $c - b_1$ of strength $s_1 a^2 \dot{c}$ to compensate for the effect of the pole in $-c$, viz

$$\lambda \approx a^2 \dot{c} \left(-\frac{1}{z-c} + \frac{1}{z+c} + \frac{s_1}{z-c+b_1} \right) \tag{A.162}$$

This can be achieved by choosing $b_1 = a^2/2c$ and $s_1 = a^2/4c^2$. Now the problem is that the boundary conditions on the y-axis are not right. Therefore we add another pole in $-c + b_1$ and a compensating pole in $c - b_2$ etc. The final solution is

$$\lambda = \sum_{p=0}^{\infty} a^2 \dot{c} \left(\frac{s_p}{z-c+b_p} - \frac{s_p}{z+c-b_p} \right) \tag{A.163}$$

where

$$\begin{aligned} b_{p+1} &= \frac{a^2}{2c - b_p} \\ s_{p+1} &= \frac{s_p a^2}{b_{p+1}^2} \end{aligned} \tag{A.164}$$

and $b_0 = 0$ and $s_0 = 1$. It can be shown that the kinetic energy of the fluid is equal to

$$E_{\text{kin,fluid}} = \frac{1}{2} \rho_a \pi a^2 \mu(c/a) \tag{A.165}$$

where

$$\mu(c/a) = 1 + 2 \sum_{p=1}^{\infty} s_p = 1 + \frac{1}{2} \left(\frac{a}{c} \right)^2 + \frac{1}{8} \left(\frac{a}{c} \right)^4 + \frac{3}{32} \left(\frac{a}{c} \right)^6 + \ldots \tag{A.166}$$

The method converges for $c \geqq a$. For the limiting case $c = a$, where the disk touches the ground, the series can be summed with the result $\mu(1) = \frac{\pi^2}{3} - 1 \sim 2.29$, which is considerably larger that the value $\mu = 1$ obtained for a free disk. The sharp increase of μ near the ground must be due to fluid being squeezed between the disk and the ground. A real plume is not rigid, it would itself be squeezed by

the pressure and adjust its shape. Therefore the sharp rise of μ near the ground should be replaced by a more moderate behaviour of which we make a bold guess. If the plume is allowed to deform as it approaches the ground, the restriction $c > a$ is no longer necessary and μ could be defined even for $c < a$. In that case c can be defined as the centre of mass of the plume, and a can be defined so that πa^2 is the area (i.e. constant a). A simple way to deform the cloud would be to let it be a circular shape with the part that below ground cut off. Unfortunately the repair scheme sketched above does not to work for this problem, and we will not pursue a numerical solution. It is noted that a disk moving parallel with the ground has the same added mass function mu. For this problem we find $\mu = 1$ for a semicircle sliding on the ground (note that the solution (145) is symmetric). By analogy one would therefore expect $\mu = 1$ for a rising (and contracting) semicircle. This indicates that μ has a maximum around $c = a$. We therefore suggest

$$\mu(c/a) = 1 + \frac{1}{2}\,\frac{1}{\left(\frac{a}{c} - \frac{c}{a}\right)^2 + \gamma} \tag{A.167}$$

where γ is an adjustable constant. This form has the right asymptotic limit $\sim 1 + \frac{1}{2}(a/c)^2$ and allows for adjustment of the maximum. With μ varying with position the dynamic equation becomes slightly more complicated

$$\begin{aligned} &\frac{\mathrm{d}}{\mathrm{d}t}\pi a^2\dot{c}(\rho + \mu(c/a)\rho_a) - \frac{1}{2}\pi a^2\dot{c}^2\frac{\partial\mu(c/a)}{\partial c} = \\ &\pi a^2(\rho + \mu(c/a)\rho_a)\frac{\mathrm{d}^2c}{\mathrm{d}t^2} + \frac{1}{2}\pi a^2\dot{c}^2\frac{\partial\mu(c/a)}{\partial c} = -\frac{\partial E_{\mathrm{pot}}}{\partial c} = F(c) \end{aligned} \tag{A.168}$$

Thus spatial variation of μ gives rise to a force term. When μ has a maximum, the force is downward near the ground, which will resist lift-off of a buoyant plume. This is similar to the Coanda effect, the phenomena that jets follow surfaces. Added mass could therefore conveniently simulate the Coanda effect, even if added mass may not fully explain it.

Governing equations

We proceed with a derivation of a set of dynamic equations for a plume taking added mass into account.

We continue to assume a uniform wind field, and use a reference frame at rest with respect to the wind. We also postpone entrainment until later and let ρ be fixed, while the cross-section area $A(s)$ is variable. It is convenient to express the plume centreline as a map $m \to \mathbf{X} = (X, Z)$ where $m = -\dot{M}t + \int_0^s \rho A ds$. Thus m is the mass (not counting added mass) contained in the plume between $\mathbf{X}$ and the source minus the mass injected by the plume ($\dot{M}$ is the source strength). Defined in this way m is a Lagrangian coordinate, since a given value of m specifies a moving slice of the plume. We define a time variable t' to go with m. The meaning of t' is that $t' = t$, but $\partial/\partial t'$ should denote the partial derivative with respect to time for fixed m. Since $\partial/\partial t'$ is the Lagrangian time derivative we can also write it as $\mathrm{d}/\mathrm{d}t$. Note that $\partial/\partial t'$ commutes with $\partial/\partial m$.

The plume is completely specified by the function $\mathbf{X}(m, t')$ and we may express other variables in terms of it. The variables that we shall use are: the velocity $\mathbf{U}$, the plume mass per unit length $A\rho$, the distance from the source measured along the centreline s, the unit vector $\mathbf{k} = (\cos\theta, \sin\theta)$ tangent to the centreline, and the effective plume radius a. Expressed in terms of $\mathbf{X}(m, t')$ these quantities are

$$\mathbf{U} = \frac{\partial \mathbf{X}}{\partial t'} \tag{A.169}$$

$$A\rho = \left|\frac{\partial \mathbf{X}}{\partial m}\right|^{-1} \tag{A.170}$$

$$s = \int_0^m \left|\frac{\partial \mathbf{X}}{\partial m}\right| \,\mathrm{d}m \tag{A.171}$$

$$\mathbf{k} = \frac{\partial \mathbf{X}}{\partial m}\left|\frac{\partial \mathbf{X}}{\partial m}\right|^{-1} \tag{A.172}$$

$$a = \sqrt{A/\pi} \tag{A.173}$$

The added mass only affects the kinetic energy corresponding to the transverse velocity component $\hat{\mathbf{k}}\cdot(\mathbf{U}-\mathbf{u}_a)$, where $\hat{\mathbf{k}} = (-\sin\theta, \cos\theta)$. Thus the kinetic energy of a plume slice is given by

$$\mathrm{d}E_{\mathrm{kin}} = \frac{1}{2}\left(\mathbf{U}^2 + \mu\rho_a\rho((\mathbf{U}-\mathbf{u}_a)\cdot\hat{\mathbf{k}})^2\right)\,\mathrm{d}m \tag{A.174}$$

Note that$\mathbf{U}$ need not be parallel with $\mathbf{k}$. The Lagrangian of the system then becomes

$$\mathcal{L} = \int\left(\frac{1}{2}\Delta\mathbf{U}^2 + \frac{1}{2}\frac{\mu\rho_a}{\rho}(\Delta\mathbf{U}\cdot\hat{\mathbf{k}})^2 - E_{\mathrm{pot}}\right)\,\mathrm{d}m \tag{A.175}$$

where $\Delta\mathbf{U} = \mathbf{U}-\mathbf{u}_a$ and $E_{\mathrm{pot}} = gZ(\rho-\rho_a)/\rho$ for a buoyant plume. The added mass function μ is a function of Z and θ. In order to use (A.167) we must decide what c to use. For a horizontal plume ($\theta = 0$) we evidently must use $c = Z$. For inclined plumes the flow around it is not really two-dimensional, but a value of c between Z and $Z/\cos\theta$ seems plausible, and it probably does not matter much whether we include the $\cos\theta$ since θ can be expected to be small for a rising plume. We therefore choose $c = Z$ because this yields the simplest equations.

We now turn to the principle of least action in order to derive the dynamic equation. The action integral is given by

$$\mathcal{S} = \int_{t_1'}^{t_2'} \mathcal{L}\,\mathrm{d}t' \tag{A.176}$$

The solution is obtained by minimizing $\mathcal{S}$ with respect to the function $\mathbf{X}(m,t')$ for fixed values of $\mathbf{X}(m,t_1')$ and $\mathbf{X}(m,t_2')$. If $\delta\mathbf{X}$ is a variation of $\mathbf{X}$ then

$$\delta\mathbf{U} = \frac{\partial\delta\mathbf{X}}{\partial t'} \tag{A.177}$$

$$\delta\mathbf{k} = A\rho\hat{\mathbf{k}}\cdot\frac{\partial\delta\mathbf{X}}{\partial m}\,\hat{\mathbf{k}} \tag{A.178}$$

These expressions are used in the standard procedure where two integrations by part are used to turn $\delta\mathcal{S} = 0$ into the form $\int dt' \int \delta\mathbf{X}\cdot\mathbf{F} = 0$. Since this should hold for any perturbation $\delta\mathbf{X}$, we end up with the governing equation $(\mathbf{F}) = 0$. In our case the following equation is obtained

$$\begin{aligned} & \frac{\partial}{\partial t'}\left(\mathbf{U} + \frac{\mu\rho_a}{\rho}(\Delta\mathbf{U}\cdot\hat{\mathbf{k}})\hat{\mathbf{k}}\right) \\ - \quad & \frac{\partial}{\partial m}\left(\rho_a A\mu(\Delta\mathbf{U}\cdot\hat{\mathbf{k}})(\Delta\mathbf{U}\cdot\mathbf{k})\,\hat{\mathbf{k}}\right) - \frac{1}{2}(\Delta\mathbf{U}\cdot\hat{\mathbf{k}})^2\frac{\rho_a}{\rho}\nabla\mu \\ = \quad & -\nabla E_{\mathrm{pot}} \end{aligned} \tag{A.179}$$

where $\nabla = (\partial/\partial X, \partial/\partial Z)$. As a check of this equation we derive an energy equation from it. This is most conveniently done in a frame of reference in rest with respect to the ambient flow. We could have chosen this from the start, in which case $\mathbf{U}$ would be the same as $\Delta\mathbf{U}$. Hence we take the vector product with $\Delta\mathbf{U}$ on both sides of (A.179) and rearrange terms. Using the identity $\hat{\mathbf{k}} \cdot \frac{\partial \Delta\mathbf{U}}{\partial m} = \frac{1}{\rho A}\hat{\mathbf{k}} \cdot \frac{\partial \mathbf{k}}{\partial t'}$ the following equation is obtained

$$\frac{\partial}{\partial t'}\left(\frac{1}{2}\Delta\mathbf{U}^2 + \frac{1}{2}\frac{\rho_a \mu}{\rho}(\Delta\mathbf{U}\cdot\hat{\mathbf{k}})^2 + E_{\rm pot}\right) = \frac{\partial}{\partial m}\left(\rho_a A \mu (\Delta\mathbf{U}\cdot\hat{\mathbf{k}})^2(\Delta\mathbf{U}\cdot\mathbf{k})\right) \tag{A.180}$$

The left hand side represents the rate of change of the total mechanical energy of a plume slice. Evidently energy is not conserved separately for each plume slice, since the right hand side of the equation represents an interaction with the rest of the plume. There is nothing wrong with that as long as the rate of change of the energy of a finite plume segment only depends on contributions at the endpoints. In other words, the right hand side of the equations must be of the form $\partial J/\partial m$, which it actually is.

For a time independent plume we may now make use of the fact that $\mathbf{U}$ is parallel with $\mathbf{k}$, e.g. $\Delta\mathbf{U} = U\,\mathbf{k} - \mathbf{u}_a$. In the stationary case it is convenient to use s instead of t' and m, which is effected by the substitutions $\partial/\partial t' = U\mathrm{d}/\mathrm{d}s$ and $\partial/\partial m = (\rho A)^{-1}\mathrm{d}/\mathrm{d}s$. From (A.179) we then get the following two equations by projecting along $\mathbf{k}$ and $\hat{\mathbf{k}}$.

$$\rho U\frac{\mathrm{d}U}{\mathrm{d}s}\rho_a\mu u_a^2\cos\theta\sin\theta\frac{\mathrm{d}\theta}{\mathrm{d}s} = \frac{1}{2}\rho_a u_a^2\sin^2\theta\frac{\mathrm{d}\mu}{\mathrm{d}s} + (\rho_a - \rho)g\sin\theta \tag{A.181}$$

$$\begin{aligned}&\left[\rho U^2 + \mu\rho_a u_a^2(\cos^2\theta - \sin^2\theta)\right]\frac{\mathrm{d}\theta}{\mathrm{d}s} - \mu\rho_a\frac{u_a^1}{U}\sin\theta\cos\theta\frac{\mathrm{d}U}{\mathrm{d}s}\\ = \;& -\frac{1}{2}\rho_a u_a^2\sin\theta\cos\theta\frac{\mathrm{d}\mu}{\mathrm{d}s} + (\rho_a - \rho)g\cos\theta\end{aligned} \tag{A.182}$$

References

Bennett, M., Jørgensen, H. E., Lyck, E., Løfstrøm, P., Mikkelsen, T. and Ott, S.: 1999, A Case Study of Plume Dispersion During the Evolution of a Stable Nucturnal Boundary Layer, *in* P. A. Davies (ed.), *Mixing and Dispersion in Stably Stratified Flows*, Claradon Press, Oxford, pp. 439–453. Dundee Sept. 1996.

Blewitt, D. N., Yohn, J. F., Koopman, R. P. and Brown, T. C.: 1987, Conduct of Anhydrous Hydrofloric Acid Spill Experiment, *Proceedings of the International Conference on Vapor Cloud Modeling,*, Boston, pp. 1–38.

Bricard, P. and Friedel, L.: 1989, Two-phase jet dispersion, *Journal of Hazardous Materials* **59**, 287–310.

Briegleb, G.: 1941, Modelbetrachtungen zur „Wasserstoffbibdung", *Z. f. Electrochemie* **51**, 9–38.

Briegleb, G. and Strohmeier, W.: 1953, Über den Assoziationszustand des HF im Gaszustand. II, *Z. f. Electrochemie* **57**, 668–674.

Briggs, G. A.: 1973, Theoretical estimates of lift off of buoyant gas initially on the ground, *Technical Report Contribution No. 87*, Atmospheric Turbulence and Diffusion Laboratory, Oak Ridge, Tennesee.

Briggs, G. A.: 1982, Similarity forms for ground-source surface-layer diffusion, *Boundary Layer Meteorology* **23**, 489–502.

Brosheer, J. C., Lenfesty, F. A. and Elmore, K. L.: 1947, Vapor pressure of hydrofloric acid solutions, *Ind. Eng. Chem.* **39**, 423–431.

Bussinger, J. A., Wyngaard, J. C., Izumi, Y. and Bradley, E. F.: 1971, Flux-profile relationship in the atmospheric surface layer, *J. Atmos. Sci.* **28**, 181–189.

Chhibber, S. and Kaiser, G. D.: 1996, Issues of the Estimation of Risk from the Atmospheric Dispersion and Consequence Modeling of Hydrofluoric Acid, *in* P. C. Cacciabue and I. A. Papazoglou (eds), *ESREL:Probabilistic safety assessment and management '96; ESREL'96-PSAM-III; June 24-28,Crete,Greece*, pp. 1788–1792.

Clough, P. N., Grist, D. R. and Wheatley, C. J.: 1987a, The mixing of anhydrous hydrogen fluoride with moist air, *in* J. L. Woodward (ed.), *International Conference on Vapor Cloud Modeling, Nov. 2–4, 1987, Cambridge, MN*, American Institute of Chemical Engineers, New York, pp. 39–55.

Clough, P. N., Grist, D. R. and Wheatley, C. J.: 1987b, Thermodynamics of mixing and final state of a mixture formed by the dilution of anhydrous hydrogen fluoride with moist air, *Technical Report SRD R 396*, United Kingdom Atomic Energy Authority, Safety and Reliability Directorate.

Escuder, M. P. and Maxworthy, T.: 1973, On the motion of turbulent thermals, *Journal of Fluid Mechanics* **61**, 541–552.

Franck, E. U. and Meyer, F.: 1959, Flourwasserstoff III, Spezifiche Värme und Assoziation im Gas bei niedrigem Druck, *Z. f. Electrochemie* **63**, 571–582.

Franck, E. U. and Spalthoff, W.: 1957, Flourwasserstoff I, Spezifiche Värme, Dampfdruck und Dichte bis zu 300°C und 300 at, *Z. f. Electrochemie* **61**, 348–357.

Fredenhagen, K.: 1933, Physikalisch-chemische Messungen am Flourwasserstoff., *Z. anorg. algem. Chem.* **210**, 210–223.

Fredenhagen, K.: 1934, Physikalisch-chemische Messungen am Flourwasserstoff II., *Z. anorg. algem. Chem.* **218**, 161–168.

Fredenhagen, K. and Wellmann, M.: 1932, Verteiligungszahlen des Flourwasserstoffs über dem Zweistoffsystem $[H_2O - HF]$ und die Siedepunktskurve dieses Systems bei Atmosphärendruck, *Z. physik. Chem.* **A 162**, 454–466.

Galindo, A., Whitehead, P. J., Jackson, G. and Burgess, N.: 1997, Predicting the Phase Equilibria of Mixtures of Hydrogen Fluoride with Water, Difluoromethane (HFC-32), and 1,1,1,2-Tetrafluoroethane (HFC-134a) Using a simplified SAFT Approach, *J. Phys. Chem. B* **101**, 2082–2091.

Gmelins Handbuch der anorganischen Chemie: 1959, Verlag Chemie, Weinheim. System Nummer 5: Fluor. 8. edition.

Gore: 1869, *J. Chem. Soc.* **22**, 368. data reproduced in Gmelin.

Guggenheim, E. A.: 1957, *Thermodynamics*, North Holland Publishing Company, Amsterdam.

Hall, D. J.: 1997, A Note on the Scaling Principles Used in the URAHFREP AHF Releas Filed Trials, *Technical Report 76080*, Building Research Establishment.

Hall, D. J. and Walker, S.: 1997, Scaling rules for reduced-scale field release of hydrogen flouride, *Journal of Hazardous Materials* **54**, 89–111.

Hall, D. J. and Walker, S.: 2000, Plume rise from buoyant sources at the ground, *Technical report*, Building Research Establishment. Report No 80921.

Hoult, D. P., Fay, J. A. and Forney, L. J.: 1969, A Theory of Plume Rise Compared with Field Observations, *Journ. Air. Pollut. Contol Assoc.* **19**, 585–590.

Hu, J.-H., White, D. and Johnston, H. L.: 1953, The Heat Capacity, Heat of Fusion and Heat of Vaporization of Hydrogen Fluoride, *J. Amer. Chem. Soc.* **75**, 1232–1236.

Jarry, R. L. and Davies, W.: 1953, The vapour pressure, association and heat of vaporisation of hydrogen fluoride, *J. Phys. Chem.* **57**, 600–604.

Johnson, G. K., Smith, P. N. and Hubbard, W. N.: 1973, The enthalpies of solution and neutralization of HF(l); enthalpies of dilution and derived thermodynamic properties of HF(aq), *J. Chem. Thermodynamics* **5**, 793–809.

Jørgensen, H. E. and Mikkelsen, T.: 1993, Lidar measurements of plume statistics, *Boundary-Layer Meteorology* **62**, 361–378.

Kemp, C. C. and Newland, M. S.: 2000, HF Thermodynamics Tests: Data Report, *Technical Report AEAT/R/NS/0028*, AEA Technology plc.

Kirk-Othmer: 1980, *Encyclopedia of Chemical Technology, third edition*, Vol. 10, John Wiley & Sons, New York. Entry: Flourine Compounds, Inorganic, Hydrogen.

Long, R. L., Hildebrand, J. H. and Morell, W. E.: 1943, The Polymerization of Gaseous Hydrogen Flouride and Deuterium Fluoride, *J. Amer. Chem. Soc.* **65**, 182–187.

Maclean, J. N., Rosetti, F. J. and Rosetti, H. S.: 1962, The Self-Association of Hydrogen Fluoride Vapour, *J. Inorg. Nucl. Chem* **24**, 1549–1554.

McBean, G. A. and Elliott, J. A.: 1975, The Vertical Transport of Kinetic Energy by Turbulence and Pressure in the Boundary Layer, *J. Atmos. Sci.* **32**, 753–766.

Meroney, R. N.: 1979, Lift off of buoyant gas initially on the ground, *Journal of Indistrial Aerodynamics* **5**, 1–11.

Miki, N., Maeno, M. and Maruhashi, K.: 1990, Vapor-Liquid Equilibrium of the Binary System HF-H_2O Extended to Extremely Anhydrous Hydrogen Fluoride, *J. Electrochem. Soc.* **137**, 787–790.

Monin, A. S. and Obukhov, A. M.: 1953, Dimensionless characteristics of turbulence in the atmospheric surface layer, *Doklady AN SSSR* **93**, 223–226.

Monin, A. S. and Yaglom, A. M.: 1975, *Statistical Fluid Mechanics*, Vol. 2, The MIT Press.

Moore, W. J.: 1972, *Physical Chemistry*, Prentice-Hall, New Jersie.

Munter, P. A., Aepli, O. T. and Kossatz, R. A.: 1947, Hydrofluoric Acid-Water and Hydrofloric Acid-Hydrofluorosilicic Acid-Water, *Ind. Eng. Chem.* **39**, 427–431.

Munter, P. A., Aepli, O. T. and Kossatz, R. A.: 1949, Partial Pressure Measurements on the System Hydrogen Fluoride-Water, *Ind. Eng. Chem.* **41**, 1504–1508.

Nelder, J. A. and Mead, R.: 1965, A simplex method for function minimization, *Computer Journal* **7**, 308–313.

Nieuwstadt, F. T. M.: 1980, Application of mixed layer similarity to the observed dispersion from ground-level sources, *J. Appl. Meteor.* **19**, 157–162.

Ooms, G.: 1972, A new method for the calculation of the plume path of gases emitted by a stack, *Atmospheric Environment* **6**, 899–909.

Ott, S. and Jørgensen, H. E.: 2001, Meteorology and lidar data from the URAH-FREP field trials, *Technical Report Risø-R-1212(EN)*, Risø National Laboratory.

Ott, S. and Mann, J.: 2000, An experimental investigation of the relative diffusion of particle pairs in three-dimensional turbulent flow, *Journal of Fluid Mechanics* **422**, 207–223.

Paulson, C. A.: 1970, The mathematical representation of wind speed and temperature profiles in the unstable atmospheric surface layer, *Journal of Applied Meteorology* **9**, 57–861.

Peng, D. and Robinson, D. B.: 1976, A New Two-Constant Equation of State, *Ind. Eng. Chem. Fundam.* **15**, 59–64.

Potter, R. L.: 1957, Thermodynamic Functions of Some Simple Fluorine Compounds, *J. Chem. Phys.* **26**, 394–397.

Ramsdale, S. A. and Tickle, G. A.: 1998, Review of Lift-Off Models for Ground Based Buoyant Clouds, *Technical Report AEAT–4262*, AEA Technology.

Redington, R. L.: 1982, Nonideal-Associated Vapor Analysis of Hydrogen Fluoride, *J. Phys. Chem.* **86**, 552.

Richards, J. M.: 1963, The penetration of interfaces by cylindrical thermals, *Quart. J. Roy. Meteor. Soc.* **89**, 254–264.

Richardson, L. F.: 1926, Atmospheric Diffusion shown on a Distance-Neighbour Graph, *Proc. Roy. Soc. London* A **110**, 709–737.

Schotte, W.: 1980, Collection of Phase Equilibrium Data for Separation Technology, *Ind. Eng. Chem. Process Des. Dev.* **19**, 432–439.

Schotte, W.: 1987, Fog Formation of Hydrogen Fluoride in Air, *Ind. Eng. Chem. Res.* **26**, 300–306.

Simons, J.: 1924, The preparation, Freezing point and vapor pressure of hydrogen fluoride, *J. Amer. Chem. Soc.* **46**, 2179–2183.

Simons, J. and Bouknight, W. K.: 1932, The Density and Surface Tension of Liquid Hydrogen Fluoride, *J. Amer. Chem. Soc.* **54**, 129.

Simons, J. and Hildebrand, J. H.: 1924, The density and molecular complexity of gaseous hydrogen fluoride, *J. Amer. Chem. Soc.* **46**, 2183–2191.

Smith, D. F.: 1958, Hydrogen Fluoride Polymer Spectrum, Hexamer and Tetramer, *J. Chem. Soc.* **28**, 1040–1056.

Strohmeier, W. and Briegleb, G.: 1953, Über den Assoziationszustand des HF im Gaszustand. I, *Z. f. Electrochemie* **57**, 662–667.

Thomas, R. K.: 1975, Hydrogen bonding in the vapour phase between water and hydrogen fluoride: the infrared spectrum of the 1:1 complex, *Proc. R. Soc. Lond. A.* **344**, 579–592.

Thorpe, T. E. and Hambly, F. J.: 1889, *J. Chem. Soc.* **55**, 161. Data are reproduced in Simons & Hildebrand.

Vanderzee, C. E. and Rodenburg, W. M.: 1970, Gas imperfections and thermodynamic excess properties of gaseous hydrogen fluoride, *J. Chem. Thermodyn.* **2**, 461–478.

Venkatram, A. and Du, S.: 1996, An analysis of the asymptotic behavior of cross-wind-integrated ground-level concentrations using lagrangian stochastic simulation, *Atmospheric Environment* **31**, 1467–1476.

Vieweg, R.: 1963, Betrachtungen zum System Fluorwasserstoff-Wasser, *Chem. Tech., Leipzig* **15**, 734–740.

Weast, R. C. (ed.): 1986, *CRC Handbook of Chemistry and Physics*, CRC Press, Inc., Florida.

Webber, D. M., Jones, S. J., Tickle, G. A. and Wren, T.: 1992, A Model of a Dispersing Dense Gas Cloud, and the Computer Implementation D*R*I*F*T, *Technical Report SRD/HSE R587*, AEA Technology, Helth and Safety Executive.

Weil, J. C.: 1988, Chapter 3: Plume Rise, *in* Venkatram and Wyngaard (eds), *Lectures on Air Pollution Modeling*, American Meteorological Society, Boston, pp. 119–166.

Willis, G. E. and Deardorff, J. W.: 1976, A laboratory model of diffusion into the convective planetory boundary layer, *Quart. J. Roy. Meteor, Soc.* **102**, 427–445.

Bibliographic Data Sheet **Risø–R–1293(EN)**

Title and author(s)

An integral model for continuous HF releases.

Søren Ott

ISBN
87–550–2942–6; 87–550–2943–4(Internet)

ISSN
0106–2840

Dept. or group
Systems Analysis Department

Date
September 2001

Project/contract No.
CEC D.G. XII ENV4-CT97-0630

Pages	Tables	Illustrations	References
75	4	26	68

Abstract (Max. 2000 char.)

This report describes the development of an integral model for the dispersion of HF clouds, which is part of the work done by Risø in the URAHFREP project.
The main objective has been to model the possible influence of HF thermodynamics on the dispersion of atmospheric HF clouds. Both negative buoyancy (heavy gas) effects and positive buoyancy effects are possible depending on concentration, humidity and other factors. A main question is under which conditions these effects are strong enough to dominate naturally occurring fluctuations and produce plume lift-off.
HF can form polymers in the gas phase and it forms highly non-ideal liquid mixtures with water. It is demonstrated that the HF thermodynamics needed for the dispersion model can be described by exact thermodynamical relations. Existing experimental data are scarce and of varying quality. The best data have been selected and analysed in order to obtain properties on the saturation curve. A relatively simple rings–and–chains model for the self-association in the gas phase is proposed, and it is demonstrated that the model is capable of reproducing the enthalpy and the anomalous specific heat of HF very satisfactory. A simple four parameter model for the mixture is proposed and successfully tested.
The dispersion model is a standard integral model with some additional features. The ideas and assumptions of integral models is explained and the various scaling regimes for cloud growth are discussed. Re-analyzing the Prairie Grass data set it is found that the height of the boundary layer has no direct impact on lift-off. The model is successfully tested against data from the URAHFREP field trials. A case study is made in order to determine the conditions necessary for HF induced buoyancy to have an effects on ground level concentrations. Added mass is discussed the appendix.

Descriptors

HYDROGEN FLUORIDE; HF; DISPERSION; MODEL; CONTINUOUS RELEASE; BUOYANCY; PLUME RISE

Available on request from:
Information Service Department, Risø National Laboratory
(Afdelingen for Informationsservice, Forskningscenter Risø)
P.O. Box 49, DK–4000 Roskilde, Denmark
Phone (+45) 46 77 46 77, ext. 4004/4005 · Fax (+45) 46 77 40 13
E-mail: risoe@risoe.dk